# DISSERTATION

submitted to the

Combined Faculties for the Natural Sciences and for Mathematics

of the Ruperto-Carola University of Heidelberg, Germany

for the degree of

Doctor of Natural Sciences

# MOLECULAR CHARACTERIZATION OF MUTATED HISTONE H3.3 IN CHILDHOOD GLIOBLASTOMA

presented by

Dipl.-Biol. Sebastian Bender

Born in Heidelberg, Germany

# DISSERTATION

submitted to the

Combined Faculties for the Natural Sciences and for Mathematics

of the Ruperto-Carola University of Heidelberg, Germany

for the degree of

Doctor of Natural Sciences

presented by

Dipl.-Biol. Sebastian Bender

Born in Heidelberg, Germany

Day of oral examination: April 10th, 2013

# MOLECULAR CHARACTERIZATION OF MUTATED HISTONE H3.3 IN CHILDHOOD GLIOBLASTOMA

Referees: Prof. Dr. Werner Buselmaier

Prof. Dr. Peter Lichter

# DECLARATION

I hereby declare that I have written the submitted dissertation ‘Molecular characterization of mutated Histone H3.3 in childhood glioblastoma’ myself and in this process have used no other sources or materials than those expressly indicated. I hereby declare that I have not applied to be examined at any other institution, nor have I used the dissertation in this or any other form at any other institution as an examination paper, nor submitted it to any other faculty as a dissertation.

_____ _____

(Place, Date) Sebastian Bender

To my parents

**SUMMARY**

In recent years, affordable costs of next-generation sequencing technologies set the basis for the characterization of a multitude of cancer genomes. In doing so, scientists all over the world reconfirmed that cancer is a disease of the (epi)genome. The growing number of genetic abnormalities found in chromatin remodeling factors in various cancer entities produced evidence that aberrant chromatin modification plays an essential role in cancer initiation and progression.

Besides numerous mutations of histone modifying factors in different cancer types, two recurrent mutations within the histone H3.3 coding gene *H3F3A* have been identified in about 50% of pediatric glioblastoma. Both mutations result in amino acid substitutions at two critical residues of the histone tail of H3.3 (K27M or G34R/V). Since glioblastomas harboring one of these H3.3 mutations are characterized by a complex but stereotypic pattern of genetic and epigenetic alterations, the project presented here uses a variety of molecular techniques to study the functional mechanisms associated with both H3.3 mutations.

By using confocal imaging of fluorescently labeled H3.3 mutants and genome-wide sequencing-based chromatin immunoprecipitation (ChIP-Seq) of ectopically expressed H3.3 mutants, it was demonstrated that deposition and incorporation of histone H3.3 into chromatin is not affected by the mutations. Furthermore, experiments with different cell lines, which were genetically modified to stably overexpress mutant H3.3, provide evidence that (at least) some of the genome-wide changes that were originally found in H3.3 mutated glioblastomas, can be faithfully recapitulated *in vitro*.

The investigation of several epigenetic marks by Western blot analysis and immunohistochemistry identified a strong dominant negative effect of the K27M mutant H3.3 protein, which causes global reduction of the key epigenetic mark H3K27me3. Moreover, this epigenetic alteration found in primary tumors, was induced *in vitro* by overexpression of K27M mutant H3.3 in different cell lines.

By using mass spectrometry to dissect the pattern of posttranslational modifications (PTM) at the histone tail of G34R mutant H3.3, a new PTM has been identified, namely dimethylation of arginine 34. Furthermore, first evidence is provided that this new PTM is causative for the downregulation of K36 trimethylation at G34R mutant H3.3.

Finally, overexpression of mutant H3.3 in the brain of neonatal mice was performed by retroviral gene transfer. In doing so, this study aims at the elucidation of the *in vivo* tumorigenic potential of both histone H3.3 mutations alone or in combination with impaired *TP53* function.

In summary, the findings of this thesis provide novel insights into the comprehensive epigenetic changes caused by mutant histone H3.3 in pediatric GBMs. These results might provide the basis for the development of novel therapeutic strategies targeting the epigenetic changes induced by H3.3 mutations, which have been identified recently in nearly half of the tumors in children suffering from this devastating brain tumor.

## ZUSAMMENFASSUNG

In den vergangenen Jahren bildeten die fallenden Kosten für die Hochdurchsatzsequenzierung die Grundlage für die genetische Analyse einer Vielzahl von Tumorgenomen. Hierdurch konnten Forscher weltweit bestätigen, dass es sich bei Krebs um eine Erkrankung des (Epi)Genoms handelt. In unterschiedlichen Krebsarten wurden vermehrt genetische Defekte in Chromatin-modifizierenden Faktoren gefunden, die den Beweis erbrachten, dass Veränderungen der Chromatinmodifizierung eine entscheidende Rolle bei der Krebsentstehung und beim Fortschreiten der Erkrankung spielen.

Neben der Identifizierung einer Vielzahl von Mutationen in Histon-modifizierenden Faktoren in unterschiedlichen Krebsentitäten, wurden in pädiatrischen Glioblastomen (pedGBMs) zwei rekurrente Mutationen im Histon H3.3 kodierenden Gen *H3F3A* entdeckt. Beide Mutationen führen zum Austausch von Aminosäuren an wichtigen Positionen des Histonproteins (K27M bzw. G34R/V). Glioblastome, die eine dieser Mutationen tragen, zeichnen sich durch ein komplexes aber sehr charakteristisches Muster an genetischen und epigenetischen Veränderungen aus. Um beide H3.3 Mutationen funktionell zu charakterisieren, wurde eine Vielzahl von molekularen Untersuchungsmethoden verwendet.

Unter Verwendung konfokaler Mikroskopie Flurochrom-gekoppelter H3.3 Mutanten und Genom-weiten Sequenzierdaten einer Chromatin Immunopräzipitation (ChIP-Seq) belegt diese Arbeit, dass die Inkorporation von Histon H3.3 in Chromatin durch keine der beiden Mutationen beeinträchtigt wird. In *in vitro* Experimenten wurden unterschiedlichen Zelllinien genetisch manipuliert, sodass sie mutiertes H3.3 überexprimieren. Die Ergebnisse zeigen, dass (zumindest) ein Teil der Genom-weiten Veränderungen, wie sie ursprünglich in H3.3 mutierten Glioblastomen gefunden wurden, im Zellkulturmodell rekapituliert werden.

Die Untersuchung mehrerer epigenetischer Modifikationen durch Western Blot Analysen und Immunohistochemie identifizierte einen starken dominant-negativen Effekt des K27M mutierten H3.3 Proteins, welcher zu einer globalen Reduktion der H3K27me3 Expression führt. Diese epigenetische Veränderung in Primärtumoren konnte durch die Überexpression von K27M mutiertem H3.3 in mehreren Zelllinien *in vitro* nachgebildet werden.

Massenspektrometrie wurde verwendet um posttranslationale Modifikationen (PTMs) am G34R mutierten Histon zu untersuchen. Das dadurch detektierte Dimethyl-Arginin 34 stellt eine bisher nicht beschriebene PTM dar. Darüber hinaus liefert diese Arbeit erste Hinweise dafür, dass diese neuartige PTM die H3K36 Trimethylierung an G34R mutiertem H3.3 negativ reguliert.

Überdies wurden die Histon H3.3 Mutanten im Gehirn von neugeborenen Mäusen mittels retroviralen Gentransfers überexprimiert, um zu untersuchen, ob dies alleine oder in Kombination mit defektem *TP53* Tumore induziert.

Zusammenfassend gibt die vorliegende Arbeit neue Einblicke in die umfassenden epigenetischen Veränderungen, die durch H3.3 Mutationen in pädiatrischen GBMs hervorgerufen werden. Diese richtungsweisenden Ergebnisse könnten den ersten Schritt in der Entwicklung neuer Therapien zur Behandlung der durch H3.3 Mutationen verursachten epigenetischen Veränderungen bedeuten. Diese wurden kürzlich in nahezu der Hälfte aller Tumore in Kinder und Jugendlichen beschrieben, die an diesem in der Regel tödlich verlaufenden Hirntumor leiden.

## ABBREVIATIONS

| | |
|---|---|
| ADMA | Asymmetric dimethylarginine |
| ALL | Acute lymphoblastic leukemia |
| ALT | Alternative lengthening of telomeres |
| AML | Acute myeloid leukemia |
| ATRX | A-thalassaemia/mental retardation syndrome X-linked |
| BRD | Bromodomain |
| BSA | Bovine serum albumin |
| CAF1 | Chromatin assembly factor 1 subunit A |
| cDNA | Complementary DNA |
| CFP | Cyan fluorescent protein |
| CHD1 | Chromodomain helicase DNA binding protein 1 |
| ChIP | Chromatin immunoprecipitation |
| CHOP | CpG hypomethylator phenotype |
| CIMP | CpG island methylator phenotype |
| CMV | Cytomegalovirus |
| CNS | Central nervous system |
| C-terminal | Carboxy-terminal |
| DAB | Diaminobenzidine |
| DAPI | 4',6-Diamidino-2-phenylindole |
| DAXX | Death-domain associated protein |
| DDR | DNA damage response |
| DIPG | Diffuse intrinsic pontine glioma |
| DKFZ | German cancer research center |
| DNA | Deoxyribonucleic acid |
| dNTPs | Deoxynucleotide triphosphates |
| DTT | Dithiothreitol |
| E. coli | Escherichia coli |
| EED | Embryonic ectoderm development |
| EGFP | Enhanced green fluorescent protein |
| EGFR | Epidermal growth factor receptor |
| EZH1 | Enhancer of zeste 1 |
| EZH2 | Enhancer of zeste 2 |
| FCS | Fetal calf serum |
| FOXG1 | Forkhead box protein 1 |
| G | Glycine (IUPAC: one letter notation for amino acids) [1] |
| GBM | Glioblastoma multiforme |
| gDNA | Genomic DNA |

| | |
|---|---|
| HAT | Histone acetyltransferase |
| HDAC | Histone deacetylase |
| HDM | Histone demethylase |
| HE | Hematoxylin and eosin |
| HeLa | Cervical cancer cell line derived from Henrietta Lacks |
| HMTs | Histone methyltransferase |
| HP1 | Heterochromatin protein 1 |
| HRP | Horseradish peroxidase |
| ICGC | International Cancer Genome Consortium |
| IDH1/2 | Isocitrate dehydrogenase ½ |
| IF | Immunofluorescence |
| IHC | Immunohistochemistry |
| IRX1 | Iroquois homeobox 1 |
| IUPAC | International union of pure and applied chemistry |
| JMJD2A | Jumonji C domain-containing histone demethylase 2A |
| K | Lysine (IUPAC: one letter notation for amino acids) [1] |
| kB | Kilobase (1000 base pairs) |
| KDM6A | Lysine (K)-specific demethylase 6A |
| LYPD | LY6/PLAUR domain containing 6 |
| M | Methionine (IUPAC: one letter notation for amino acids) [1] |
| MCF7 | Michigan Cancer Foundation–7 |
| MECP2 | Methyl-CpG Binding protein 2 |
| MLL1 | myeloid/lymphoid or mixed-lineage leukemia |
| MOI | Multiplicity of infection |
| MS | Mass spectrometry |
| MTS | 3-(4,5-dimethylthiazol-2-yl)-5-(3-carboxymethoxyphenyl)-2-(4-sulfophenyl)-2H-tetrazolium |
| NF1/2 | Neurofibromin 1/2 |
| N-terminal | Amino-terminal |
| OLIG1/2 | Oligodendrocyte lineage marker 1/2 |
| ORF | Open reading frame |
| PBS | Phosphate buffered saline |
| PCNA | Proliferating cell nuclear antigen |
| PTCH1 | Patched 1 |
| pedGBM | Pediatric glioblastoma multiforme |
| PHD | Plant homeodomain |
| PI | Propidium iodide |
| PRC2 | Polycomb repressive complex 2 |

| | |
|---|---|
| PRMT | Protein arginine methyltransferases |
| PTM | Posttranslational modification |
| PVDF | Polyvinylidene fluoride |
| PWWP | Proline-tryptophan-tryptophan-proline |
| qRT-PCR | Quantitative realtime PCR |
| R | Arginine (IUPAC: one letter notation for amino acids) [1] |
| RCAS | Replication competent ASLV long terminal repeat with splice acceptor |
| RNA | Ribonucleic acid |
| RBAPA48 | Retinoblastoma-binding protein p48 |
| SDMA | Symmetric dimethylarginine |
| SOX10 | SRY (sex determining region Y)-box 10 |
| SUFU | Suppressor of fused homolog (Drosophila) |
| SUZ12 | Suppressor of zetse 12 |
| TMA | Tissue microarray |
| TP53 | Tumor protein p53 |
| US | United States of America |
| UTR | Untranslated region |
| UTX | Ubiquitously-transcribed X chromosome tetratricopeptide repeat protein |
| V | Valine (IUPAC: one letter notation for amino acids) [1] |
| WHO | World health organization |
| ZNF233 | Zinc finger protein 233 |

## DEFINITIONS

Gene symbols written as capital letters indicate human protein (e.g. ATRX).

Gene symbols written in italic as capital letters indicate human gene (e.g. *ATRX*).

Gene symbols written in lower case starting with a capital letter indicate mouse protein (e.g. Atrx).

Gene symbols written in italic in lower case starting with a capital letter indicate mouse gene (e.g. *Atrx*).

# 1 INTRODUCTION

## 1.1 Cancer - A Disease of the (Epi)Genome

Since the early 19th century, defects within the genetic information were suspected to cause cancer. At this time, Theodor Boveri and David von Hansemann described an abnormal number of chromosomes due to aberrant mitosis in cancer cells [2, 3]. Today, there is overwhelming evidence that cancer is a disease of the genome. Cancer is believed to start when a single cell in one part of the body has acquired the ability to uncontrolled cell proliferation. Although this might sound harmless, in worst case uncontrolled cell growth ends up in cancer related death, as it was the case for 7.6 million people worldwide, who died due to cancer in 2008 [4]. According to the World Health Organization (WHO), cancer is the leading cause of death all over the world, accounting for 13% of all deaths worldwide [5]. Current estimates assume that every day within the year 2013, approximately 1600 people will die due to cancer in the US [6].

Cancer is a genetic disease which develops in a multistep process. At the end of this process a cell has acquired several properties, which allow for tumor growth and progression. Within recent years, our knowledge about these malignant properties, which are essential to drive cancerous transformation, increased rapidly. Some years ago, six malignant properties, also known as the hallmarks of cancer, have been reported to be necessary to transform normal cells into cancerous ones [7]. In order to become malignant, a tumor cell has to acquire the capability to escape programmed cell death (apoptosis), replicate without limit, be independent of exogenous growth signals and resistant to anti-proliferative signals. Moreover, the capability to grow into healthy neighboring tissues by invasion or metastasis and the ability to supply the developing tumor with nutrients by the growth of new blood vessels (angiogenesis) enhances mortality of cancer enormously [7]. Today, it is well accepted that cells have to obtain additional properties to become malignant. These include the potential to use different metabolic pathways to produce all classes of macromolecules. This hallmark of cancer is based on the observation that cancer cells show fundamental differences in metabolic pathways to produce energy, a phenomenon called Warburg effect [8]. Furthermore cancer cells have to evade immune destruction but might benefit from the tumor supportive effect of immune cells. Last but not least, an essential hallmark of cancer is the development of genome instability [9].

Genomic instability is a crucial hallmark of cancer as it promotes the acquisition of all other malignant properties described above via accumulation of numerous genomic aberrations and/or mutations. On the one hand, these genomic changes target genes which in principal have the ability to promote cancer development (proto-oncogenes). When activated, e.g. by mutation, these genes are called oncogenes. On the other hand, both alleles of genes named tumor suppressors have to be inactivated to drive a cell into cancerous development.

Since new DNA sequencing technologies provide the possibility to decipher the mutational landscape of tumor genomes in a fast and cost effective way, the number of mutations identified in both of these classes of cancer related genes, oncogenes and tumor suppressor genes, has increased rapidly. As an example, the detailed analysis of hundreds of genomes of medulloblastoma, which represents one of the most devastating brain tumors in childhood, led to the identification of several new oncogenes and tumor suppressor genes, which have been found to be recurrently mutated [10, 11]. One of the most comprehensive cancer sequencing efforts worldwide has recently been launched by the International Cancer Genome Consortium (ICGC), which initiated the genomic analysis of more than 25,000 tumor genomes from 50 different cancer entities [12]. The results of this international large scale sequencing effort will decisively improve our knowledge of the genetic disease named cancer.

The past decade of cancer research has underlined the fact that cancer is not only a disease of the genome but also a disease of the epigenome. The epigenome is defined as cellular information, other than the DNA sequence itself, which is heritable through cell division [13]. Alterations within the epigenome are an alternative/additional mechanism to promote tumorigenesis. These alterations include the activation and inactivation of oncogenes or tumor suppressor genes, respectively, by DNA methylation and the regulation of DNA accessibility by altered chromatin structure via histone modifications [14]. In general, the cancer genome has been found to show global loss of DNA methylation (hypomethylation) which is complemented by specific genomic regions displaying aberrantly high DNA methylation (hypermethylation) [15, 16]. Basically, regions of DNA hypomethylation are associated with activated gene transcription, while genes located within hypermethylated regions of the genome are transcriptionally downregulated. Abnormal histone modifications in cancer change the overall structure of chromatin leading to a more open or condensed nucleosome configuration which allows or inhibits gene transcription, respectively. Epigenetic (in)activation of cancer related genes is assumed to be at least as frequent as mutational events [17]. Therefore, the sequencing results of each of the cancer genomes coordinated by the ICGC are strongly recommended to be complemented with genome-wide information on DNA methylation [12].

Basically, every cell in the human body can undergo malignant transformation. However, some cells/tissues are much more susceptible to malignant transformation. This is mainly due to differences in exposure to exogenous stimuli (carcinogens) like irradiation, tobacco, alcohol or diet. Tissues, which are exposed to these carcinogens like skin, lung or colon are much more prone to develop cancer. Variable incidence rates of nearly all cancer types are mainly linked to environmental risk factors including behavioral, geographical and cultural differences [18]. Unlike many cancers in adults, childhood cancers are not linked to

environmental risk factors, as they arise sporadically, as a consequence of developmental defects or due to heritable causes. As for many diseases, gender is an essential factor influencing the development and prognosis of cancers. It has been shown that for the majority of different tumor entities including brain tumors, the overall incidence and mortality rates among males was significantly higher than in females [19]. In general, breast cancer is the most frequent and deadly cancer in females (23% of all diagnosed cancer cases resulting in 14% of total cancer deaths), while lung cancer is the most commonly diagnosed cancer type and most deadly entity in males (17% of all cancer cases resulting in 23% of total cancer deaths) [4].

One of the most outstanding factors influencing the development of cancer is age, as almost all cancer incidence rates rise dramatically with age. However, brain tumors in infants and children are frequent and the second most common cause of death in this age group, surpassed only by traffic accidents.

## 1.2 Childhood Brain Tumors

More than 7% of the 300,000 individuals that were diagnosed with a primary brain tumor in the United States between 2004 and 2008 were younger than 20 years [20]. In this age group, tumors of the central nervous system (CNS) are the second most common malignancy after leukemia. Although incidence rates of leukemia are much higher, solid malignancies of the brain are the leading cause of cancer related mortality in childhood. This is mainly attributed to recent advances in leukemia treatment including precise risk stratification and personalized therapy, which have pushed the cure rate for some leukemias like acute lymphoblastic leukemia (ALL) in children and adolescents to more than 90% [21]. In comparison, advances in diagnosis and treatment of solid malignancies of the brain did not keep pace. Just nowadays, as researchers continuously unravel the molecular basis of childhood brain tumors, new treatment protocols, adapted to the needs and specific features of brain tumors in children, find their way into clinics.

Given the fact that brain tumors of childhood and adolescence differ substantially from their adult counterparts, there is a desperate need of adapted diagnostic algorithms and treatment protocols for brain tumors in young patients. A subset of brain tumors, called embryonal tumors, can be found almost exclusively in children. These embryonal CNS tumors develop during intrauterine or early postnatal development due to dysregulation of signaling pathways crucial for normal CNS development [22]. In addition, genetic disorders, which are known to predispose children to develop a brain tumor, are found in about 10% of all pediatric brain tumor patients [23]. Genetic disorders associated with a higher risk to develop a brain tumor include Li-Fraumeni syndrome, characterized by mutations within the tumor suppressor gene

coding for p53 (*TP53)*, Gorlin syndrome (*PTCH1* or *SUFU*), Turcot syndrome (*APC*) and Neurofibromatosis type 1/2 (*NF1*/*NF2*) [24-27]. Most brain tumors, however, originate sporadically with notable differences between children and adults. Some brain tumors like benign gliomas are much more frequent in young patients, while highly malignant gliomas predominate in adult patients. In addition, pediatric brain malignancies often develop in the hindbrain, whereas hemispheric tumors dominate in adulthood. Consequently, approximately 50% of all pediatric brain tumors arise infratentorially in the posterior fossa [28]. While being histopathologically indistinguishable, tumors of the same entity also dramatically differ in several genetic and epigenetic features between children and adults [29]. This includes the frequency of genomic aberrations such as hot spot mutations, which has been shown to be significantly higher in adult medulloblastoma compared to subgroup-matched tumors of pediatric patients [11].

The main part of the thesis presented here deals with the functional consequences of histone H3.3 mutations, which represent a genetic alteration exclusively found in high grade gliomas of pediatric and adolescent patients [30]. Considering all aforementioned differences between pediatric and adult brain tumors, it is not surprising that current treatment protocols of brain tumors in childhood have to be adapted specifically to their characteristics. Additionally, treatment of pediatric brain tumors always faces the problem that the developing brain is highly vulnerable to aggressive treatment options, in particular radiotherapy [31]. This has led to limitations of radiotherapy usage in very young children (below 4 years of age), who have to be treated by postoperative chemotherapy alone [32]. In young patients quality of survival is of special importance since these patients have to live the rest of their life with all treatment-induced cognitive deficits.

### 1.3 Glial Tumors

The most common category of brain tumors diagnosed in children are tumors of glial origin (glioma). These tumors account for 53% of all brain tumors in very young patients (0-14 years) and 38% in adolescent patients (15-19 years) [20]. Gliomas represent the most frequent type of central nervous system neoplasms. In Europe and the United States 77,000 new cases are diagnosed every year [33]. For almost a century, gliomas have been classified according to histological features, which resemble features of normal glial cells [34]. Thus, gliomas are classified into one of the three main groups: astrocytomas (astrocytes), oligodendrogliomas (oligodendrocytes) or ependymomas (ependymal cells) [35]. Whether these cells represent indeed the respective tumor initiating cells, however, requires further investigation. All three main groups of gliomas are further subdivided by additional histologic features of the respective tumors (Figure 1).

Based on the grade of malignancy, gliomas are graded into one of the four World Health Organization (WHO) grades (grade I to grade IV) [36]. While benign grade I gliomas generally can be treated by surgery alone, grade II tumors are low-risk tumors which grow infiltrative and need to be treated with adjuvant therapy. Unlike in children, grade II gliomas in adults frequently progress to grade IV glioblastomas. Grade III gliomas show much higher proliferation rates and tend to progress into grade IV tumors, the most malignant form of glioma. A summary of the WHO glioma classification by cellular origin and grading is given in Figure 1.

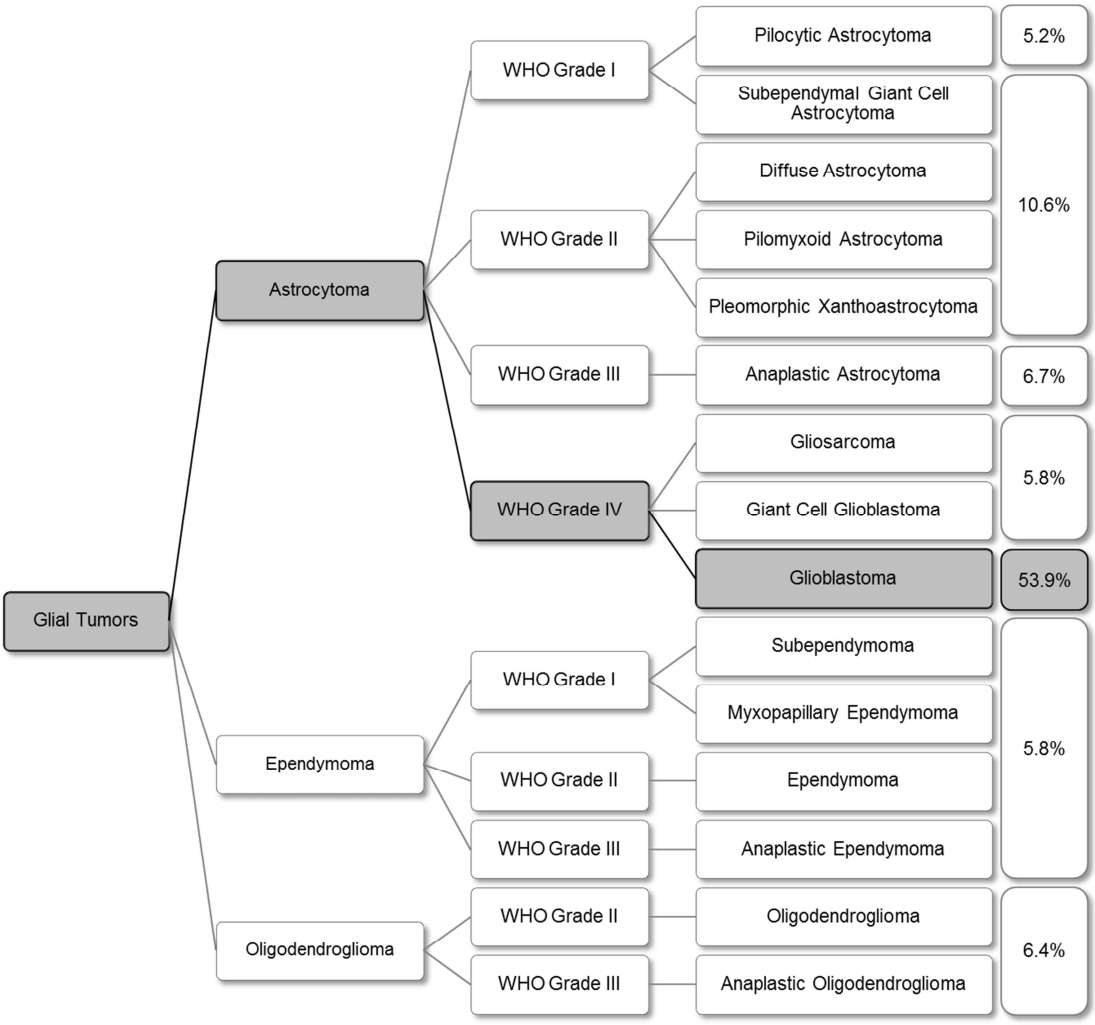


**Figure 1. Classification of Glial Brain Tumors.** Overview of histological subtypes and WHO grading of glial brain tumors based on the 2007 WHO brain tumor classification [36]. In addition, relative frequency of tumors of glial origin are shown based on the 2004-2008 report of the Central Brain Tumor Registry of the United States (CBTRUS) [20]. Percentages represent the relative distribution of the respective glioma subtype within the total number of 89,617 tumors diagnosed between 2004 and 2008 in the US.

The most common and most life threatening type of glioma are grade IV astrocytomas, also termed glioblastoma multiforme (GBM), which account for approximately 54% of all glial tumors [20].

### 1.3.1 Glioblastoma

Glioblastoma multiforme (GBM; WHO grade IV astrocytoma) represents the most common and most lethal type of glioma in children and adults [36]. Every year, there are 3 to 5 newly diagnosed cases per 100,000 individuals [37]. Three years after diagnosis more than 95% of all glioblastoma patients have died from disease due to the aggressive clinical behavior of this brain tumor [38]. This dismal prognosis is mainly a consequence of the invasive growth of GBMs and the resistance to conventional treatment, including surgery, radio- and chemotherapy. The large majority of these tumors (> 90%) develop rapidly *de novo* (primary GBMs), while only a subset progress gradually from grade II/grade III glioma within 5 to 15 years and are therefore also referred to as secondary glioblastoma [37]. Based on their histology, primary and secondary GBMs are indistinguishable, but substantial molecular differences including genetic aberrations and distinct gene expression profiles strongly suggest that primary and secondary GBMs represent different disease entities sharing a comparable fatal prognosis [39, 40].

GBMs mainly affect the adult population with a median age of 64 years at diagnosis. Yet, 3% of all childhood primary brain tumors are pediatric glioblastomas (pedGBMs) [20, 37]. Almost all children, diagnosed with a pedGBM, die due to this fatal brain tumor within the next 3 years. Like in adults, pedGBMs may develop within one of the two cerebral hemispheres (or other regions of the brain), but some pedGBMs affect the brain stem and are then named diffuse intrinsic pontine gliomas (DIPGs). These tumors, which are almost exclusively found in children, are unresectable and are characterized by an even inferior prognosis compared to their hemispheric counterparts. Histologically, pedGBMs are indistinguishable from adult GBMs but substantially differ from adult GBMs in their hallmark molecular and genetic features, which are of major biological and clinical significance. Like adult primary GBMs, pedGBMs develop *de novo* but numerous studies have shown that pedGBMs harbor recurrent genomic aberrations, gene expression and DNA methylation profiles distinct from their adult counterparts [29, 41, 42]. Due to these fundamental genetic and epigenetic differences, it became obvious that distinct biological pathways are responsible for gliomagenesis in adults and children. Low incidence rates in children and the consequential paucity of frozen pedGBM samples has been hindering efforts to establish new treatment protocols specifically for childhood GBMs. Therefore, standard therapy is currently mainly based on clinical experience in adults.

### 1.3.2 The (Epi)Genome in Childhood Glioblastoma

Compared to malignant glioma in adults, which are characterized by genomic instability and a complex series of genomic aberrations, pediatric glioblastoma display a much more limited

spectrum of genomic aberrations, including a subset of tumors with an almost stable karyotype and more favorable prognosis [29, 41]. The most frequent genomic aberrations found in pedGBMs are amplification of the *PDGFRA* locus (4q12) and deletions of *CDKN2A/B* (9p21) [29, 41]. Focal chromosomal gains or losses have been found to mainly perturb gene function within the p53, PI3K/RTK, and RB pathways [41, 43]. In addition, deletions of other well-known tumor suppressor genes (e.g. *PTEN*) or amplifications of oncogenes have been reported at much lower frequency than in adults, including amplifications *of EGFR* (epidermal growth factor receptor) at 7p12, which is a very common event in adult primary glioblastoma [41]. The same holds true for mutations of *IDH1* and *IDH2* (isocitrate dehydrogenase 1/2), which are present in more than 90% of adult secondary GBMs but are hardly found in pedGBMs [44]. Large scale genomic alterations of pedGBMs include gain of 1q, which is described to be a common event in other childhood cancers as well, including aggressive pediatric ependymoma [45]. Notably, besides high *PDGFRA* expression due to gene amplification, aberrant PDGF signaling has been reported in a high proportion of pedGBMs, underscoring the importance of this signaling pathway in pedGBM [46].

Recently, we and others identified a high frequency of pedGBMs harboring mutations within the H3.3/ATRX/DAXX chromatin remodeling pathway [30]. Two recurrent mutations within the *H3F3A* gene*,* encoding the replication independent replacement histone H3.3, were found in about 50% of pedGBMs [30, 47]. These mutations state the first described recurrent mutations within any of the highly conserved human histone genes. The first *H3F3A* mutation affects the codon for lysine 27 (K27) of H3.3, which was always found to be substituted by a methionine (K27M). The same mutation was found in DIPGs at a very high frequency, and at a lower frequency within the gene *HIST1H3A*, coding for the canonical histone H3.1 [47]. The second mutation leads to the replacement of glycine 34 (G34) by an arginine (R34R) and in some rare cases by a valine (G34V) [30, 47]. Interestingly, both mutations were also significantly associated with clinical parameters such as patient age or tumor location. While patients suffering from a K27M mutated pedGBM tend to be younger (median age 10.5 years), G34R mutated tumors develop in adolescent patients/young adults with a median age of 18 years [48]. Furthermore, most of the K27M mutated tumors are midline tumors affecting the thalamus, brain stem or pons and are therefore commonly found in DIPGs [47, 49]. In contrast, pedGBMs with G34R mutations are located within one of the two cerebral hemispheres [48].

In a subsequent analysis, we were able to demonstrate that H3.3 mutated pedGBMs not only exhibit a distinct gene expression profile, but are also characterized by mutation specific genome-wide DNA methylation patterns [48]. Based on their methylome, pedGBMs can be subdivided into 5 different subgroups: All pedGBMs lacking *H3F3A* or *IDH1* mutations either

belong to a group with high frequency of *PDGFR* amplifications (receptor tyrosine kinase 1 group (RTK1_PDGFR)) or the so-called mesenchymal group, which mainly consists of tumors with a mesenchymal gene expression signature. All other pedGBMs can be subdivided into three subgroups, which are tightly correlated with mutations of *IDH1* or *H3F3A,* that have been shown to be mutually exclusive. The methylome of *IDH1* mutated tumors is very distinct from any other methylation profile as it is characterized by global DNA hypermethylation. *IDH1* mutations are gain-of-function mutations, which have been shown to increase the intracellular level of the onco-metabolite 2-hydroxyglutatrate, a potent inhibitor of histone lysine demethylases and DNA methylases [50, 51]. The association of *IDH1* mutations and global DNA hypermethylation, which is predominantly found in adult GBMs, is also known as the Glioma CpG island methylator phenotype (G-CIMP) [52]. In addition, tumors harboring either K27M or G34R mutations of *H3F3A* also form a separate DNA methylation cluster each, with G34R mutated tumors displaying global DNA hypomethylation, which is predominantly affecting subtelomeric regions [48]. According to the CpG island methylator phenotype in *IDH1* mutated GBMs, this hypomethylated pattern of G34R mutated pedGBMs was named CHOP (CpG hypomethylator phenotype).

Differences have also been identified when correlating patient survival of all three mutation-defined subgroups. As already reported for adult GBMs, *IDH1* mutated pedGBMs are characterized by a slightly more favorable prognosis compared to their non-mutated counterparts. While patients suffering from a G34R mutated tumor are doing significantly better than *H3F3A* wildtype tumors, patients with K27M mutated tumors tend to do even worse without reaching statistical significance [48, 49].

By applying an integrated analysis combining DNA methylation and gene expression data, our laboratory identified marker genes, which show differential methylation and expression within the described subgroups. A region of the *FOXG1* (forkhead box protein 1) promoter was found to be specifically hypermethylated in K27M mutated pedGBMs, leading to loss of *FOXG1* gene expression in K27M mutated tumors. The promoter of the two oligodendrocyte lineage marker genes *OLIG1* and *OLIG2* displayed concerted hypermethylation exclusively in G34R mutated pedGBMs, resulting in abolished *OLIG1/2* gene expression. Hence, protein expression of *OLIG1/2* and *FOXG1* analyzed by immunohistochemistry (IHC) can be used as a surrogate marker to identify H3.3 mutated pedGBMs [48].

In summary, more than 50% of pediatric high grade gliomas are characterized by recurrent genetic mutations of *H3F3A* and *IDH1*, which have been shown to directly impact the epigenome including the methylation of DNA and histone proteins. In addition, mutations within the genes coding for the two H3.3 specific histone chaperones ATRX (a-thalassaemia/mental retardation syndrome X-linked) and DAXX (death-domain associated protein) were identified in 31% of all pedGBMs, including 100% of G34R mutated tumors and

approximately 67% of K27M mutants. Both, ATRX and DAXX, are essential components of the complex mediating H3.3 incorporation at pericentric heterochromatin and at telomeres. Loss of function mutations of *ATRX* have recently been proven to be associated with alternative lengthening of telomeres (ALT), a phenomenon which is significantly associated with G34R mutated pedGBMs [30, 53]. The potential link between global DNA hypomethylation at subtelomeric regions detected in G34R mutated pedGBMs and the existence of the ALT phenotype in these tumors requires further elucidation. The presence of ALT has been best explained in pedGBMs having simultaneous mutations within *H3F3A*, *ATRX* and the tumor suppressor gene *TP53* [30]. Mutations of *TP53* are reported to exist in all G34R mutated pedGBMs and about 67% of K27M mutant tumors. In adults, *ATRX* alterations are frequently found together with *IDH1/2* and *TP53* mutations in astrocytic tumors across all WHO grades [54].

The high frequency of mutations directly interfering with epigenetic integrity together with the comparably low number of other genetic alterations commonly found in adult GBMs once more indicate that pedGBMs develop differently from adult GBMs. There is growing evidence that pedGBMs are primarily driven by genetic alterations resulting in defective epigenetic regulation.

## 1.4 The Structure of Chromatin

Within the eukaryotic cell nucleus, genetic information is organized in structures, called chromosomes, which allow enormous compaction of the entire hereditary information. Each of these chromosomes consists of a single DNA molecule, which is wrapped around highly conserved nucleoprotein complexes. This complex of DNA and proteins is called chromatin with nucleosomes being the repeating unit of this structure. In more detail, nucleosomes are composed of 146 base pairs of DNA wrapped around an octamer of the four core histones H2A, H2B, H3 and H4 [55, 56]. During nucleosome assembly, two pairs of H3-H4 heterodimers form a heterotetramer, which is deposited onto DNA. Afterwards, a heterotetramer of two H2A-H2B pairs is added to complete the nucleosomal octamer [57]. Packaging of DNA around histone octamers leads to a chromatin fiber of about 10 nm in diameter [58]. This conformation represents the first packaging level of genomic information, which is mediated by intra- as well as internucleosomal interactions. A higher order of compaction is achieved by the presence of the linker histone H1, which is located between the nucleosomes at the DNA entry and exit sites [59]. Histone H1 allows the establishing of a more condensed chromatin fiber, which was formerly known as the 30 nm fiber [60, 61]. The existence of this 30 nm fiber *in vivo* is not supported by more recent data [62, 63]. Fiber-fiber interactions, which are regulated by structural components of the nucleosomes themselves

(internucleosomal) as well as additional architectural chromatin proteins (non-histone proteins) allow further condensation into a higher-order chromatin structure [64, 65]. A schematic representation of chromatin and its different organization levels is given in Figure 2.

The binding of architectural chromatin proteins like the methyl-CpG-binding protein 2 (MECP2) or heterochromatin protein HP1 are substantially affected by the pattern of posttranslational modifications (PTMs) of the histone proteins or the exchange of histone variants. Besides the basic function of chromatin in storage and organization of the entire genetic information, it also provides the basis for substantial processes where the genetic information must be accessible such as during DNA replication, DNA repair or gene transcription. Overall, histone proteins are key players in the regulation of DNA accessibility.

In 1910 Albrecht Kossel was awarded the Nobel Prize in Physiology and Medicine, for his pioneering work, describing histones as the major protein component of cellular nuclei (Kossel 1884). Histones are small proteins with a length of 102 (histone H4) to 135 (histone H3) amino acids. Due to a high content of the two basic amino acids arginine (R) and lysine (K), histones are overall positively charged. This characteristic facilitates interactions with the negatively charged DNA backbone. Histones are among the evolutionarily most conserved proteins and consist mainly of two important parts: A carboxy-terminal (C-terminal) histone fold, which forms the nucleosome scaffold, and a comparably short amino-terminal (N-terminal) tail, which protrudes outward from the nucleosome [66].

The carboxy-terminal histone fold domain forms the biggest part of the histone protein (approximately 75%). It shares low sequence homology with other core histones, but a common motif of tertiary structure, which is made up of three helices separated by short loop and ß strand structures [67]. These helices are responsible for the pairing of 2 heterodimers of H3-H4 or H2A-H2B during nucleosome assembly [55]. Mutations within the domain promoting the association of two H3-H4 pairs have been shown to interfere with nucleosomal incorporation by formation of aberrant histone interactions [68].

The flexible amino-terminal tail of all core histone proteins is highly conserved and varies in length from 13 (histone H2A) to 42 (histone H3) amino acids. While the major part of histone proteins forms a globular structure, the histone tails protrude from the nucleosome core particle. This exposed position ensures its accessibility to enzymes establishing posttranslational modifications, which directly affect chromatin structure.

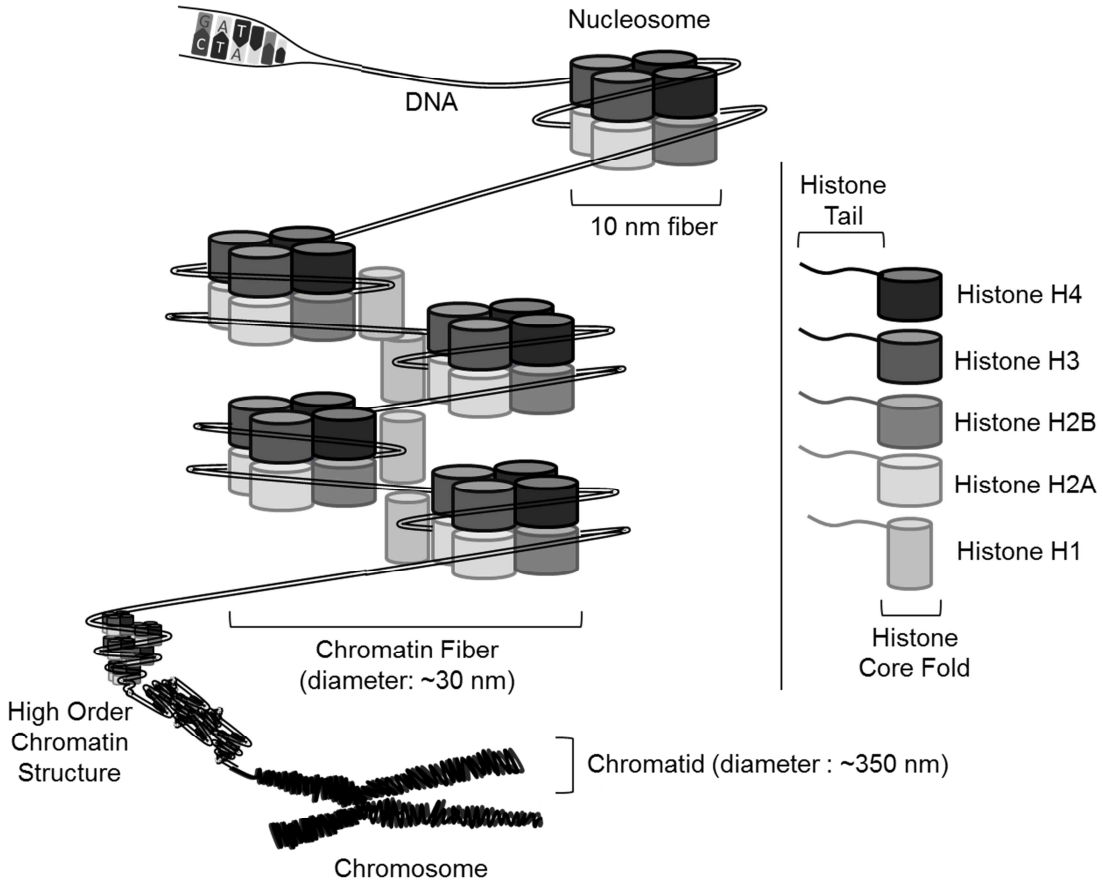


**Figure 2. Chromatin Structure.** Schematic representation of chromatin and its different organization levels. Genomic DNA is wrapped around a nucleosome comprising the histone octamer with a diameter of approximately 10 nm. Further chromatin condensation is achieved by addition of the linker histone H1, which stabilizes the more condensed chromatin fiber with a diameter of approximately 30 nm. High order chromatin structures built up the condensed (mitotic) chromosome, which consists of the two sister chromatids.

### 1.4.1 The Histone Code

For about half a decade it has been known that residues within the amino-terminal tail of histones can be subjected to posttranslational modifications (PTMs) [69]. Since then, the number of different modifications, which have been found at the histone tail of all core histones H2A, H2B, H3 and H4, has rapidly increased. Today, histone methylation, phosphorylation and acetylation have been studied extensively but the list of known PTMs targeting the histone tail also includes ubiquitination, sumoylation, biotinylation, ADP ribosylation, glycosylation, carbonylation and others [70-79]. Just recently, a mass spectrometry-based study reported on the identification of 67 new PTMs including crotonylation of lysine residues, which have been found at the amino-terminal tail and within the histone fold domain of all 4 core histones [80]. Depending on type and location of PTMs, the combination of these chemical modifications builds up the so called histone code, which directly regulates chromatin structure and gene transcription [81-83]. These highly dynamic

changes of the chromatin template take place during many fundamental cellular processes such as gene transcription or DNA replication. Moreover, chromatin organization and modifications of specialized histone variants like H2AX are essential to ensure genome integrity during DNA damage response (DDR) [84].

According to their association with chromatin structure and gene expression, PTMs can be classified as heterochromatic/repressive or euchromatic/activating histone marks. Some of the extensively studied repressive histone modifications are the trimethylation of histone H3 at lysine 9 (H3K9me3) or lysine 27 (H3K27me3) [85]. Other PTMs like H3K4me3 or H3K36me3 are associated with open chromatin and active gene expression [86]. Besides this simplified view on PTMs and their association with either active or inactive transcription, it has been shown that the precise enrichment pattern of a PTM at a gene of interest should be considered as well, as it might be linked to distinct regulatory consequences. Depending on the exact enrichment profile, H3K27me3, considered to be a repressive histone mark, has also been found at actively transcribed genes [87]. Moreover, several studies on embryonic stem cells and differentiated T-cells report on the existence of so-called bivalent domains within the genome, which are marked simultaneously by activating and repressive marks (e.g. H3K27me3 and H3K4me3) [88, 89]. Since these bivalent domains have been found at developmental genes, their existence has been suggested to play a fundamental role in cell differentiation.

In general, the highly dynamic state of chromatin has to be tightly regulated by antagonizing chromatin modifying enzymes. These enzymes are responsible for the introduction (epigenetic writers) or removal (epigenetic erasers) of modifications in a site-specific manner.

Methylation of lysine residues is mediated by enzymes known as histone methyltransferases (HMTs). Two families of HMTs have been described, which catalyze the addition of methyl groups from S-adenosylmethionine to histone proteins. Both families are characterized by distinct protein domains catalyzing the methylation: The SET-domain containing HMTs and enzymes harboring a DOT1-domain [70]. Histone demethylases (HDMs) like the lysine-k specific demethylase 1A (KDM1A or LSD1) have been identified as epigenetic erasers removing methyl groups from histones [90]. While lysine residues are subjected to mono-, di- and trimethylation, methylation of the second basic amino acid arginine (R) includes only mono- and dimethylation, but with the differentiation of symmetric dimethylarginines (SDMA) and asymmetric dimethylarginines (ADMA). Arginine methylation is performed by a separate family of enzymes called protein arginine methyltransferases (PRMTs). This family includes 11 members, which catalyze either the reaction producing symmetrically or asymmetrically methylated arginines [71, 91]. Antagonizing enzymes, mediating the removal of methyl groups from arginines, are for instance the jumonji-domain containing protein 6 (JMJD6) [92]. For the sake of completeness it should be noted that the third basic amino acid histidine is

known to become monomethylated but this PTM has not been characterized in more detail to date [93].

Lysine residues of histone proteins are not only subjected to posttranslational methylation but also acetylation, which is accomplished by epigenetic writers called histone acetyltransferases (HATs). These enzymes uniquely use acetyl coenzyme-a as the donor to transfer acetyl groups to the lysine residues of histones. The opposing activity is governed by histone deacetylases (HDACs), which are important for the regulation of dynamic levels of lysine acetylation.

In addition to these modifications of the basic amino acids within the histone tail, there are also modifications of other amino acids, such as phosphorylation of the polar amino acids serine and threonine. Histone phosphorylation takes place at all known histones including all 4 core histones and the linker histone H1 and is mediated by a large variety of different kinases [94]. As other PTMs, histone phosphorylation directly affects the dynamics of other key PTMs. One of the most intensively studied histone phosphorylation events is that of serine 10 at the tail of histone H3 (H3S10p), which affects other modifications including methylation of H3K9 in close vicinity [95]. Serine/threonine-specific phosphatases are described as the epigenetic erasers of this PTM.

In order to be catalytically active *in vivo*, all aforementioned epigenetic writers and erasers are dependent on incorporation into large multiprotein complexes. Other subunits of these complexes ensure proper nucleosomal association or modulation of the catalytic activity. One of these multiprotein complexes is the Polycomb repressive complex 2 (PRC2), which contains the H3K27 specific histone methyltransferase enhancer of zeste 2 (EZH2) [96]. Besides its catalytically active subunit EZH2, PRC2 comprises additional core subunits, including suppressor of zetse 12 (SUZ12), retinoblastoma-binding protein p48 (RBAP48) and embryonic ectoderm development (EED). While SUZ12 and RBAP48 are involved in targeting the complex to nucleosomes, EED is able to enhance the catalytic activity of EZH2 [97]. Loss of one of these subunits such as SUZ12 leads to genome-wide alterations in H3K27me3 levels [98]. The presence of activating PTMs such as H3K4me3 is known to inhibit PRC2 function [97]. Interestingly, recent work shows that the PRC2 subunits EED and SUZ12 are also able to bind to trimethylated lysine 27 at histone H3, leading to a model for propagation of the repressive histone mark H3K27me3 in proliferating cells [99, 100]. The role of the EZH2 homolog EZH1 in the establishment and maintenance of the H3K27me3 mark (particularly in stem cells) is currently being intensively studied [101, 102]. A summary of PTM of the amino-terminal tail of histone H3.3 is given in Figure 3.

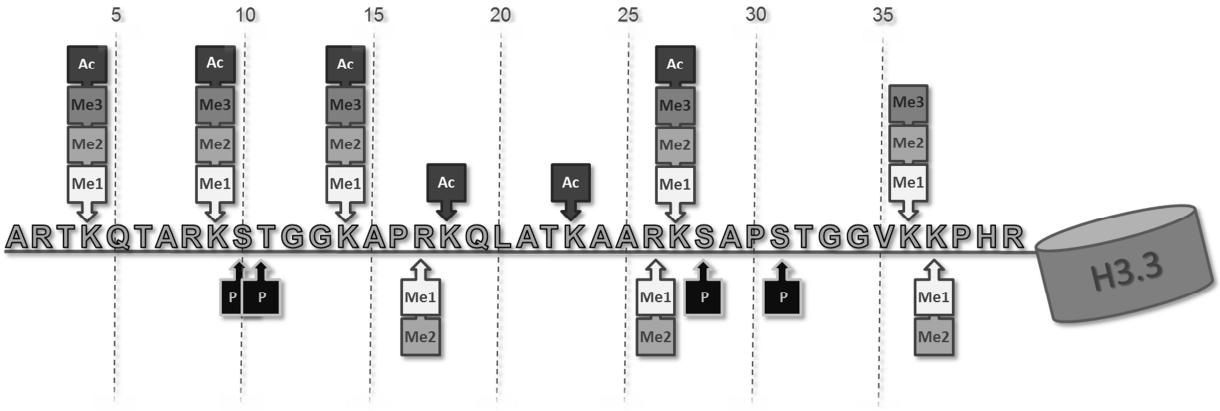


**Figure 3. Posttranslational Modifications of the amino-terminal Histone H3.3 Tail.** Occurrence and localization of several PTMs at the tail of histone H3.3 (amino acid position 1-40). This overview includes mono- and dimethylation of lysine (K) and arginine (R) residues, trimethylation of lysines, acetylation of lysines and phosphorylation of serine (S) and tyrosine (T) residues.

Although some PTMs *per se* such as acetylation of lysines are known to directly change the highly positive charge of histone tails and thereby its physicochemical properties, translation of the highly dynamic epigenetic code into cellular processes like gene transcription or DNA repair is mainly mediated by protein complexes called epigenetic readers [103]. These protein complexes harbor highly-conserved protein domains recognizing and binding to the temporal and spatial pattern of PTMs. Methylated lysine residues for example are recognized by numerous proteins harboring either a plant homeodomain (PHD), PWWP domain (named after the core amino acid sequence prolin-tryptophan-tryptophan-prolin), tudor domain or chromodomain (chromatin organization modifier) [104-106]. In contrast, the existence of a bromodomain (BRD) allows the binding to acetylated lysine residues [107]. The existence of proteins containing more than one of these reader domains further increases the level of complexity. Not surprisingly, epigenetic readers were shown to be recurrently mutated in a large variety of different tumor entities [108].

In addition, the deposition of histone variants adds another layer of complexity to the histone code. Structural differences of histone variants are capable to change the biophysical properties of the core octamer. With the exception of histone H4, there are histone variants for all core histone proteins [109]. The amino-terminal tail of histone H3 (amino acid 1 to 40) is the most heavily modified tail of all four core histones with 21 potential modification sites [110].

### 1.4.2 The Human Histone H3 Repertoire

Histones are among the most highly conserved proteins throughout evolution. Phylogenetic trees for all four core histones show that histone H3 has diverged much slower than other histone proteins like H2A, H2B or the linker histone H1 [111]. The human non-centromeric H3 histone repertoire comprises three different groups of H3 proteins, which are classified according to their expression pattern. The expression of the first group of H3 proteins is directly linked to DNA replication during S-phase of the cell cycle, when large amounts of newly synthesized histones are needed to wrap up the duplicated DNA. Thus, this group is termed the replication-dependent or canonical group of H3 proteins. The expression of the second group of H3 proteins, named replication-independent or non-canonical H3 proteins, is generally not upregulated during DNA replication, although incorporation can also take place at this time point [112]. These replication-independent H3 proteins, as well as the third group of H3 histones, which are termed after their tissue specific expression patterns, are used to replace the canonical H3 in non-dividing cells to actively modulate chromatin structure and gene expression.

Within the human genome, canonical histone H3 genes are found in two separate gene clusters on chromosome 6p22.1 (HIST1) and 1q21.2 (HIST2). While the gene cluster HIST1 on chromosome 6 is composed of 10 genes (*HIST1H3A*-*HIST1H3J*), producing canonical H3 termed H3.1, HIST2 on chromosome 1 produces canonical H3.2 from 3 gene copies (*HIST2H3A*, *HIST2H3C*, *HIST2H3D*). H3.2 differs in only one amino acid (serine at position 96 instead of a cysteine) from the H3.1 protein. Like all canonical histone genes, HIST1 and HIST2 produce intronless mRNAs without poly-A tails, which are processed by a unique pathway including the recognition of a stem-loop structure within the 3’ UTR of canonical H3 mRNAs, which allows massive production of these proteins at the beginning of S-phase [113]. Deposition of replication-dependent H3 is mediated by the chromatin assembly factor 1 subunit A (CAF1), which is directly tethered to the DNA replication fork by the DNA polymerase clamp PCNA (proliferating cell nuclear antigen) [114, 115].

The second source of human H3 proteins, also known as the non-canonical H3 or H3.3, is encoded by two single copy genes *H3F3A* on 1q42.12 and *H3F3B* on 17q25.1. Both genes are transcribed into substantially different mRNAs, but translation produces an exactly identical H3.3 protein. While canonical H3 is encoded by multicopy, intronless genes, producing mRNA without a polyadenyl tail, *H3F3A* as well as *H3F3B* are transcribed into a polyadenylated mRNA from single copy genes containing several exons. The H3.3 protein differs in only 4 to 5 amino acids from canonical H3.2 and 3.1, respectively. Comparing solely the amino-terminal tail, there is only one single amino acid at position 31, which discriminates between replication-dependent H3 (alanine) and the replacement histone H3.3 (serine). This serine at position 31 of H3.3 represents an extra phosphorylation site besides the known

serine residues at position 10 and 28, which is not present in all other non-centromeric H3 variants. Phosphorylated serine 31 of H3.3 has been found in metaphase cell nuclei at specific regions of the chromosomes bordering the centromeres [116]. In addition, the H3.3 specific PTM H3.3S31p was detectable during mitosis and female meiosis in the urochordate *Oikopleura dioica*, indicating the evolutionary conservation of this epigenetic mark [117].

Phylogenetic analysis of all H3 variants suggests that a histone protein, similar to the mammalian histone H3.3, is the ancestor of all H3 variants in animals [118]. The uniquely present single H3 protein in some algae such as *Nuclearia simpex* differs from mammalian H3.3 in only one amino acid (serine 87 instead of alanine in mammals). A protein absolutely identical to human H3.3 is the unique H3 protein in unicellular eukaryotes like yeast [118]. Here, the histone protein has to undergo replication-independent as well as replication-coupled assembly to chromatin. Although sharing more than 95% amino acid similarity, the subtle differences between H3.3 and canonical H3.1/H3.2 are sufficient to ensure that factors like the H3.3-specific chaperone DAXX discriminate between H3 and H3.3, thereby leading to fundamental differences in H3 and H3.3 localization. Recently, it has been shown that two amino acids within the histone fold domain at position 87 (alanine) and 90 (glycine) are responsible for the H3.3-specificity of its chaperone DAXX [119].

While canonical H3 is incorporated in a genome-wide manner during formation of new nucleosomes in S-phase via its chaperone CAF1, H3.3 incorporation is mediated by two distinct deposition pathways, depending on the H3.3 incorporation site [120, 121]. Deposition of H3.3 protein to gene bodies of actively transcribed genes is mediated by a mechanism including the histone chaperone HIRA (HIR histone cell cycle regulation defective homolog A) [120, 122, 123]. Furthermore, the chromodomain helicase DNA-binding protein 1 (CHD1) contributes to the HIRA mediated deposition of H3.3 in fruit flies [124]. Reflecting its euchromatic deposition, the amino-terminal tail of H3.3 contains more activating/euchromatic PTMs (e.g. acetylation of lysine 4) than canonical H3.1 and H3.2 [125].

Independently, the second H3.3 incorporation pathway uses the chaperones ATRX and DAXX to load H3.3 into pericentric and telomeric heterochromatin [121, 126]. The genes coding for these two proteins are frequently mutated in pedGBMs harboring *H3F3A* mutations, emphasizing the importance of the H3.3 chromatin remodeling pathway in pedGBM development. Further evidence for a specific H3.3 function is provided by H3.3 knockout experiments, demonstrating that H3.3 deletions are not always lethal but do result in infertility in the fruit fly *Drosophila melanogaster* and the ciliate *Tetrahymena thermophile* [127-129]. This clearly indicates the importance of H3.3 in germline-specific chromatin remodeling.

In addition to canonical H3 and non-canonical H3.3, several H3 protein variants, which show tissue specific expression patterns, have been recently identified in humans. A gene on 1q42 outside the known histone gene cluster codes for the H3 histone variant H3.4, which is also termed H3.T due to its testis-specific expression in human primary spermatocytes [130]. H3.4 differs in only 4 to 5 amino acids from H3.1/H3.2 and presumably uses a unique chromatin incorporation pathway [131]. A second testis-specific H3 variant is H3.5, which is encoded by *H3F3C*, a retrotransposed copy of *H3F3B* on chromosome 12p11.21 [132]. Compared to its ancestor H3.3, the H3.5 protein shows 5 amino acid differences including deletion of one of the two lysines at position 36 or 37. Furthermore, two additional H3 variants at chromosome 5, termed H3.X and H3.Y have been identified in recent times, which are expressed in malignant and normal tissues including parts the human brain like the hippocampus, cerebellum or cerebral cortex [133]. H3.X/H3.Y protein fundamentally differs from H3.3 in at least 25 amino acids. The amino acid alignment of all non-centromeric histone H3 variants is given in Figure 4**,** illustrating their high sequence homology.

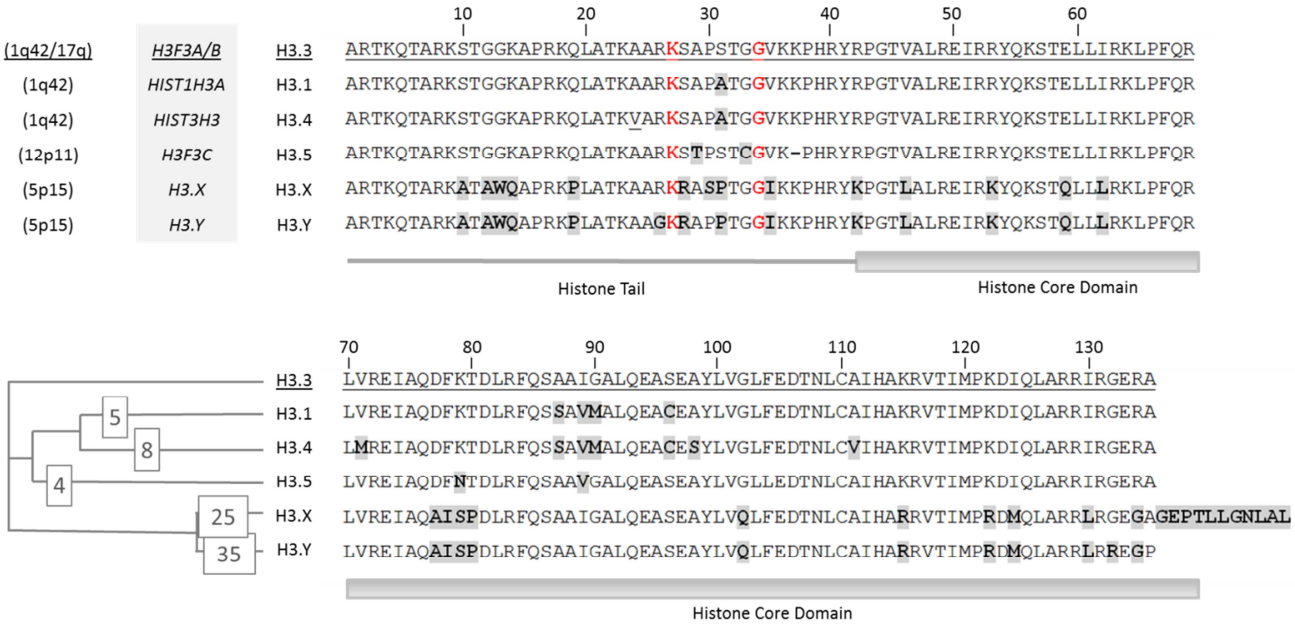


**Figure 4. Protein Sequence Alignment of Human Non-Centromeric Histone H3 Variants.** Chromosomal localization and gene symbols of human H3 variant coding genes are given for histone proteins H3.3 (ENSP00000355780), H3.1 (ENSP00000350275), H3.4 (ENSP00000355657), H3.5 (ENSP00000339835) and H3.X/H3.Y [133]. Canonical H3.2 is not listed but differs from canonical histone H3.1 by only one amino acid (position 96: serine (S) instead of cysteine (C)). Amino acid residues differing from histone H3.3 are highlighted in grey. Protein similarity is also illustrated by the distance tree including the number of diverging amino acids from H3.3. Amino acids K27 and G34 that are mutated in pedGBM are highlighted in red.

To complete the human H3 repertoire, there is the centromeric H3 variant CENP-A (centromere protein A), which in many aspects differs from all non-centromeric H3 variants listed above [134]. CENP-A incorporation is unique to nucleosomes at the centromeres, which are required for proper chromosome segregation during cell division [135]. Sharing only about 50% amino acid identity with any other H3 histone, CENP-A harbors several structural differences, which define its exclusive deposition at centromeric nucleosomes.

### 1.4.3 Histone Modifications in Cancer

Genome integrity is of pivotal importance for survival of every single organism. Throughout lifetime, every cell is encountered by endogenous events or exogenous environmental agents, which interfere with genome stability. Efficient DNA repair as well as proper chromosome replication are key processes to ensure intactness of the genome. Chromatin structure, which is tightly regulated by a diverse set of mechanisms including covalent histone modifications and incorporation of histone variants, has been shown to essentially contribute to genome stability.

Over the last decades it became obvious that cancer is a disease of the genome. If genomic stability is not ensured, alterations in the genome is one of the major driving forces of tumor development. Based on this knowledge, international efforts like the one conducted by the International Cancer Genome Consortium (ICGC) were initiated to find recurrent genetic alterations in different cancer types by using next generation sequencing technologies [12]. In doing so, mutations within the *H3F3A* gene, coding for the replication independent histone variant H3.3, were identified in pedGBMs, which formed the basis for the project presented in this thesis [30]. Never before, recurrent mutations within one of the highly conserved histone genes have been identified in cancer. However, the list of deregulated histone modifications in cancer is long and constantly growing.

Several studies reported on global changes in histone methylation in various cancers types [70, 136]. In most of these entities, downregulated arginine and lysine methylation is associated with a higher risk of tumor recurrence and unfavorable outcome. One possible explanation for deregulated histone modifications in different neoplasms is the growing number of mutations within chromatin modifying genes including epigenetic writers, readers, and erasers. Epigenetic writers like the methyltransferases EZH2 or MLL1 are reported to be frequently altered in different tumor entities [137-139]. Looking at brain tumors, the epigenetic writers MLL2 and MLL3 are mutated in about 16% of medulloblastomas [11]. Furthermore, the translation of the epigenetic code in cancerous cells is frequently interfered by mutations of catalytically active and non-catalytic epigenetic readers [108]. Genetic alterations of epigenetic regulators with reader domains have been found within the

*SMARCB1* or *SMARCA4* gene in atypical teratoid/rhabdoid tumors (AT/RTs) and *SMARCA4 in* medulloblastoma [11, 140, 141]. Lastly, impaired removal of histone modifications due to mutations of epigenetic erasers has also been identified in numerous human cancers including *UTX/KDM6A* (lysine (K)-specific demethylase 6A) mutations in approximately 12% of group 4 medulloblastomas [11].

Besides point mutations in chromatin remodeling genes, complex genomic rearrangements have also been reported to contribute to deregulated histone modifications in cancer. In acute myeloid leukemia (AML), a recurrent translocation of chromosomes fuses the gene of the histone methyltransferase NSD1 to the *NUP98* gene, leading to *HOXA* gene activation due to aberrant H3K36 trimethylation [142]. With regard to the different genetic events leading to deregulation of histone modifiers, it is obvious that specific chromosomal translocations are much more common in hematopoietic malignancies compared to solid tumors. However, deregulation of histone modifiers in solid tumors seem to be much more often caused by point mutations, deletions or amplifications [143].

On top of alterations directly targeting the establishing, interpreting or erasing machineries of the histone code, mutations in other genes like *IDH1* or *IDH2* are described to interfere with histone modifications in cancer. Alterations of the *IDH1* gene have been detected in about 12% of glioblastoma, leading to high intracellular levels of the onco-metabolite 2-hydroxyglutatrate, a potent inhibitor of histone demethylases [50, 144].

On the basis of these genetic events, it becomes apparent that genetic hits and the resulting epigenetic alterations actively contribute to cancer initiation and progression. This especially applies to tumors developing in the human brain, as a multitude of histone modifiers play a central role in nervous system development. This is underscored by various cognitive disorders that are caused by alterations in chromatin remodeling genes (reviewed in [145]). Diverse genetic events resulting in haploinsufficiency of the methyltransferase NSD1 are reported to result in Sotos syndrome, a genetic disorder associated with intellectual impairment [146]. While NSD1 is inactivated due to promoter hypermethylation in neuroblastomas and gliomas, this mechanism of NSD1 inactivation has never been described in entities outside of the nervous system like leukemias, lymphomas, breast or colon cancer [147]. Other examples of genetic alterations found to result in intellectual disability syndromes affect the methyl-CpG binding protein MECP2 in Rett syndrome, the histone demethylase JARID1C in X-linked mental retardation syndrome or the histone chaperone ATRX in alpha thalassemia/mental retardation syndrome [148-150].

In conclusion, histone modifications play a fundamental role in human brain development. As a consequence, genetic alterations causing deregulated histone modification in the brain result in abnormal developmental defects or in tumorigenesis. The identification of histone

H3.3 mutations in pedGBMs represents a completely new field of research. It identifies mutations of histone proteins themselves as the cause of changes in the epigenetic code.

## 2 AIMS AND PROCEDURES

Recent studies have shown that almost 50% of glioblastoma diagnosed in children harbor mutations in the H3.3/ATRX/DAXX chromatin remodeling pathway [30]. Noteworthy, recurrent mutations within the gene encoding the histone variant H3.3 (*H3F3A*) always led to amino acid substitutions at lysine 27 (K27M) or glycine 34 (G34R or G34V in rare cases) in the tail of H3.3. Furthermore, it has been shown that H3.3 mutated glioblastomas are characterized by mutation specific gene expression and DNA methylation profiles [48]. Following-up on these exciting findings, the thesis presented here aimed at the functional characterization of both H3.3 mutations (K27M or G34R) originally found in pediatric high grade gliomas.

In order to do so, several cell lines including the pediatric glioblastoma cell line SF188 were genetically modified to stably overexpress mutant H3.3. These cell lines provided the basis for a main aspect of this project, focusing on the genetic and epigenetic differences between wildtype and mutant H3.3 overexpressing cells. While incorporation of mutant H3.3 protein into chromatin was analyzed by immunofluorescence and chromatin immunoprecipitation followed by next generation sequencing, alterations in posttranslational modifications of mutant H3.3 were investigated by immunohistochemistry, Western blot analysis and mass spectrometry. In addition, mutant H3.3 overexpressing cells were studied by genome-wide gene expression and DNA methylation profiling as well as functional readouts, assessing differences in cell proliferation and cell cycle progression.

The second part of the work presented here was pointing at the tumorigenic potential of H3.3 mutations. To determine whether mutant H3.3 is able to induce glioblastoma *in vivo*, retroviral gene transfer using the RCAS/Ntv-a system was used to overexpress H3.3 mutants in nestin-positive neural precursor cells in neonatal mice. Furthermore, this part of the project was conducted to establish new mutant H3.3 driven cell culture systems which would provide an excellent basis for subsequent preclinical studies.

Complementing these functional analyses, this work was also thought to include molecular data generated on primary glioblastoma samples, which directly reflect the genetic and epigenetic situation in the patients suffering from these highly aggressive brain tumors.

Taken together, this thesis aimed at the elucidation of the role and molecular mechanisms underlying glioblastoma initiation and progression, which in nearly half of the tumors seems to be tightly linked to H3.3 mutations.

# 3 MATERIALS & METHODS

## 3.1 Materials

### 3.1.1 Antibodies

| Antibody | Source | Dilution | Company |
|---|---|---|---|
| AU1-Tag | Rabbit | 1:1000 | Abcam, Cambridge, UK |
| GFP-Tag | Mouse | 1:1000 | Roche Diagnostics, Mannheim, Germany |
| H3.3 | Rabbit | 1:1000 | Millipore, Billerica, USA |
| H3.3S31p | Rabbit | 1:1000 | Abcam, Cambridge, UK |
| H3K27ac | Mouse | 1:1500 | Diagenode, Liège, Belgium |
| H3K27me1 | Mouse | 1:2000 | Abcam, Cambridge, UK |
| H3K27me3 | Rabbit | 1:3000 | Abcam, Cambridge, UK |
| H3K27me3 | Mouse | 1:5000 | Abcam, Cambridge, UK |
| H3K36me3 | Rabbit | 1:2000 | Abcam, Cambridge, UK |
| H3K4me3 | Rabbit | 1:1000 | Diagenode, Liège, Belgium |
| H3K9me3 | Rabbit | 1:1000 | Diagenode, Liège, Belgium |
| H4 | Rabbit | 1:5000 | Abcam, Cambridge, UK |
| HA-Tag (ChIP grade) | Rabbit | 1:5000 | Abcam, Cambridge, UK |
| Mouse (HRP) | Goat | 1:5000 | Santa Cruz Biotechnology, Santa Cruz, USA |
| Rabbit (HRP) | Goat | 1:2500 | Cell Signaling, Danvers, USA |

### 3.1.2 Primers & shRNAs

| Primer | Sequence (5'-3') |
|---|---|
| dnTP53-AU1-ClaI-rev | AATCGATTCAAATATAACGATAAGTATC |
| dnTP53-AU1-rev | ATCAAATATAACGATAAGTATCGTCTGAGTCAGGCCCCAC |
| dnTP53-NotI-for | TAGCGGCCGCGCCATGGAGGAGTCACAG |
| H3.3-for | GGATCCTCTCTGTACCATGGCTCGTAC |
| H3.3-G34R-SDM-Dm-for | CGGCGCCATCCACCGGCAGGGTGAAGAAGCC |
| H3.3-G34R-SDM-Dm-rev | GGCTTCTTCACCCTGCCGGTGGATGGCGCCG |
| H3.3-G34R-SDM-Hs-for | GTGCGCCCTCTACTGGAAGGGTGAAGAAACC |
| H3.3-G34R-SDM-Hs-rev | GGTTTCTTCACCCTTCCAGTAGAGGGCGCAC |
| H3.3-HA-ClaI-rev | GGAATCGATTCAAGCGTAGTCTGGGACGTC |
| H3.3-HA-rev | GCGGCCGCTCAAGCGTAGTCTGGGACGTCGTATGGGTATCCAGCACGTTCTCCACGTATGC |

| | |
|---|---|
| H3.3-K27M-SDM-Dm-for | AGGCGGCCCGTATGTCGGCGCCATC |
| H3.3-K27M-SDM-Dm-rev | GATGGCGCCGACATACGGGCCGCCT |
| H3.3-K27M-SDM-Hs-for | AAGCCGCTCGCATGAGTGCGCCCTC |
| H3.3-K27M-SDM-Hs-rev | GAGGGCGCACTCATGCGAGCGGCTT |
| H3.3-MutAnalysis for | GTGATCGTGGCAGGAAAAGT |
| H3.3-MutAnalysis rev | CAAGAGAGACTTTGTCCCATTTT |
| H3.3-NotI-for | GAAGCGGCCGCTCTGTACCATGGCTCGTAC |
| H3.3-TS-for | TGGCTCGTACAAAGCAGACT |
| H3.3-TS-rev | GAAGGGAAGTTTGCGAATCA |
| H3F3A for | CAAACTTCCCTTCCAGCGTC |
| H3F3A/B for | CAGAGCGCAGCCATCGGTGC |
| H3F3A/B rev | TGGATGGCACACAGGTTGGT |
| H3F3B for | GAAGCTGCCCTTCCAGAGGT |
| H3F3B rev | CTCACTTGCCTCCTGCAAA |
| H3F3B rev | TTCGCTAGCCTCCTGCAGC |
| SDHA for | GACCATCTACGGAGCAGAGG |
| SDHA rev | TAGGACAGGGTGTGCTTCCT |
| shH3F3A_1 | CCGGGCGGAGACGTAAAGCATTAATCTCGAGATTAATGCTTTACGTCTCCGCTTTTTTG |
| shH3F3A_2 | CCGGCCACTATGATGGGAAACATTTCTCGAGAAATGTTTCCCATCATAGTGGTTTTTTG |
| shH3F3A_3 | CCGGGATGGCAACTAAATGGTGTTTCTCGAGAAACACCATTTAGTTGCCATCTTTTTTG |
| shH3F3B_1 | CCGGGCGCATTTATACCTTGCATAACTCGAGTTATGCAAGGTATAAATGCGCTTTTTG |
| shH3F3B_2 | CCGGGACTTGTTGGGTAGCTATTAACTCGAGTTAATAGCTACCCAACAAGTCTTTTTG |

### 3.1.3 Instruments

| **Instrument** | **Company** |
|---|---|
| ABI PRISM 3100 Genetic Analyzer | Life Technologies, Darmstadt, Germany |
| ABI PRISM 7700 PCR System | Life Technologies, Darmstadt, Germany |
| Agilent 2100 Bioanalyzer | Agilent, Santa Clara, USA |
| Bioruptor Sonication Device | Diagenode, Denville, USA |
| Eppendorf PCR Cycler (Mastercycler Gradient) | Eppendorf, Hamburg, Germany |
| L8-M Ultracentrifuge | Beckmann Coulter, Krefeld, Germany |
| Leica DM IRB/E inverted microscope | Leica, Wetzlar, Germany |
| Micro-Dismembrator | Braun Biotech, Melsungen, Germany |

| | |
|---|---|
| Mini Protean Gel Transfer System | BioRad, Munich, Germany |
| Mithras LB 940 Microplate Reader | Berthold Technologies, Bad Wildbad, Germany |
| NanoDrop ND-1000 spectrophotometer | NanoDrop, Wilmington, USA |
| Qubit 2.0 Fluorometer | Life Technologies, Darmstadt, Germany |
| TCS SP5 confocal laser scanning microscope | Leica, Wetzlar, Germany |
| ViCell XR cell counter | Beckmann Coulter, Krefeld, Germany |

### 3.1.4 Biochemicals and Reagents

| **Reagent** | **Supplier** |
|---|---|
| Absolute SYBR Green ROX Mix | ABgene, Epsom, UK |
| Acetone | Sigma-Aldrich, Munich, Germany |
| Ampicillin | Roche Diagnostics, Mannheim, Germany |
| Bovine serum albumin | Sigma-Aldrich, Munich, Germany |
| Cell culture dish (10 cm, 14.5 cm) | TPP Techno Plastic Products, Trasadingen, Switzerland |
| Cell culture plates (6 well, 12 well) | Nunc, Wiesbaden, Germany |
| Chicken egg albumin | Sigma-Aldrich, Munich, Germany |
| Coverslips (circular) | Ted Pella, Redding, USA |
| Dithiothreitol (DTT) | Sigma Aldrich, Munich, Germany |
| DMEM media (for DF1 cells) | ATCC, Wesel, Germany |
| DMEM medium (4.5 g/L glucose) | Life Technologies, Darmstadt, Germany |
| dNTP Mix (100 µM each) | Fermentas, St.Leon-Rot, Germany |
| ECL (plus) WB Detection Reagents | GE Healthcare, München, Germany |
| Ethanol (100%) | Merck, Darmstadt, Germany |
| Fetal calf serum (FCS) | Biochrom AG, Berlin, Germany |
| Fetal calf serum (FCS) (for DF1 cells) | ATCC, Wesel, Germany |
| Formaldehyde | Merck, Darmstadt, Germany |
| Formamide | Merck, Darmstadt, Germany |
| FuGENE HD transfection reagent | Roche Diagnostics, Mannheim, Germany |
| Gelatin from cold water fish skin (45%) | Sigma-Aldrich, Munich, Germany |
| $H_2O$ | Braun Biotech, Melsungen, Germany |
| Horseradish peroxidase (HRP) conjugated streptavidin | Dako, Carpinteria, USA |
| Hydrogen peroxide | Dako, Carpinteria, USA |
| L-glutamin | Life Technologies, Darmstadt, Germany |

| | |
|---|---|
| Methanol | Merck, Darmstadt, Germany |
| Milk powder | Roth, Karlsruhe, Germany |
| Needle (0.9 mm) | Braun Biotech, Melsungen, Germany |
| NuPAGE Antioxidant | Life Technologies, Darmstadt, Germany |
| NuPAGE Bis-Tris Precast Gels (12 or 10 well; 1 mm) | Life Technologies, Darmstadt, Germany |
| NuPAGE SDS Running Buffer (20x) | Life Technologies, Darmstadt, Germany |
| NuPAGE SDS Sample Buffer (4x) | Life Technologies, Darmstadt, Germany |
| Oligo(dT) primer | Thermo Fisher Scientific, Waltham USA |
| OptiMEM medium | Life Technologies, Darmstadt, Germany |
| Penicillin/Streptomycin (1000 U/ml) | Life Technologies, Darmstadt, Germany |
| Perchloric acid | Sigma-Aldrich, Munich, Germany |
| Phosphate buffered saline (PBS) | Life Technologies, Darmstadt, Germany |
| pLVX-Puro plasmid | Clontech, Mountain View, USA |
| pMD2.G plasmid | Addgene, Cambridge, USA |
| Polybrene | Millipore, Billerica, USA |
| Polyvinylidene fluoride (PVDF) membrane | Sigma-Aldrich, Munich, Germany |
| Porpidium iodide | Sigma-Aldrich, Munich, Germany |
| Protein A/G sepharose beads | GE Healthcare, München, Germany |
| ProtoBlue Safe | National Diagnostics, Atlanta, USA |
| psPAX2 plasmid | Addgene, Cambridge, USA |
| Random hexamer primers | Life Technologies, Darmstadt, Germany |
| Reaction tubes (1.5 ml/2 ml) | Eppendorf, Hamburg, Germany |
| Sodium Acetate | Roth, Karlsruhe, Germany |
| Spectra multicolor broad range protein ladder | Fermentas, St.Leon-Rot, Germany |
| Syringe filters (0.45 µm) | Millipore, Billerica, USA |
| TransIT transfection reagent | Mirus Bio, Madison, USA |
| Triton-X 100 | AppliChem, Darmstadt, Germany |
| Trypsin-EDTA (1x) | Sigma-Aldrich, Munich, Germany |
| Universal Human Reference RNA | Agilent, Santa Clara, USA |
| Vectashield HardSet Mounting Medium with DAPI | Vector Laboratories, Burlingame USA |
| X-ray films, Super RX | FUJIFilm, Tokyo, Japan |

### 3.1.5 Cells & Cell Lines

| Cell Type | Company |
|---|---|
| DF1 chicken fibroblasts | ATCC, Wesel, Germany |
| HEK293T Cells | ATCC, Wesel, Germany |
| OneShot TOP10 competent *E. coli* cells | Life Technologies, Darmstadt, Germany |
| SF188 Glioblastoma Cells | UCSF, San Francisco, USA |

### 3.1.6 Kits

| Enzyme | Company |
|---|---|
| ClaI | New England Biolabs (NEB), Ipswich, USA |
| DNase | Life Technologies, Darmstadt, Germany |
| GoTaq DNA polymerase | Promega, Mannheim, Germany |
| NotI | New England Biolabs (NEB), Ipswich, USA |
| SuperScript II reverse transcriptase | Life Technologies, Darmstadt, Germany |
| T4 DNA ligase | Roche Diagnostics, Mannheim, Germany |
| XbaI | Fermentas, St. Leon Rot, Germany |
| XhoI | Fermentas, St. Leon Rot, Germany |

### 3.1.7 Enzymes

| Kit | Company |
|---|---|
| BigDye Terminator v3.1 Cycle Sequencing Kit | Life Technologies, Darmstadt, Germany |
| CellTiter 96 AQueous Non-Radioactive Cell Proliferation Assay | Promega, Mannheim, Germany |
| CloneJet PCR cloning kit | Thermo Fisher Scientific, Waltham USA |
| DNA 1000 Kit | Agilent, Santa Clara, USA |
| High Sensitivity DNA Kit | Agilent, Santa Clara, USA |
| Histone Purification Mini Kit | Active Motif, La Hulpe, Belgium |

| | |
|---|---|
| MinElute PCR Purification Kit | Qiagen, Hilden, Germany |
| pcDNA3.1/V5-His TOPO TA Expression Kit | Life Technologies, Darmstadt, Germany |
| PCR purification kit | Norgen, Thorold, Canada |
| pGEM-T Easy Vector System Cloning Kit | Promega, Mannheim, Germany |
| QIAamp DNA Mini Kit | Qiagen, Hilden, Germany |
| QIAprep Spin Mini/MaxiPrep Kit | Qiagen, Hilden, Germany |
| QIAquick Gel Extraction Kit | Qiagen, Hilden, Germany |
| Qubit dsDNA HS Assay Kit | Life Technologies, Darmstadt, Germany |
| QuikChange II Site-Directed Mutagenesis Kit | Agilent, Santa Clara, USA |
| RNA 6000 Nano Kit | Agilent, Santa Clara, USA |
| RNeasy Mini Kit | Qiagen, Hilden, Germany |

### 3.1.8 Buffers and solutions

| **Buffer** | **Ingredients** |
|---|---|
| ChIP Buffer A | 100 mM Tris-HCl pH 9.4, 10 mM DTT |
| ChIP Buffer B | 10 mM HEPES pH 6.5, 10 mM EDTA, 0.5 mM EGTA, 0.25% Triton X-100 |
| ChIP Buffer C | 100 mM HEPES pH 6.5, 10 mM EDTA, 0.5 mM EGTA, 200 mM NaCl |
| ChIP Buffer D | 50 mM Tris-HCl pH 8.0, 10 mM EDTA, 1% SDS, protease inhibitors |
| ChIP Dilution Buffer | 20 mM Tris-HCl pH 8.0, 1% Triton X-100, 2 mM EDTA, 150 mM NaCl, protease inhibitors |
| ChIP Elution Buffer | 100 mM $NaHCO_3$, 1% SDS |
| ChIP High salt buffer | 20 mM Tris-HCl pH 8.0, 1% Triton X-100, 2 mM EDTA, 500 mM NaCl |
| ChIP LiCl Buffer | 100 mM Tris-HCl pH 8.0, 400 mM LiCl, 1% NP-40, 1% Na-deoxycholate, 1mM EDTA |

| | |
|---|---|
| Citrate buffer (pH 6.0) | 10 mM sodium-citrate, 0.05% Tween-20 |
| TBST | 150 mM NaCl, 10 mM Tris, 0.1% Tween-20, pH 7.4 |
| TE Buffer (pH 8.0) | 10 mM Tris pH 8.0, 1 mM EDTA |
| Western Blot Transfer Buffer | 25 mM Tris pH 8.8, 200 mM glycine, 20% methanol |

## 3.2 Methods

### 3.2.1 Extraction of genomic DNA (gDNA)

For isolation of high quality gDNA out of tumor tissue, frozen tissue was pulverized before lysis using a Micro-Dismembrator (Braun Biotech). Afterwards, gDNA was extracted as previously described [151]. Genomic DNA out of cell pellets was conducted by using the QIAamp DNA Mini Kit (Qiagen) following the manufacturer's protocol. After extraction, DNA concentration was measured by using a NanoDrop ND-1000 Spectrophotometer (NanoDrop). If necessary, DNA quality was assessed by running a DNA 1000 Kit (Agilent) on an Agilent 2100 Bioanalyzer (Agilent) as described in the manufacturer's protocol.

### 3.2.2 Extraction of RNA

Isolation and purification of RNA from cell pellets (minimum $1x10^5$ cells) was performed by using the RNeasy Mini Kit (Qiagen). For isolation of RNA out of primary tissue, at least 30 mg of frozen tissue was pulverized before lysis by using a Micro-Dismembrator (Braun Biotech). Subsequently, starting material was lysed by adding 350 µl RLT buffer and passing the lysate through a 0.9 mm needle (Braun). Afterwards, cell lysates were applied to RNeasy spin columns (Qiagen) and RNA isolation was carried out according to the manufacturer's protocol. Total RNA was eluted in a final volume of 30 µl $H_2O$ (Braun Biotech). RNA concentration was measured by using a NanoDrop ND-1000 Spectrophotometer (NanoDrop). If necessary, RNA quality was assessed by running a RNA 6000 Nano Chip (Agilent) on an Agilent 2100 Bioanalyzer (Agilent) as described in the manufacturer's protocol.

### 3.2.3 Preparation of Plasmid DNA

Plasmid DNA from transformed OneShot TOP10 competent *E. coli* cells (Life Technologies) was isolated using either the QIAprep Spin MiniPrep or MaxiPrep Kit (Qiagen). Therefore, transformed bacteria were grown in LB-media containing 100 µg/ml ampicillin (Roche) at 37℃ for at least 8 hours with constant shaking. After centrifugation at 4000 rpm at 4℃ for 15 minutes, pelleted bacteria were resuspended in buffer P1 and lysed by adding the respective amount of buffer P2. By adding neutralization buffer P3 and centrifugation at 13300 rpm at 4℃ for 10 minutes, genomic DNA and proteins were removed and circular plasmid DNA was purified using QIAprep spin column with silica-membranes and several washing steps according to the manufacturer's protocol. Finally, purified plasmid DNA was eluted in 50 µl (MiniPrep) or 300 µl (MaxiPrep) $H_2O$ (Braun Biotec). Plasmid DNA concentration was measured by using a NanoDrop ND-1000 Spectrophotometer (NanoDrop).

### 3.2.4 Reverse Transcription (cDNA Synthesis)

Synthesis of cDNA from purified RNA was carried out using SuperScript II reverse transcriptase (Life Technologies). Before reverse transcription, 1 µg total RNA was digested with 1 µl DNase (1 U/µl) (Life Technologies) and 2 µl first strand buffer (5x) in a total volume of 10 µl at 20℃ for 20 minutes. After adding 1 µl EDTA (25 mM), cDNA priming was performed by using Oligo(dT) primers (Thermo Scientific) as well as random hexamer primers (3 µg/µl) (Life Technologies). Primer annealing was carried out by heating the reaction to 42℃ for 10 minutes followed by 65℃ fo r additional 10 minutes. After the addition of 1 µl DTT (0.1 M) (Sigma), 2 µl first strand buffer (5x), 1 µl dNTP Mix (10 µM each) (Fermentas) and 1 µl H20 (Braun), the reaction was incubated at 42°C for 2 minutes. Reverse transcription was initiated by adding 1 µl SuperScript II and incubation at 42℃ for 50 minutes. The enzymatic reaction was stopped by incubation at 70°C for 15 minutes. Finally, 20 µl of cDNA were diluted with $H_2O$ (Braun) to a total volume of 60 µl.

### 3.2.5 Sanger Sequencing

Sequencing of purified PCR products or plasmid DNA was performed by using the BigDye Terminator v3.1 Cycle Sequencing Kit (Life Technologies). In short, 20 ng of PCR product or 500 ng of plasmid DNA was mixed with 1 µl BigDye solution, 2 µl BigDye sequencing buffer (5x) and 1 µl sequencing primer (10 µM) in a total volume of 10 µl on ice. Sequencing PCR was done for 25 cycles (step 2-4) using an Eppendorf PCR Cycler (Eppendorf) as follows: Initial denaturation at 96℃ for 3 minutes (1), den aturation at 96℃ for 30 seconds (2), primer annealing at 51℃ for 15 seconds (3), extension at 60℃ for 4 minutes (4) and constant cooling at 4℃ (5). Afterwards PCR products were pu rified by precipitation by adding and 25 µl 100% ethanol (Merck) and 1 µl 3 M sodium acetate (Roth). After centrifugation at 13300 rpm at 4℃ for 30 minutes, precipitates were washed with 200 µl 60% ethanol (Merck) and centrifuged again at 13300 rpm at 4℃ for 15 mi nutes. Finally, precipitates were air dried at room temperature, resuspended in 10 µl formamide (Merck) and sequenced using an ABI PRISM 3100 Genetic Analyzer (Life Technologies).

### 3.2.6 Mutation Analysis of the Genomic *H3F3A* Locus

To determine the *H3F3A* mutation status in pedGBM samples, the first exon of *H3F3A* was PCR amplified out of genomic DNA using GoTag DNA polymerase (Promega) and primers H3.3-MutAnalysis for/H3.3 MutAnalysis rev (annealing temperature 56℃; 30 seconds extension time at 72℃). After PCR purification usi ng the PCR purification Kit (Norgen), amplicons were sequenced by using the BigDye Terminator v3.1 Cycle Sequencing Kit (Life Technologies) and an ABI PRISM 3100 Genetic Analyzer (Life Technologies).

### 3.2.7 Mutation Analysis of *H3F3A* Transcripts

Isolated RNA of pedGBM samples was reverse transcribed into cDNA using SuperScript II reverse transcriptase (Life Technologies). A region including the codons for both H3.3 mutations was amplified out of this cDNA by PCR amplification using GoTag DNA polymerase (Promega) and primers H3.3-TS-for/H3.3-TS-rev (annealing temperature 60°C; 30 seconds extension time at 72°C). After purification using the PCR purification Kit (Norgen), PCR products were cloned into the pGEM-T Easy Vector System (Promega) according to manufacturer's instructions. After transformation into OneShot TOP10 competent *E. coli* cells (Life Technologies), single clones were grown on agar plates containing 100 µg/ml ampicillin (Roche). The next day, clones were picked to perform PCR amplification with GoTag DNA polymerase (Promega) and primers H3.3-TS-for/H3.3-TS-rev (annealing temperature 60°C; 30 seconds extension time at 72°C). PCR products were again purified and subjected to Sanger sequencing using primers H3.3-TS-for or H3.3-TS-rev.

### 3.2.8 Polymerase Chain Reaction (PCR)

PCR reaction using GoTaq DNA polymerase (Promega) was performed using 0.25 µl DNA polymerase (5 U/µl), 5 µl GoTag Reaction Buffer (5x), 1 µl dNTP Mix (10 µM each) (Fermentas), 1 µl forward primer (10 µM), 1 µl reverse primer (10 µM) and 20 ng of template (gDNA, cDNA, or plasmid DNA) in a total volume of 25 µl. If not denoted differently, PCR was performed for 40 cycles (steps 2-4) in an Eppendorf PCR Cycler (Eppendorf) with the following Cycler Conditions: Initial denaturation at 95°C for 2 minutes (1), denaturation at 95°C for 30 seconds (2), primer annealing (3) and extension (4) as indicated, followed by final extension at 72°C for 5 minutes (5) and constant cooling at 10°C (6). GoTaq DNA polymerase lacks proofreading activity and produces PCR products with 3'dA overhangs.

### 3.2.9 Quantitative Realtime PCR (qRT-PCR)

For mRNA expression analysis, high quality RNA was isolated and reverse transcribed into cDNA as described earlier. Each cDNA sample was analyzed in triplicates using the ABI PRISM 7700 PCR System (Applied Biosystems) and Absolute SYBR Green ROX Mix (ABgene). Gene expression was normalized to the endogenous housekeeping gene succinate dehydrogenase complex subunit A (*SDHA*) using primers SDHA for/rev. Amplification of genomic DNA was excluded by using intron-spanning primers if possible. Relative gene expression levels were calculated as described by Pfaffl *et al.* [152].

### 3.2.10 Cloning of C-terminally HA-tagged H3.3 Overexpression Constructs

The open reading frame (ORF) of histone H3.3 was amplified out of reverse-transcribed Universal Human Reference RNA (Agilent) using the GoTaq DNA polymerase (Promega) and primers H3.3-for/H3.3-HA-rev (annealing temperature 59°C; 45 seconds extension time at 72°C). After PCR amplification, 20% of the PCR reaction was separated by agarose gel

electrophoresis (1.5%) to check for correct amplicon size. The remaining 80% of the PCR reaction was subjected to PCR clean up using the PCR purification kit (Norgen). Purified PCR product was cloned into the mammalian overexpression vector pcDNA3.1 (Life Technologies) followed by transformation into OneShot TOP10 competent *E. coli* cells (Life Technologies). Single clones were subjected to Sanger sequencing to confirm the integrity of the C-terminally HA-tagged H3.3-WT overexpression construct (pcDNA_H3.3-WT-HA). C-terminally HA-tagged K27M and G34R mutated overexpression constructs were generated by using H3.3-WT-HA, which was subjected to site-directed mutagenesis using primers H3.3-K27M-SDM-Hs-for/ H3.3-K27M-SDM-Hs-rev and H3.3-G34R-SDM-Hs-for/ H3.3-G34R-SDM-Hs-rev and the QuikChange II Site-Directed Mutagenesis Kit (Agilent). Integrity of C-terminally HA-tagged K27M (pcDNA_H3.3-K27M-HA) and G34R (pcDNA_H3.3-G34R-HA) mutated overexpression constructs was verified by Sanger sequencing.

### 3.2.11 EGFP/CFP-tagged H3.3 Overexpression Constructs

The wildtype histone H3.3 overexpression construct (H3.3-WT-pEGPF-N1), which was C-terminally tagged with the enhanced green fluorescent protein (EGFP), was provided by Philippe Collas (Institute of Basic Medical Sciences, Oslo, Norway). C-terminally EGFP-tagged K27M and G34R mutated overexpression constructs were generated by performing site-directed mutagenesis. Therefore, H3.3-WT-pEGPF-N1, was chosen as the template to conduct site-directed mutagenesis using primers H3.3-K27M-SDM-Dm-for/H3.3-K27M-SDM-Dm-rev and H3.3-G34R-SDM-Dm-for/H3.3-G34R-SDM-Dm-rev. Mutagenesis was performed using the QuikChange II Site-Directed Mutagenesis Kit (Agilent). Finally, all constructs were analyzed by Sanger sequencing to confirm sequence integrity.

The overexpression construct of wildtype H3.3 fused to the cyan fluorescent protein (CFP) was a generous donation of Karsten Rippe (Genome Organization & Function, German Cancer Research Center (DKFZ), Heidelberg, Germany). It consists of the H3.3 ORF cloned into the pEYFP-C1 backbone (Clontech), which was modified to express CFP instead of EYFP.

### 3.2.12 Transfection

Transfection of SF188 glioblastoma or HEK293T cells was performed by using TransIT transfection reagent (Mirus Bio). After seeding $1x10^6$ cells in a 14.5 cm cell culture dish (TPP) in high glucose DMEM medium (Life Technologies) supplemented with 10% FCS (v/v) (Biochrom), 1% penicillin/streptomycin (v/v) (Life Technologies) and 1% 200 mM L-glutamin (v/v) (Life Technologies), cells were cultivated for 24 hours at 37℃ and 5% $CO_2$. For transfection, 200 µl OptiMEM medium (Life Technologies) were mixed with 20 µg overexpression plasmid and 60 µl TransIT transfection reagent. For double transfections the amount of each plasmid was reduced to 10 µg. Formation of transfection complexes was

performed at room temperature for 20 minutes, before adding the mixture dropwise to the cells and cultivation for 24 hours at 37℃ and 5% $CO_2$. The next day, cells were washed with PBS (Life Technologies) and supplemented with new DMEM medium (Life Technologies). Expression of EGFP- and CFP-tagged H3.3 proteins was analyzed by fluorescence microscopy 72 hours after transfection.

For imaging of fluorescently-labeled H3.3 proteins, SF188 glioblastoma cells were grown on circular glass coverslips (Ted Pella) in 12 well cell culture plates (Nunc) in DMEM medium (Life Technologies). The day before transfection, $5x10^4$ cells were seeded in a 12 well and incubated for 24 hours at 37℃ and 5% $CO_2$. Transfection was performed as described above using 3 µl TransIT transfection reagent (Mirus Bio) and 1 µg plasmid DNA. After medium exchange 24 hours post transfection, cells were fixed and permeabilized at least another 48 hours later. For fixation, cells were treated with 2% formaldehyde (Merck) in PBS (Life Technologies) at room temperature for 20 minutes. After three washing steps in PBS, cells were incubated with 0.1% Triton-X 100 (AppliChem) at room temperature for 30 minutes. After additional three washing steps in PBS, coverslips were mounted in Vectashield HardSet Mounting Medium with DAPI (Vector) on glass slides followed by confocal imaging using a TCS SP5 confocal laser scanning microscope (Leica).

### 3.2.13 Cloning of C-terminally HA-tagged H3.3 pLVX-Puro Constructs

In order to overexpress H3.3 variants by lentiviral transduction, the ORF of H3.3 was cloned into the pLVX-Puro plasmid (Clontech). Therefore, H3.3-pJet1.2 constructs (pJet1.2_H3.3-WT-HA, pJet1.2_H3.3-K27M-HA, pJet1.2_H3.3-G34R-HA), generated in 3.2.24 were double-digested with XhoI and XbaI restriction enzymes (Fermentas). Digested constructs were separated by agarose gel electrophoresis (1%) and inserts were gel extracted using the QIAquick Gel Extraction Kit (Qiagen) according to manufacturer's instructions. Subsequently, DNA concentration was quantified by using a NanoDrop ND-1000 spectrophotometer (NanoDrop). T4 DNA ligase (1 U/µl) (Roche) was used to ligate the insert into linearized pLVX-Puro plasmid in a vector/insert ratio of 1:3. Ligation was performed overnight at 4℃ before transformation into OneShot TOP10 competent *E. coli* cells (Life Technologies). Single clones, growing on agar plates containing 100 µg/ml ampicillin (Roche), were subjected to Sanger sequencing before using H3.3-pLVX constructs (pLVX_H3.3-WT-HA, pLVX_H3.3-K27M-HA, pLVX_H3.3-G34R-HA) for lentivirus production.

### 3.2.14 Production of Lentiviral Particles

To generate lentiviral particles, HEK293T cells (passage number < 10) were co-transfected with the following three constructs: The transgene containing pLVX-Puro vector (4 µg), the packaging vector psPAX2 (2 µg) (Addgene) and the envelope vector pMD2.G (2 µg) (Addgene). For each transfection, $4x10^6$ cells were seeded in a 10 cm cell culture dish (TPP)

in high glucose DMEM medium (Life Technologies) supplemented with 30% fetal calf serum (FCS) (v/v) (Biochrom), 1% penicillin/streptomycin (v/v) (Life Technologies) and 1% 200 mM L-glutamin (v/v). Cells were cultivated till reaching 70% confluency at 37℃ and 5% $CO_2$. Co-transfection was performed using the respective amount of plasmid (see above) and 30 µl TransIT transfection reagent (Mirus Bio) in a total volume of 600 µl OptiMEM medium (Life Technologies). After formation of transfection complexes for 20 minutes at room temperature, the mixture was added dropwise to the HEK293T cells. Medium exchange 24 hours later was followed by the first virus harvest another 24 hours later (48 hours after transfection) and a second virus harvest 72 hours after transfection. Transfection efficiency was simultaneously monitored by confirming GFP expression in HEK293T cells using fluorescence microscopy (Leica). Virus harvest was executed by removing the virus containing supernatant, filtering using a 0.45 µm syringe filter (Millipore) and ultracentrifugation using a SW41 rotor in a L8-M Ultracentrifuge (Beckmann) for 90 minutes at 4℃ at 25,000 rpm. Subsequently, the supernatant was removed and the virus pellet was dried at room temperature. Viral particles were resuspended in 100 µl OptiMEM medium (Life Technologies) and stored in 10 µl aliquots at -80℃.

Virus titer and the multiplicity of infection (MOI) was determined by transduction of HEK293T cells or respective target cells with different amounts of GFP containing lentiviral particles of the same virus harvest, which were generated simultaneously. At least 48 hours after transduction, the number of GFP positive cells was determined by flow cytometry. Virus titer was calculated as follows:

Titer [transduction units/µl] = (cell number at transduction time point) x (percentage of GFPpositive/100) x (dilution factor) x (1/volume).

### 3.2.15 Lentiviral Transduction

Transduction of SF188 glioblastoma or HEK293T cells was performed in 6 well cell culture plates (Nunc), seeding $1x10^5$ cells the day before transduction. Lentiviral particles containing either one of the three H3.3 variants (H3.3-WT-HA, H3.3-K27M-HA, H3.3-G34R-HA) or a shRNA targeting the untranslated region (UTR) of endogenous *H3F3A* or *H3F3B* gene were added to the cells with an MOI of 5 in the presence of 8 µg/ml polybrene (Millipore). After 24 hours the virus containing supernatant was removed, cells were washed with PBS (Life Technologies) and new DMEM medium (Life Technologies) was added. For overexpression experiments, viral particles containing empty pLVX-Puro vectors were used in parallel as a control. As a control for all H3.3 silencing experiments, viral particles harboring non-target shRNA were used simultaneously. Transduction efficiency was calculated by flow cytometry of GFP overexpressing cells, which were transduced in parallel.

### 3.2.16 Chromatin Immunoprecipitation (ChIP)

Transduced SF188 glioblastoma cells were seeded in 14.5 cm cell culture dishes (2x each) (TPP) and incubated in DMEM medium (Life Technologies) at 37℃ and 5% $CO_2$ until reaching 90% confluence. ChIP experiments were performed on SF188 cells transduced for 4 weeks with H3.3 variants (pLVX_H3.3-WT-HA, pLVX_H3.3-K27M-HA, pLVX_H3.3-G34R-HA, pLVX-EMPTY) with an MOI of 5. Cells were harvested by trypsination (Sigma) and centrifugation at 1000 rpm at 4℃ for 10 minutes. Pellet was resuspended in 1 ml ChIP Buffer A and incubated at 4℃ for 15 minutes followed by 30℃ for 15 minutes. After centrifugation at 1000 rpm at 4℃ for 5 minutes, the pellet was resuspended in 1 ml ChIP Buffer B and incubated at 4℃ for 5 minutes. Subsequently, samples were centrifuged and pellets were incubated in 1 ml ChIP Buffer C at 4℃ for 5 minutes. Centrifugation was repeated before resuspending the pellet in 300 µl ChIP Buffer D and sonification at 4℃ for 60 cycles (power ON for 30 seconds followed by power OFF for 30 seconds) in a 1.5 ml reaction tube (Eppendorf) using a Bioruptor Sonication Device (Diagenode). In doing so, chromatin was adjusted to an average fragment size of 300 bp. Cell debris was removed by centrifugation at 13300 rpm at 4℃ for 5 minutes and chromatin containing supernatant was diluted by adding 2.5 ml ChIP-dilution buffer. An aliquot of 100 µl was removed and stored at -80℃ (Input). Each ChIP experiment was split into 3 parts containing 900 µl chromatin each. Preclearing was performed at 4℃ for 1 hour by using 20 µl of a mixture of protein A and protein G sepharose beads (1:1) (GE Healthcare), which were washed three times in ChIP dilution buffer and blocked with 5% bovine serum albumin (Sigma) in ChIP dilution buffer, gelatin (Sigma) and chicken egg albumin (Sigma) at 4℃ for 2 hours and constant tumbling. After removal of sepharose beads and unspecifically bound DNA by centrifugation at 2000 rpm at 4℃ for 2 minutes, precleared chromatin was added to 20 µl fresh sepharose beads, which were washed and blocked as described above. Immunoprecipitation was performed at 4℃ overnight and constant tumbling by adding 2 µl (2 µg) ChIP-grade anti-HA antibody (Abcam ab9110). The following day, beads, were washed as indicated by addition of the respective buffer (4℃), incubation at room temperature with constant tumbling for 10 minutes and subsequent centrifugation at 2000 rpm at 4℃ for 2 minutes (3x High salt buffer, 3x LiCl Buffer, 1x TE buffer). Finally, bound DNA was eluted by adding 60 µl Elution buffer and constant shaking at 1200 rpm at room temperature for 15 minutes followed by centrifugation (10000 rpm at room temperature for 1 minute). The elution step was repeated once and both elutions were pooled (120 µl). Reverse crosslinking was performed by adding 3.6 µl 5 M sodium acetate (Roth) and incubation at 65℃ overnight. Input samples (100 µl) were thawed and reverse crosslinked at 65℃ overnight by adding 2 µl 5 M sodium acetate. The next day, all three samples of one ChIP experiment were pooled by using a shared MinElute PCR purification Column (Qiagen) and a final $H_2O$ elution volume of 12 µl. Total

amount of precipitated DNA was calculated by using Qubit 2.0 Fluorometer (Life Technologies) and a dsDNA HS assay Kit (Life Technologies). In addition, fragment size was checked by running a High Sensitivity DNA Chip (Agilent) on an Agilent 2100 Bioanalyzer (Agilent).

Library preparation and sequencing of bound DNA fragments was performed according to the manufacturer's instructions at the DKFZ Genomics and Proteomics Core Facility (Heidelberg, Germany) by using an Illumina HiSeq 2000 sequencing system.

For ChIP-Seq data analysis, sequencing reads were aligned to human genome build GRCh37 using a Burrows–Wheeler aligner (BWA). Post-processing of the aligned reads included merging of lane-level data and removal of duplicate read pairs using Picard tools (http://picard.sourceforge.net). Only uniquely aligned reads were considered for downstream analysis, and aligned reads were converted to the SAM/BAM format using SAMtools [153]. Reads within bins of 10 kB were counted using custom Python scripts and resulting data was interpreted using R.

### 3.2.17 Cell Proliferation Assay (MTS Assay)

Cell growth characteristics were assessed by performing MTS (3-(4,5-dimethylthiazol-2-yl)-5-(3-carboxymethoxyphenyl)-2-(4-sulfophenyl)-2H-tetrazolium) assay using the CellTiter 96 AQueous Non-Radioactive Cell Proliferation Assay (Promega). Equal amounts of transduced cells were seeded in triplicates into 96-well plates and incubated in a 5% $CO_2$ humidified incubator at 37℃ for 24 hours. The next day, MTS solution was added followed by incubation at 37℃ for 1-3 hours. Finally, absorbance at 490 nm was measured by using an Mithras LB 940 microplate reader (Berthold Technologies). As described, the absorbance at 490 nm is proportional to the number of living cells in a 96-well [154].

### 3.2.18 Cell Cycle Analysis (Nicoletti Assay)

Quantitative information about cell proportions residing in different cell cycle phases was determined by performing Nicoletti assay, which uses the immunofluorescence detection of the DNA-intercalating substance propidium iodide (PI) to calculate the amount of DNA in the cell nucleus [155]. Transduced cells were seeded in equal amounts in 6-well plates (Nunc) and cultured in a 5% $CO_2$ humidified incubator at 37℃ for 24 hours. Afterwards, cells were incubated in hypotonic Nicoletti buffer containing 50 µg/ml PI (Sigma Aldrich), 0.1% sodium citrate and 0.1% Triton X-100 (Sigma Aldrich) protected from light at 4℃ for 4 hours. Finally, DNA content of cell nuclei was analyzed by flow cytometry.

### 3.2.19 Isolation of Histone Proteins

The Histone Purification Mini Kit (Active Motif) was used to isolate and purify histone proteins from cell culture and tissue samples. For isolation of histones out of primary tissue,

approximately 100 mg of frozen tissue were pulverized by using a Micro-Dismembrator (Braun Biotech). Cell pellets (minimum $5x10^6$ cells) or pulverized tissue was directly resuspended in an appropriate volume of ice cold extraction buffer and lysed on a rotating platform at 4℃ for at least 1 hour. After removal of cell debris by centrifugation at 13300 rpm at 4℃ for 5 minute, the supernatant was neutralized by adding 1:4 volume of neutralization buffer (5x). In parallel, spin columns were equilibrated by the addition of 500 µl equilibration buffer and centrifugation at 800 rpm at 4℃ for 3 minutes to load neutralized sample in 500 µl steps to the column with the same centrifugation conditions. Afterwards, columns were washed three times with 500 µl ice cold washing buffer and centrifugation at 800 rpm at 4℃ for 3 minutes. Finally, columns were transferred to a new 1.5 ml reaction tube (Eppendorf) and elution was performed by adding 100 µl histone elution buffer and centrifugation at 800 rpm at 4℃ for 3 minutes. To further purify the isolated histone proteins, 6 µl 70% perchloric acid (Sigma) were added to precipitate histone proteins over night at 4℃. The following day, samples were centrifuged at 13300 rpm at 4℃ for at least 1 hour and pelleted histones were washed with 1 ml ice cold 4% perchloric acid followed by centrifugation at 13300 rpm at 4℃ for 5 minutes. T wo additional washing steps with ice cold acetone (Sigma) containing 0.2% HCl and pure acetone were carried out before drying the pellet at room temperature. Finally, the histone pellet was resuspended in at least 100 µl $H_2O$ (Braun Biotech) and stored at 4℃.

### 3.2.20 Western Blot Analysis

Electrophoretic separation of protein samples was performed by using 4-12% gradient NuPAGE Bis-Tris Precast Gels (Life Technologies) with a maximum loading capacity of 20 µl (12 well; 1mm). First, protein samples were mixed with 1:3 volume NuPAGE LDS Sample Buffer (4x) (Life Technologies) followed by denaturation at 95℃ for 5 minutes. Together with protein samples, 10 µl Spectra multicolor broad range ladder (Fermentas) was loaded to the gel and protein separation was carried out in 1x NuPAGE Running Buffer (Life Technologies), which was partially mixed with NuPAGE Antioxidant (Life Technologies). Gel electrophoresis was performed at 140 V for 75 minutes. Afterwards, separated proteins were transferred to a polyvinylidene fluoride (PVDF) membrane (Sigma) by a full wet blotting procedure using a Mini Protean Gel Transfer system (Biorad), Western blot transfer buffer and a stepwise increasing current (100 mA for 10 minutes, 200 mA for 10 minutes, 300 mA for 10 minutes 400 mA for 10 minutes 500 mA for 10 minutes). Subsequently, PVDF membranes were blocked in TBS-T containing 3% bovine serum albumin (BSA) (Sigma) and 10% milk (Roth). If required, NuPAGE gels were coomassie stained by using ProtoBlue Safe (National Diagnostics). Primary antibodies were diluted as indicted in 3.1.1 in 10% blocking solution in TBS-T and incubated with the membrane over night at 4℃ with constant rolling. After three washing steps with TBS-T at room temperature for 5 minutes, horseradish

peroxidase (HRP) coupled secondary antibodies were applied at room temperature for at least 1 hour with constant rolling. Chemiluminescent detection using ECL or ECLplus (GE Healthcare) and X-ray films (FUJI) was performed as described in the manufacturer's protocol. Hereby, exposure time was individually adjusted.

### 3.2.21 Gene Expression Profiling

Genome-wide mRNA expression profiling was performed by isolating high quality RNA from SF188 glioblastoma cells. Sample library preparation, hybridization and quality control was carried out at the Microarray Department of the University of Amsterdam (Netherlands) using the Affymetrix GeneChip® Human Genome U133 Plus 2.0 Array according to manufacturer's instructions.

### 3.2.22 DNA Methylation Analysis

More than 450,000 single CpG sites per DNA sample were analyzed for their methylation status using the Infinium HumanMethylation450 BeadChip (Illumina) and high quality DNA isolated from transduced SF188 cells. Bisulfite conversion, array hybridization and data normalization was performed by the Genomics & Proteomics Core Facility of the German Cancer Research Center (DKFZ) (Heidelberg) according to standardized protocols.

### 3.2.23 Immunohistochemistry (IHC)

Protein expression analysis by immunohistochemistry was performed by staining a custom-made tissue microarray (TMA) of pediatric GBM samples. For all tissue cores, regions representing neoplastic tissue were identified by hematoxylin and eosin staining (HE staining). As a control, non-neoplastic reference tissue cores were stained in parallel. Immunohistochemistry was performed based on an indirect streptavidin-biotin method. The TMA containing 10 µm sections was deparaffinized using xylene two times for 5 minutes. Rehydrating was performed by an ethanol series (100%, 96%, 70%: 2 minutes each). Epitopes were uncovered by applying pre-heated citrate buffer (pH 6.0) and heating in a microwave oven (400 W for 10 minutes). Inhibition of endogenous peroxidase activity was accomplished by incubation with 3% hydrogen peroxide (Dako) followed by incubation (4°C overnight in a wet chamber) with primary antibodies diluted 1:1000 in antibody diluent (Dako). The next day, tumor cores were incubated with horseradish peroxidase (HRP) conjugated streptavidin (Dako) at room temperature for 15 minutes. Finally, slides were stained with diaminobenzidine hydrochloride (DAB) supplemented with hydrogen peroxide followed by counterstaining with hematoxylin and mounting.

Immunopositivity was evaluated by Prof. Andrey Korshunov (Clinical Cooperation Unit Neuropathology, German Cancer Research Center (DKFZ), Heidelberg, Germany).

### 3.2.24 Cloning of C-terminally HA-tagged H3.3 RCAS Constructs

Retroviral overexpression of H3.3 variants in the brain of neonatal mice required cloning of H3.3 variants into the RCASBP(A) plasmid. PCR amplification using GoTag DNA polymerase (Promega) was carried out using primers H3.3-NotI-for/H3.3-HA-ClaI-rev (annealing temperature 58°C; 60 seconds extension time at 72°C) and H3.3 overexpression constructs (pcDNA_H3.3-WT-HA, pcDNA_H3.3-K27M-HA, pcDNA_H3.3-G34R-HA) as a template to introduce NotI and ClaI restriction sites. Purified PCR product was cloned into the pJet1.2 plasmid using the CloneJet PCR cloning kit (Thermo Scientific), followed by sequence verification using Sanger sequencing. Afterwards, H3.3-pJet1.2 constructs (pJet1.2_H3.3-WT-HA, pJet1.2_H3.3-K27M-HA, pJet1.2_H3.3-G34R-HA) were double-digested with restrictions enzymes NotI and ClaI (NEB). After gel extraction using the QIAquick Gel Extraction Kit (Qiagen), NotI/ClaI digested inserts were ligated into NotI/ClaI linearized RCASBP(A) using T4 DNA ligase (Roche) followed by Sanger sequencing.

### 3.2.25 Cloning of C-terminally AU1-tagged dnTP53 RCAS Constructs

Dominant-negative p53 (dnTP53) construct (MSCV-dnTP53) was kindly provided by Prof. Rob Wechsler-Reya (Sanford-Burnham Medical Research Institute, La Jolla, USA). DnTP53 ORF was amplified using GoTaq DNA polymerase (Promega) with primers dnTP53-NotI-for/dnTP53-AU1-rev (annealing temperature 60°C; 30 seconds extension time at 72°C) introducing an amino terminal NotI restriction site and a C-terminal AU1 tag. After PCR purification (Norgen PCR purification kit), the PCR product was cloned into the mammalian overexpression vector pcDNA3.1 (Life Technologies) followed by transformation into OneShot TOP10 competent *E. coli* cells (Life Technologies). Single clones were subjected to Sanger sequencing to confirm the integrity of pcDNA_dnTP53-AU1. Afterwards, a C-terminal ClaI restriction site was introduced by PCR amplification using GoTaq DNA polymerase and primers dnTP53-NotI-for/dnTP53-AU1-ClaI-rev (annealing temperature 60°C; 30 seconds extension time at 72°C). Purified PCR product was double-digested with restrictions enzymes NotI and ClaI (NEB) and ligated into NotI/ClaI digested RCASBP(A) using T4 DNA ligase (Roche) followed by Sanger sequencing.

### 3.2.26 Restriction Digestion

Digestion of plasmid DNA with restriction enzymes ClaI and NotI (NEB) was performed at 37°C overnight. In a 1.5 ml reaction tube, 5 µl ClaI (5 U/µl), 5 µl NotI (5 U/µl) and 10 µl NEB buffer 4 (5x) (NEB) were given to 20 µg plasmid DNA in a total volume of 50 µl $H_2O$ (Braun).

Digestion of plasmid DNA with restriction enzymes XhoI and XbaI (Fermentas) was performed at 37°C for 2 hours. In a 1.5 ml reaction tube, 5 µl XhoI (10 U/µl), 5 µl XbaI (10 U/µl) and 5 µl tango buffer (10x) (Fermentas) were given to 20 µg plasmid DNA in a total volume of 50 µl $H_2O$ (Braun).

### 3.2.27 Retroviral Gene Transfer using RCAS/Ntv-a System

Retroviral particles harboring HA-tagged H3.3 variants or dnTP53-AU1 were generated by transfection of DF1 chicken fibroblasts (ATCC) with RCASBP(A) constructs. Low passage DF1 cells (passage number < 5) were seeded the day before transfection in a 10 cm cell culture dish (TPP) and maintained in DMEM media (ATCC) supplemented with 10% FCS (ATCC) in a humidified 39℃ incubator with 5% $CO_2$. Transfection was conducted by using 10 µl FuGENE HD transfection reagent (Roche) and 4 µg plasmid DNA in a total volume of 200 µl OptiMEM medium (Life Technologies). After formation of transfection complexes at room temperature for 20 minutes, solution was given to the cells in a dropwise manner. Transfection efficiency was monitored every 24 hours by performing parallel transfection experiments with RCASBP(A) harboring the green fluorescent protein (GFP) and fluorescence microscopy. 72 hours after transfection, DF1 cells were washed with PBS (Life Technologies) and pelleted by trypsination and centrifugation at 800 rpm at room temperature for 5 minutes. After cell counting using a ViCell XR cell counter (Beckmann), virus producing DF1-cells were diluted to a final concentration of 40,000 cells/µl in DMEM media (ATCC). All intracranial injections were performed with virus producing DF1 cells 72h post transfection and neonatal Ntv-a mice as previously described [156].

# 4 RESULTS

## 4.1 Expression of Mutant Histone H3.3 in Primary Glioblastoma

By performing whole-genome or whole-exome sequencing, our laboratory and others identified two recurrent mutations (K27M or G34R) within the *H3F3A* gene, coding for the replication-independent histone H3.3 in pediatric glioblastoma [30, 49]. To date, *H3F3A* mutations were identified in approximately 50% of all analyzed childhood GBMs with a patient age younger than 22 years. Mutations of the second H3.3 producing gene *H3F3B* were not found. With the exception of one single K27M mutated tumor, all identified *H3F3A* alterations are heterozygous mutations, affecting only one *H3F3A* allele. Assuming biallelic expression of the *H3F3A* gene, this would lead to 50% mutated H3.3 mRNA and consequently H3.3 protein.

In order to test for biallelic expression of *H3F3A* in H3.3 mutated tumors, RNA of 6 pedGBM samples harboring either the K27M (n=3) or G34R (n=3) mutation was isolated and transcribed into cDNA. After PCR amplification of a fragment covering both mutations, PCR products were cloned into the pGEM-T Easy vector system. Twenty clones per tumor were analyzed by Sanger sequencing using vector specific primers. Thus, the percentage of mutated clones identified directly reflects the relative expression of the mutated *H3F3A* allele in the tumor. In all analyzed tumors the number of mutated clones was between 15 and 70%. Assuming a high tumor cell content within the tumor mass originally used for RNA extraction, these results reflect biallelic expression of the *H3F3A* gene in pedGBMs.

Whole-transcriptome sequencing data of one K27M and two G34R mutated GBMs were used to confirm that both alleles of the *H3F3A* gene are expressed in primary tumors. In the K27M mutated tumor, 138 sequencing reads were generated covering the respective codon within the *H3F3A* transcript. While 109 reads supported the wildtype codon GGG, coding for lysine at amino acid position 27 of H3.3, 29 reads (21%) showed the mutated codon AGG, replacing lysine by methionine at the respective amino acid position. In both G34R mutated tumors the relative number of RNA sequencing reads supporting the G34R mutation was 57% and 37%. This clearly indicates that tumor cells harboring a heterozygous *H3F3A* mutation still express approximately the same amount of wildtype H3.3 from the second (unaffected) *H3F3A* allele.

The total amount of mutated H3.3 protein can be further diluted by wildtype H3.3 protein, which is produced from the second H3.3 producing gene *H3F3B*. For this reason relative mRNA expression of *H3F3A* and *H3F3B* was analyzed by quantitative real-time PCR (qRT-PCR) in three K27M and three G34R mutated pedGBMs. As illustrated in Figure 5A, both H3.3 producing genes (*H3F3A* and *H3F3B*) are expressed in primary GBMs harboring H3.3

mutations. With the exception of one G34R mutated GBM (GBM5), relative mRNA expression levels of both genes were comparable.

Additionally, *H3F3A/B* mRNA levels were analyzed by using whole-genome expression profiling data of 81 GBM samples with known H3.3 mutation status. This data confirms the qRT-PCR results, as both H3.3 coding genes are found to be transcribed into mRNA. By trend, *H3F3A* showed slightly higher expression levels compared to the *H3F3B* gene (Figure 5B). The trend towards higher *H3F3B* expression in G34R mutated tumors measured by qRT-PCR is not confirmed by the microarray data. Furthermore, mRNA expression of *H3F3A* and *H3F3B* in K27M (n=14) and G34R (n=11) mutated tumor samples is comparable to tumors without *H3F3A* mutations (n=56), speaking against compensatory effects as a consequence of *H3F3A* mutations.

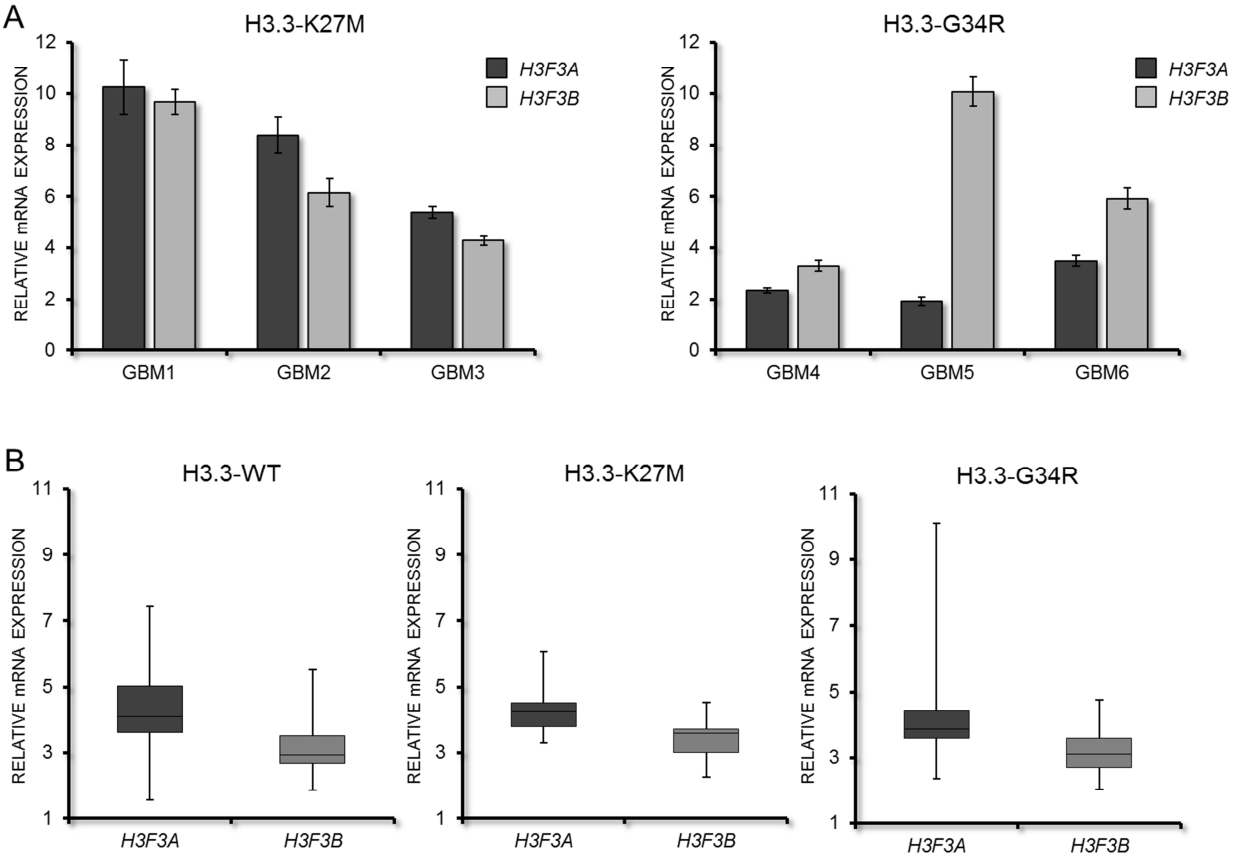


**Figure 5. *H3F3A* and *H3F3B* mRNA Expression in primary GBM Tumors. (A)** Messenger RNA expression of both H3.3 producing genes (*H3F3A* and *H3F3B*) in H3.3-K27M (n=3) and H3.3-G34R (n=3) mutated pedGBM samples was measured by quantitative RT-PCR. Relative gene expression is normalized to the housekeeping gene *SDHA*. **(B)** Affymetrix microarray expression data is visualized as boxplots to compare mRNA expression levels of both H3.3 coding genes in 81 primary GBM samples. Tumors were grouped according to their *H3F3A* mutation status (H3.3-WT (n=56), H3.3-K27M (n=14) or H3.3-G34R (n=11)). (Affymetrix probe set ID used for *H3F3A* expression: 211940_x_at. Affymetrix probe set ID used for *H3F3B* expression: probe 211999_at.)

In summary, biallelic expression of the *H3F3A* gene in combination with similar transcriptional output of both H3.3 encoding genes (*H3F3A* and *H3F3B*) results in the fact that approximately 25% of total H3.3 protein within H3.3 mutated tumor cells harbors the respective H3.3 mutation. In other words, the complex genetic and epigenetic changes originally identified in H3.3 mutated tumors are induced by a relatively low amount of mutant protein, indicating a dominant negative effect.

No differences in mRNA expression of canonical histone H3 was detected in K27M or G34R mutated pedGBMs compared to tumors without *H3F3A* mutations (Supplementary Figure 1). Microarray expression data of other histone H3 variants such as H3.4, H3.5, H3.X or H3.Y was not available since these genes are not covered by the Affymetrix microarray platform.

### 4.2 Incorporation of mutant H3.3 Protein

The non-canonical histone variant H3.3 has been reported to be enriched at transcriptionally active genes in several cell types [157-160]. In order to find out whether the identified H3.3 mutations affect the incorporation of histone H3.3 protein into chromatin, SF188 glioblastoma cells were transfected with EGFP-tagged H3.3 variants (H3.3-WT-EGFP, H3.3-K27M-EGFP and H3.3-G34R-EGFP). Afterwards, H3.3 protein localization was visualized by fluorescence microscopy 96 hours after transfection. As a result, wildtype H3.3 protein but also K27M or G34R mutated H3.3 exclusively showed nuclear localization as indicated by co-localization with blue DAPI signals (Figure 6).

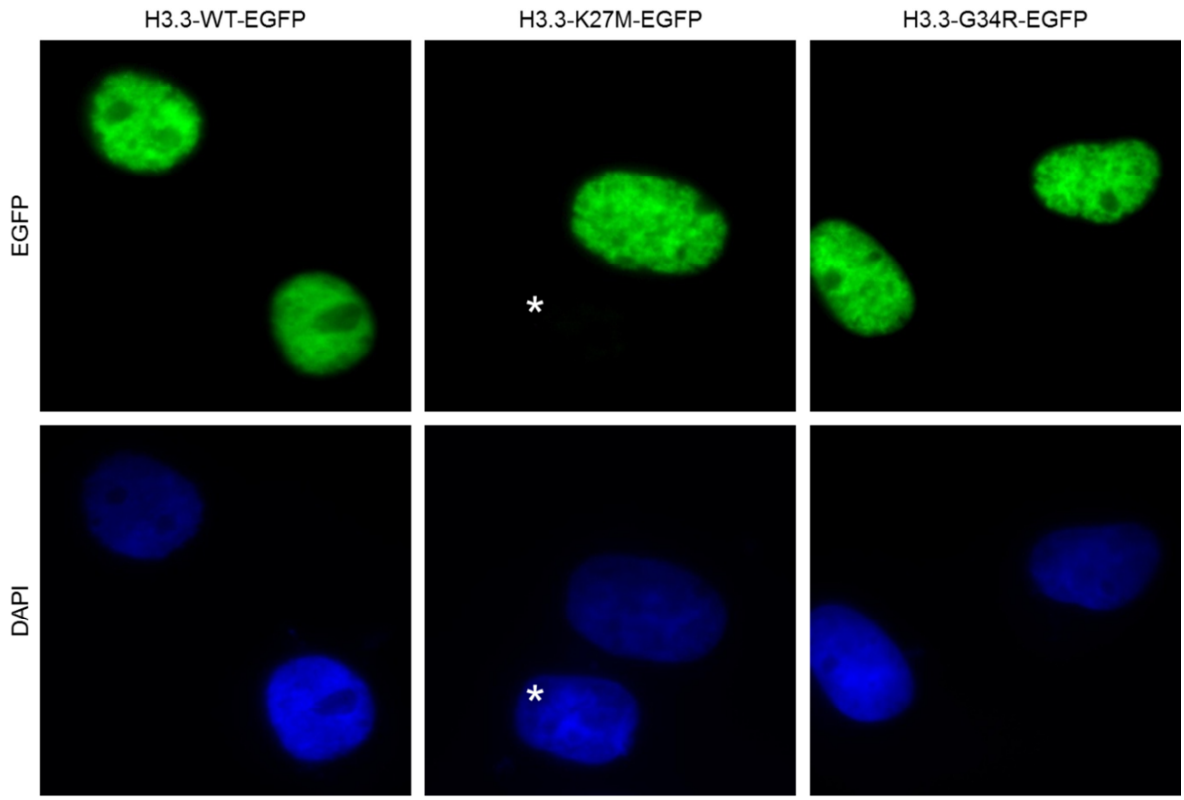


**Figure 6. Localization of mutant Histone H3.3 Protein.** Protein localization of EGFP tagged H3.3 variants (H3.3-WT-EGFP, H3.3-K27M-EGFP, H3.3-G34R-EGFP) was analyzed by fluorescence microscopy 96 hours after transfection of SF188 cells. Nuclear localization of H3.3 variants (green EGFP signal) is indicated by co-localization with nuclear DNA, labeled with 4',6-diamidino-2-phenylindole (DAPI) (blue signal). Asterisk marks an untransfected SF188 cell without H3.3-K27M-EGFP expression.

To determine whether protein localization of mutant H3.3 within the cell nucleus differs from wildtype H3.3 localization, SF188 cells expressing CFP tagged wildtype H3.3 were transfected simultaneously with EGFP tagged H3.3 harboring either the K27M or G34R mutation. Localization of both fluorescently tagged H3.3 proteins was analyzed by two-channel fluorescence confocal imaging. In doing so, protein co-localization was quantified by measuring the extent of signal overlap between wildtype H3.3 (CFP: red signal) and K27M or G34R mutated H3.3 (EGFP: green signal) (Figure 7). The extent of signal overlap between CFP tagged wildtype H3.3 protein and EGFP tagged wildtype H3.3 served as a positive control. Co-localization of both wildtype proteins was demonstrated by high correlation coefficients ($R^2$>0.95) (Figure 7A). Correlation analysis of wildtype H3.3 and one of the mutant histones (K27M or G34R) did not show any significant differences in protein localization, indicated by equally high correlation coefficients (Figure 7B/C). Alternatively, the indistinguishable protein localization of wildtype and mutant histone H3.3 is illustrated by almost identical signal intensity profiles of both color channels. Based on these results, fundamental differences in mutant histone nuclear transport or histone protein incorporation can be ruled out.

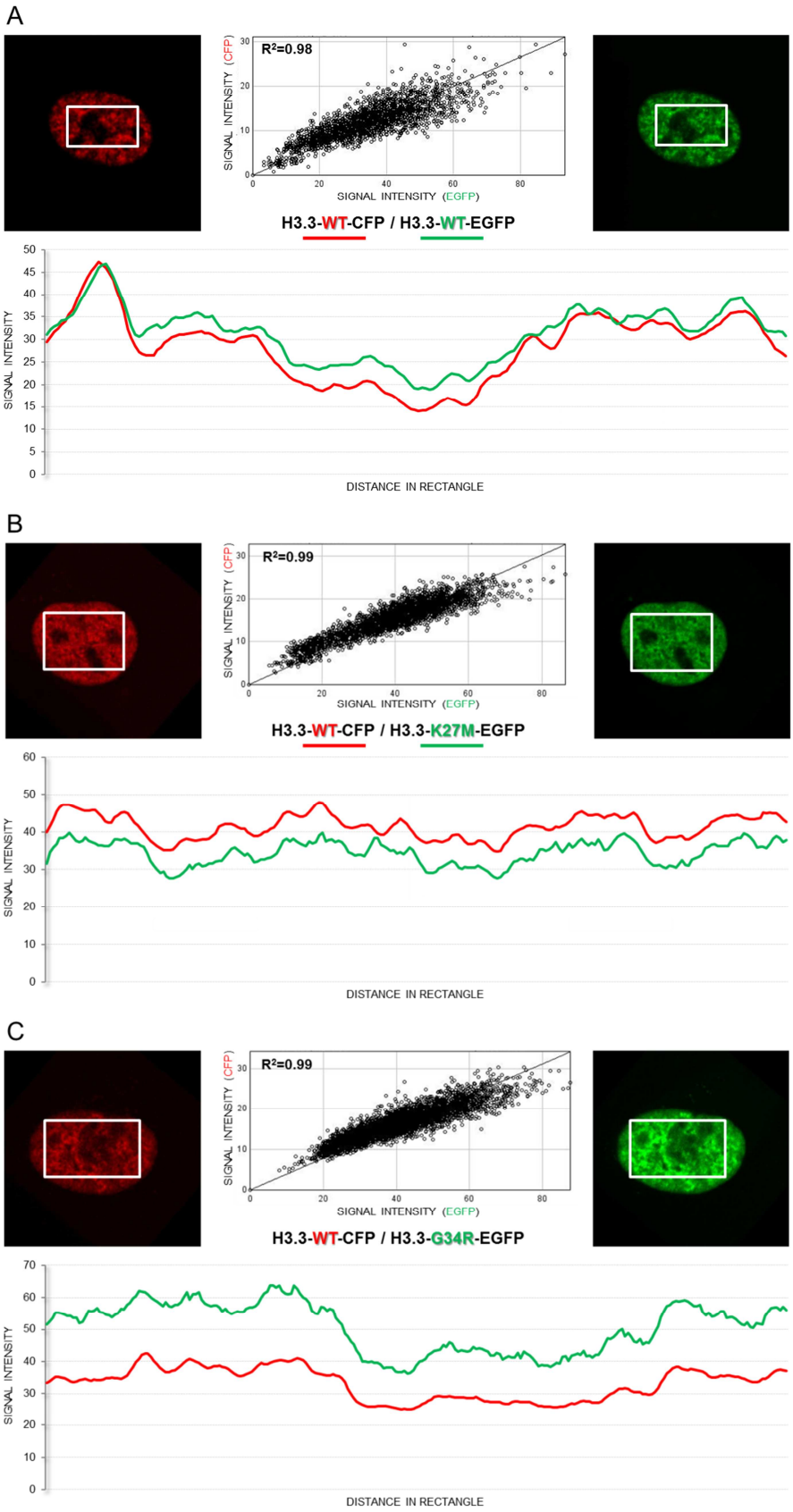


**Figure 7. Incorporation of mutant H3.3 Protein.** SF188 glioblastoma cell were co-transfected for 96 hours with CFP tagged wildtype H3.3 (red signal) and one of the following EGFP-tagged variants (green signal): H3.3-WT-EGFP **(A)**, H3.3-K27M-EGFP **(B)** or H3.3-G34R-EGFP **(C)**. Scatter plots show pixel distribution, whereby the intensity of a given pixel of the EGFP signal corresponds to the

x-coordinate and the intensity of the corresponding pixel of the CFP signal is shown as the y-coordinate. Correlation was done in the area delineated using 10 confocal images per cell nucleus (5 cell nuclei/experiment). High correlation coefficients ($R^2$) indicate high signal overlap between wildtype CFP tagged H3.3 and the respective EGFP tagged H3.3 variant. Signal intensity plots (lower part of each experiment) show the intensity of the CFP and EGFP signal along the distance in the designated rectangle within the cell nucleus.

Due to the signal density in combination with the limited resolution of quantitative confocal imaging of fluorescently labeled proteins, this technique is not able to reveal more detailed differences in mutant H3.3 localization. Therefore, a comprehensive high-resolution map of H3.3 incorporation sites was generated by performing chromatin immunoprecipitation (ChIP) followed by next generation sequencing. By using a tag-specific antibody, which allows immunoprecipitation of ectopic HA-tagged variants of H3.3, genome-wide incorporation maps of K27M mutant, G34R mutant and wildtype H3.3 protein were generated in transduced SF188 glioblastoma cells. Sequencing of DNA fragments bound to one of the three H3.3 variants (referred to as IP) produced a minimum of $3.67x10^6$ sequencing reads. For normalization, input samples of each ChIP experiment were sequenced in parallel, leading to a minimum of $4.29x10^6$ sequencing reads.

In order to compare the ChIP-Seq profiles of mutated H3.3 and wildtype H3.3, the human genome was divided into 10 kb non-overlapping windows (also called bins). Higher resolution data analysis using smaller bins (e.g. 5 kb) was not possible without increasing the sequencing depth. In average, 51 reads were located within one 10 kb bin. Data was normalized by dividing read numbers within a particular 10 kb bin of the IP experiments by the read number within the respective bin of the input sample. Afterwards, normalized ChIP-Seq profiles of one of the two mutants K27M or G34R were compared to profiles of wildtype H3.3. Finally, results were illustrated as ratio plots for each of the human chromosomes, as this figure type visualizes aberrant incorporation of mutant histone H3.3 protein. As shown for K27M and G34R mutant H3.3 in Figure 8A and Figure 8B respectively, the log2 ratio of normalized ChIP-Seq reads between mutant and wildtype H3.3 mainly did not exceed +/-1, indicating very similar incorporation sites of both proteins based on 10 kB resolution. Genomic bins showing more prominent differences between mutant and wildtype H3.3 deposition were found in pericentromeric regions of several chromosomes like chromosome 1, chromosome 9 or chromosome 14. This was of particular interest, as Histone H3.3 has been shown to be preferentially incorporated at pericentromeric heterochromatin. In addition, we found some genomic regions such as a region on chromosome 5q, where differences between mutant and wildtype H3.3 incorporation seemed to be more striking. Careful revision of ChIP-Seq data revealed that these genomic regions of differential H3.3 incorporation were poorly covered by sequencing reads. In line with this, sequencing gaps were causative for differential incorporation of mutant H3.3 at pericentromeric DNA. These

regions are known to be poorly covered by next-generation sequencing techniques due to their high repetitive complexity. Taken together, no differences between incorporation sites of mutant and wildtype H3.3 have been identified by performing ChIP-Seq of epitope tagged H3.3 mutants in SF188 glioblastoma cells at the resolution chosen.

A

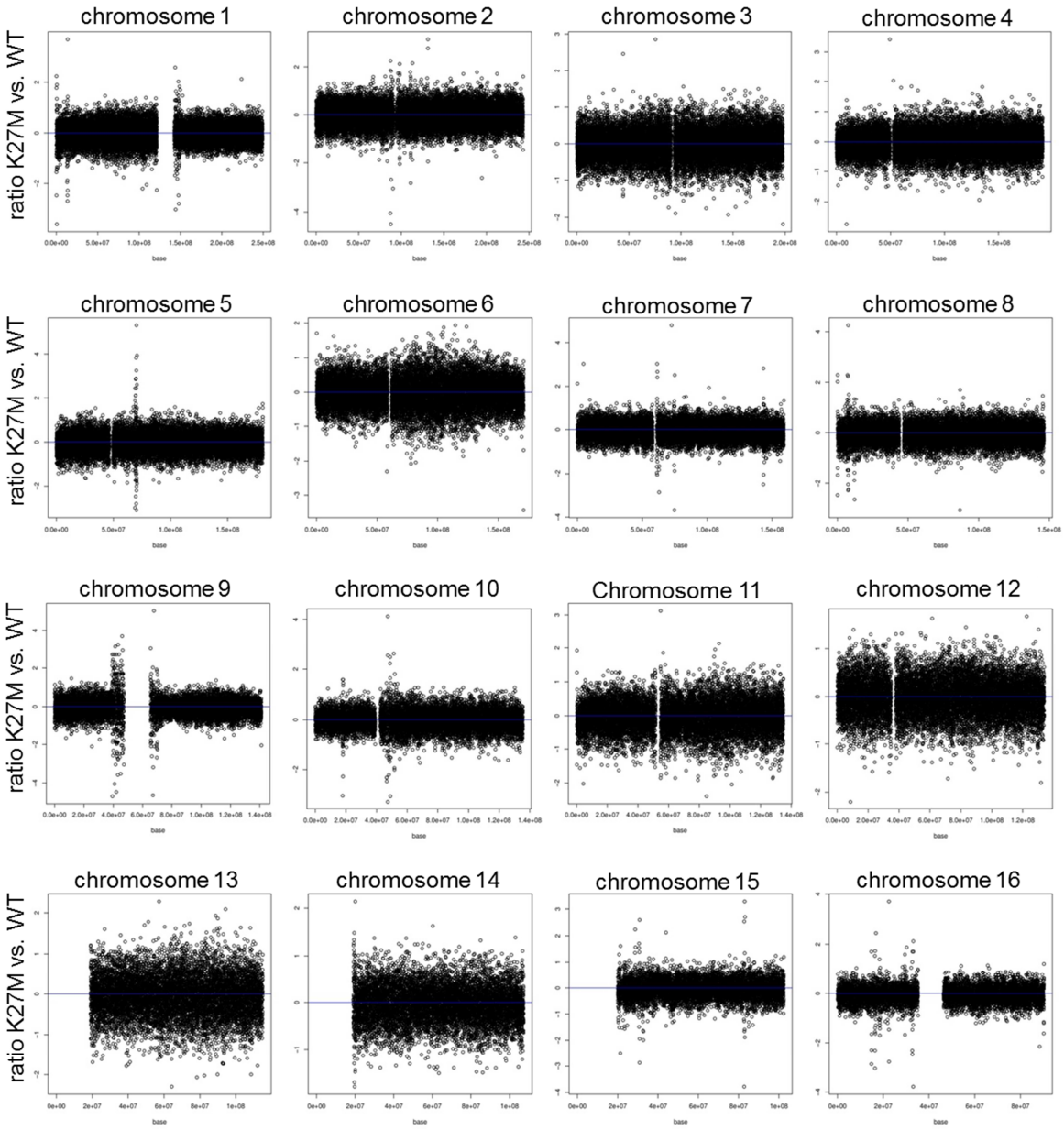

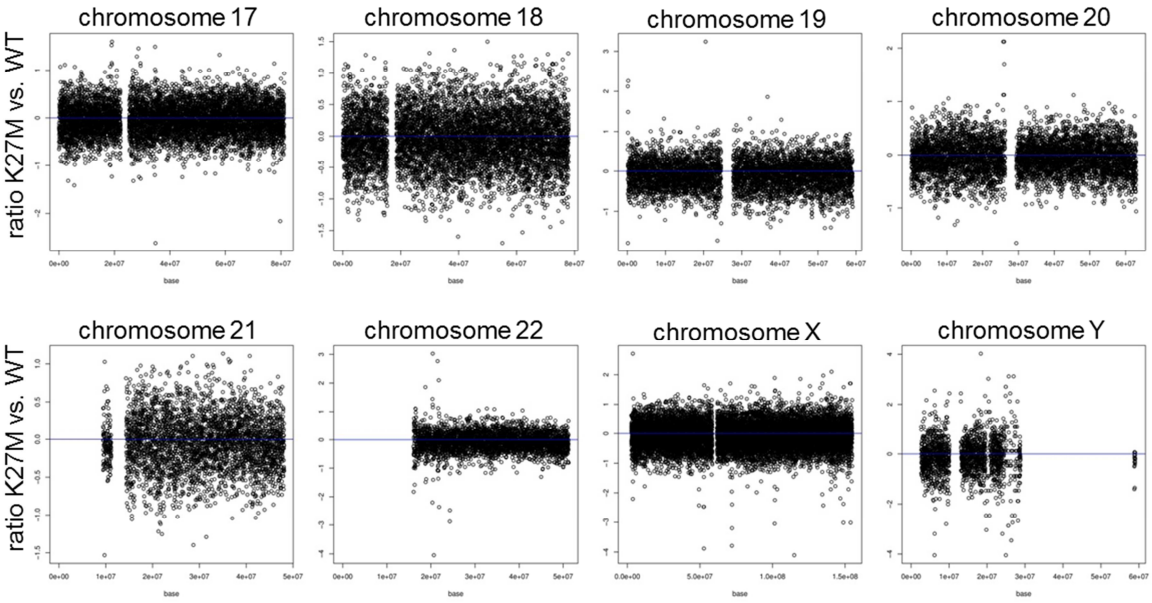
chromosome 17
chromosome 18
chromosome 19
chromosome 20
chromosome 21
chromosome 22
chromosome X
chromosome Y
ratio K27M vs. WT
ratio K27M vs. WT
base

B

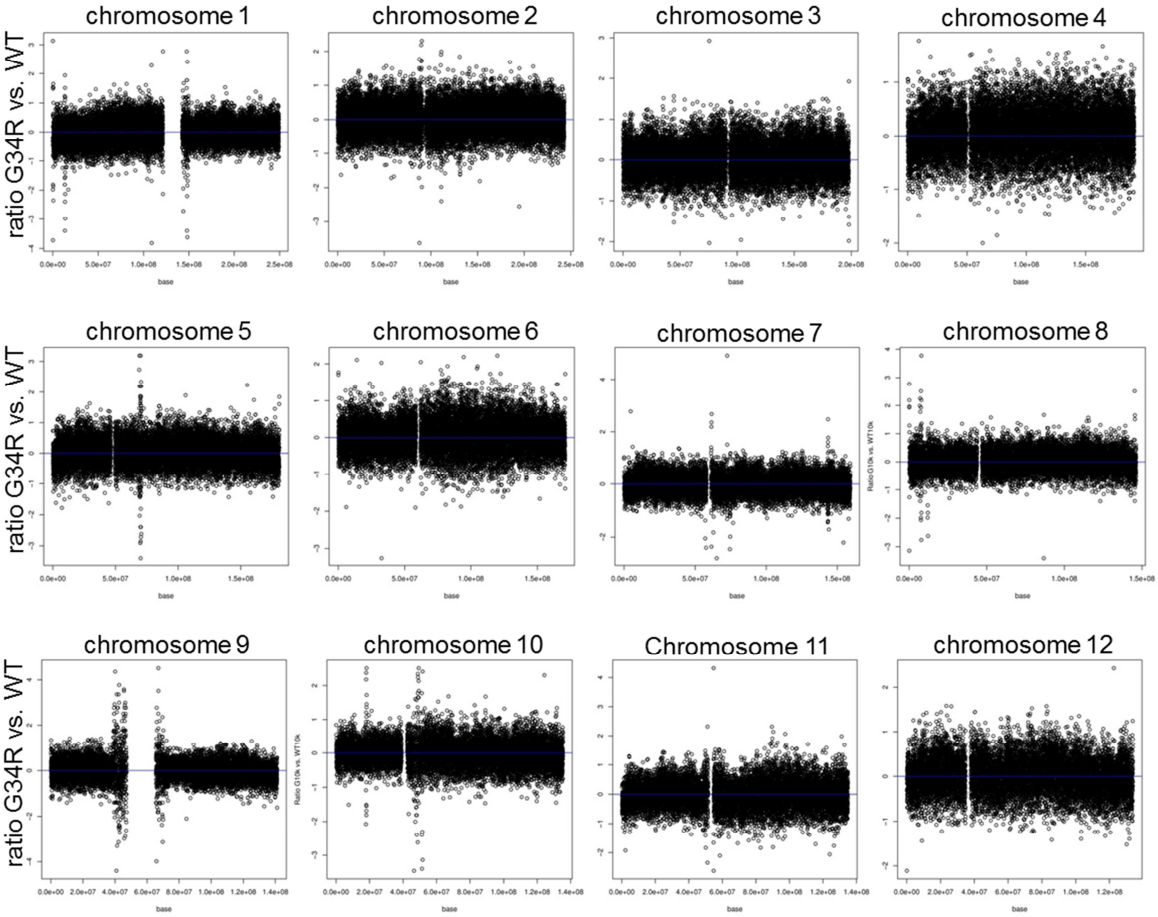
chromosome 1
chromosome 2
chromosome 3
chromosome 4
chromosome 5
chromosome 6
chromosome 7
chromosome 8
chromosome 9
chromosome 10
Chromosome 11
chromosome 12
ratio G34R vs. WT
ratio G34R vs. WT
ratio G34R vs. WT
base

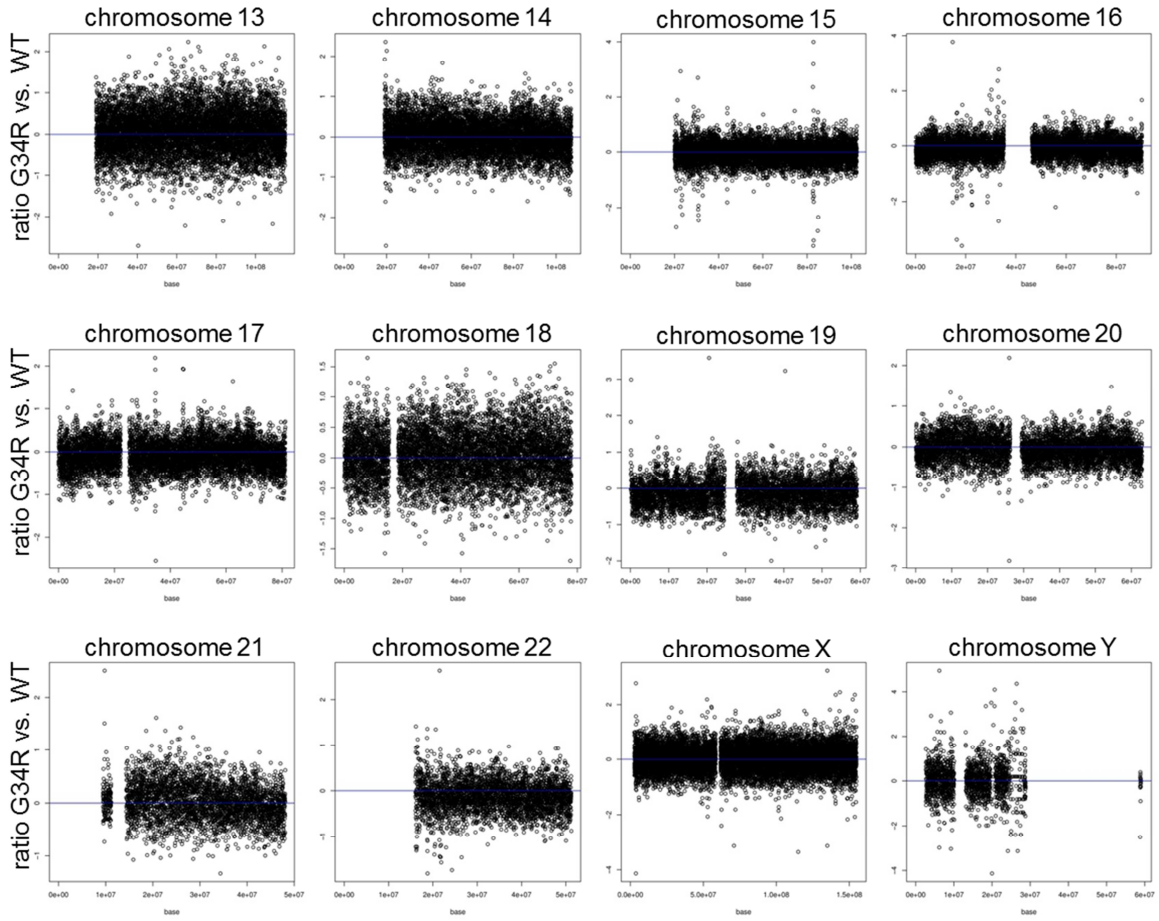


**Figure 8. Incorporation Profiles of mutant Histone H3.3.** SF188 glioblastoma cells stably expressing epitope-tagged H3.3 variants (H3.3-WT-HA, H3.3-K27M-HA, H3.3-G34R-HA) for 14 days were used to perform chromatin immunoprecipitation with an epitope-specific antibody followed by next generation sequencing (ChIP-Seq). Data is illustrated as ratio plots comparing normalized ChIP-Seq profile of the K27M **(A)** or G34R **(B)** mutant with ChIP-Seq profiles of wildtype H3.3. Each dot represent a genomic region of 10 kB.

## 4.3 Overexpression of mutant Histone H3.3

To find out if overexpression of mutant histone H3.3 is sufficient to induce similar effects on DNA methylation and gene expression, which have been originally described in primary pedGBMs, isogenic SF188 glioblastoma cells were generated, stably overexpressing either K27M or G34R mutated H3.3. Although the contribution of mutations within the H3.3 chaperone ATRX and the tumor suppressor p53 in initiation and progression of H3.3 mutated GBMs is not elucidated yet, high co-incidence rates of H3.3 mutations and mutations within *ATRX* and *TP53* indicate the importance of these additional genetic hits [30]. In order to recapitulate the genetic background of H3.3 mutated primary GBMs *in vitro*, SF188 glioblastoma cells were chosen for further examinations. SF188 cells are derived from a male 8-year old patient suffering from a highly aggressive glioblastoma, harboring several genetic alterations including a mutation within the *TP53* gene [161-163].

For subsequent overexpression experiments, the open reading frame of wildtype H3.3 as well as K27M or G34R mutated H3.3 was cloned in frame with a C-terminal HA-tag into the lentiviral overexpression vector pLVX-Puro. After lentivirus production, SF188 glioblastoma cells were transduced and the expression of exogenous H3.3 variants was analyzed by Western blot. Due to the high abundance of endogenous H3.3 protein, expression of exogenous/overexpressed H3.3 only accounts for approximately 5-10% of total H3.3 protein (Figure 9A).

To assess, whether overexpression of mutant H3.3 induces changes in cell viability or growth characteristics of SF188 cells, cell cycle analysis and a proliferation assay was conducted. Cell proliferation of mutant H3.3 overexpressing SF188 cells was analyzed by performing MTS assays using the CellTiter 96 AQueous Non-Radioactive Cell Proliferation Assay (Promega). Seven days after transduction, SF188 cells were seeded and readout was carried out another 24 hours later. Mutant as well as wildtype H3.3 overexpressing cells showed reduced cell proliferation compared to empty vector (EMPTY-pLVX) transduced cells (Figure 9B). K27M expressing cells showed a trend towards slightly higher proliferation, while mutant G34R expressing cells proliferated slower without reaching significance.

Furthermore, the cell cycle of transduced SF188 cells was analyzed by using a propidium iodide (PI) flow cytometric assay originally described by Nicoletti *et al.* [155]. Seven days after transduction, SF188 cells were seeded and incubated for additional 24 hours followed by flow cytometric analysis. As illustrated in Figure 9C, the number of apoptotic cells represented by the SubG1 fraction was marginally reduced in K27M expressing cells compared to wildtype and G34R expressing cells. Less apoptotic cells might also explain the slightly increased number K27M transduced cells in the MTS assay. In addition, the number of cells preparing for mitosis in G2 phase was slightly increased in K27M transduced cells, resembling SF188 cells transduced with the empty vector control. In conclusion, SF188 glioblastoma cells overexpressing mutant H3.3 did not show fundamental differences in cell cycle distribution compared to wildtype H3.3 overexpressing cells.

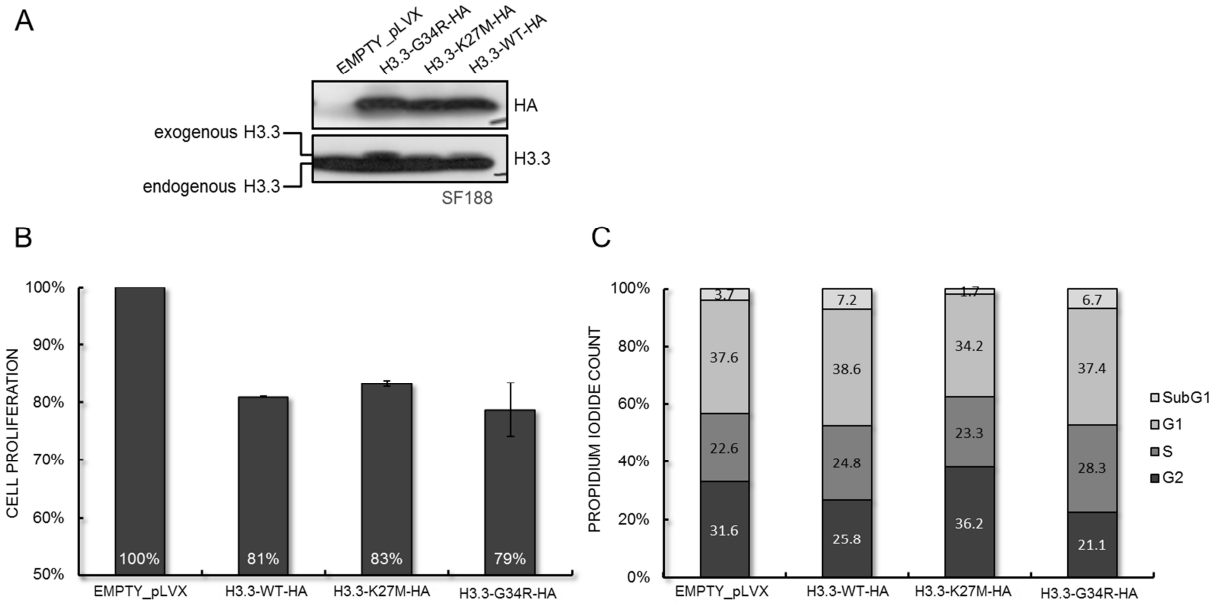


**Figure 9. Overexpression of Histone H3.3 Mutants in SF188 Cells. (A)** Western blot analysis showing overexpression of HA-tagged H3.3 variants (H3.3-WT-HA, H3.3-K27M-HA, H3.3-G34R-HA) by using an HA-specific antibody. H3.3 Western blot results illustrate the relative amount of overexpressed H3.3 protein, which is visible as a faint band above the endogenous H3.3 protein. **(B)** Cell proliferation of SF188 cells overexpressing mutant H3.3 was assessed by MTS assay 8 days after transduction. **(C)** Propidium iodide assay of H3.3 variant overexpressing cells displays marginal differences in cell cycle progression of K27M expressing cells at the same time point.

PedGBMs expressing one of the two H3.3 mutants were reported to be characterized by distinct gene expression and DNA methylation profiles [30, 48]. Differential expression of marker genes *OLIG1/2* and *FOXG1* was shown to robustly identify K27M or G34R mutated samples. Moreover, promoters of *OLIG1/2* and *FOXG1* were found to be differentially methylated in these tumors. For this reason, SF188 cells, transduced for 25 days to overexpress mutant H3.3, were profiled by whole-genome gene expression and DNA methylation arrays using the Human Genome U133 Plus 2.0 Array (Affymetrix) and the Infinium Methylation 450K Array (Illumina), respectively. In line with published results, *OLIG1* mRNA expression was also downregulated in H3.3-G34R overexpressing SF188 cells. However, hypermethylation of the *OLIG1* promoter region was not detected (Figure 10A). *OLIG2*, which was specifically downregulated in G34R mutated primary tumors, did not show differential expression or DNA methylation (Figure 10B). Compared to more distal parts of the *OLIG1/2* gene bodies, DNA methylation was substantially reduced in close vicinity to the transcriptional start sites and the adjacent part of the gene body. In contrary to the findings in K27M mutated pedGBMs, downregulation of *FOXG1* expression due to promoter hypermethylation was not detected in SF188 cells overexpressing the K27M mutant (Figure 10C). Accordingly, gene promoters of additional genes such as *SOX10*, *ZNF233*, *LYPD1* or

*IRX1*, which displayed differential methylation in primary tumors, did not show methylation differences at this early time point after transduction.

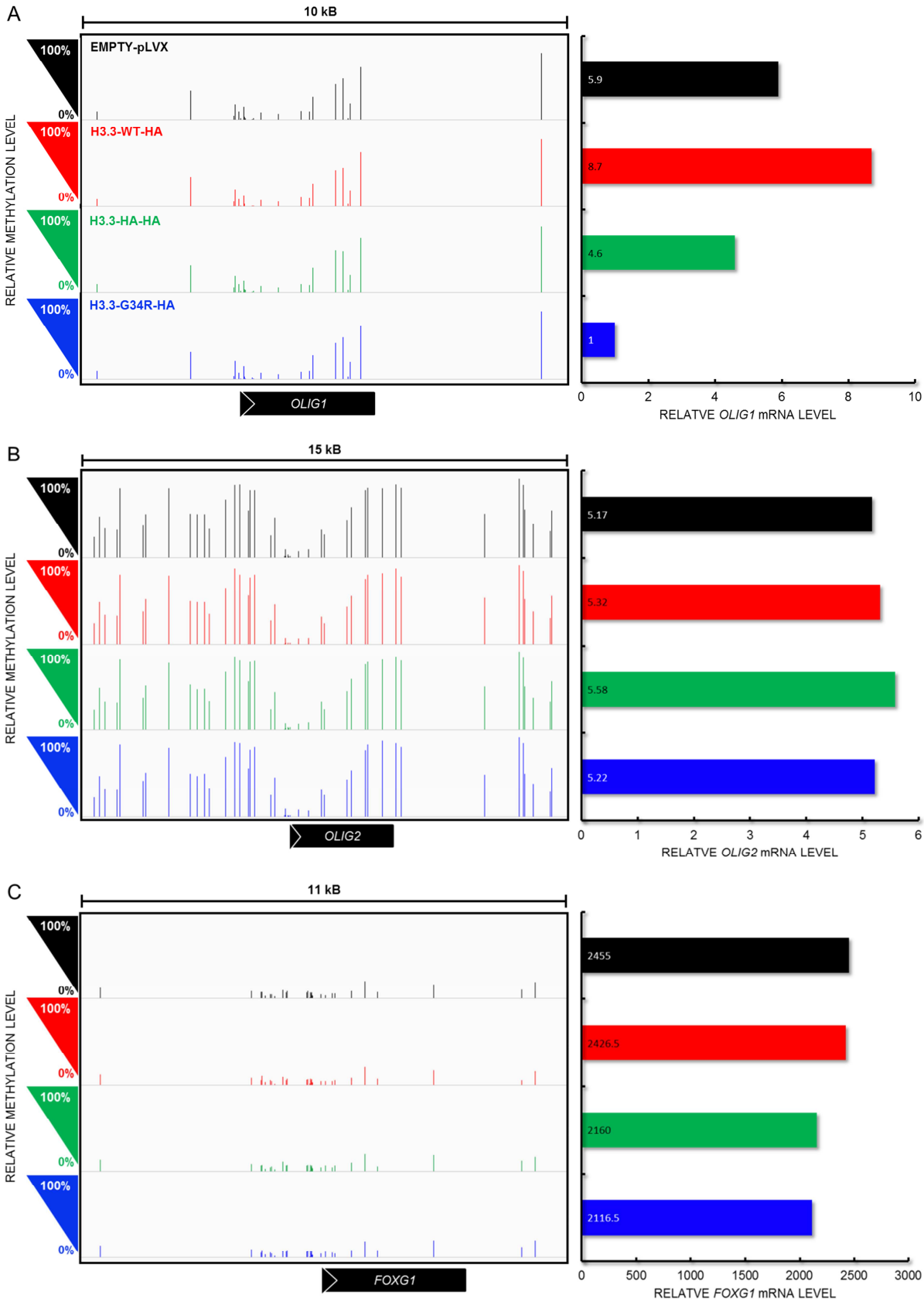


**Figure 10. Promoter Methylation and mRNA Expression of *OLIG1/2* and *FOXG1*.** DNA methylation in transduced SF188 cells at the genomic locus of *OLIG1* **(A)**, *OLIG2* **(B)** and *FOXG1* **(C)** is shown on the left side. DNA methylation levels (0-100%) of single CpGs are indicated by the height of vertical bars. Bar charts on the right illustrate mRNA expression of *OLIG1/2* and *FOXG1* in transduced SF188 cells.

### 4.4 Combined Knockdown and Overexpression Experiments

As shown for transduced SF188 glioblastoma cells, the amount of endogenous wildtype H3.3 exceeds the amount of overexpressed mutant H3.3 protein at least 10 fold (see also Figure 9A). In contrast, the relative amount of mutant H3.3 in primary pedGBM samples with *H3F3A* mutations represents 25% of total H3.3 protein. To increase the relative amount of ectopic mutant H3.3 compared to endogenous wildtype H3.3, a combined knockdown and overexpression approach was performed. As confirmed by gene expression data of transduced SF188 cells described in 4.3, H3.3 expression in (transduced) SF188 cells is driven from both endogenous H3.3 genes to an almost identical extent. Consequently, the expression of both H3.3 coding genes had to be silenced by different short hairpin RNAs (shRNAs) to reduce the overall amount of endogenous H3.3 protein. Three shRNAs targeting the untranslated region (UTR) of *H3F3A* (shH3F3A_1; shH3F3A_2 and shH3F3A_3) and two shRNAs targeting the UTR of *H3F3B* (shH3F3B_1 and shH3F3B_2) were tested for their knockdown efficiency in SF188 cells by measuring *H3F3A* or *H3F3B* mRNA expression by quantitative realtime PCR (qRT-PCR) using *H3F3A* or *H3F3B* specific primers (H3F3A for/rev or H3F3B for/rev). Compared to the non-target shRNA (NT-shRNA), SF188 cells transduced with one of the five specific shRNAs showed a significant mRNA downregulation of the respective gene (Figure 11A/B). While shH3F3A_1 led to a reduction of *H3F3A* mRNA expression by 90%, shH3F3B_2 reduced the *H3F3B* mRNA level by 85%.

As expected, simultaneous transduction of SF188 cells with lentiviral particles delivering shH3F3A_1 and shH3F3B_2 leads to a significant downregulation of overall H3.3 mRNA levels as detected by qRT-PCR using *H3F3A/B* specific primers (H3F3A/B for & H3F3A/B rev) (Figure 11C). Moreover, downregulation of total H3.3 protein in these cells was confirmed by Western blot analysis (Figure 11D).

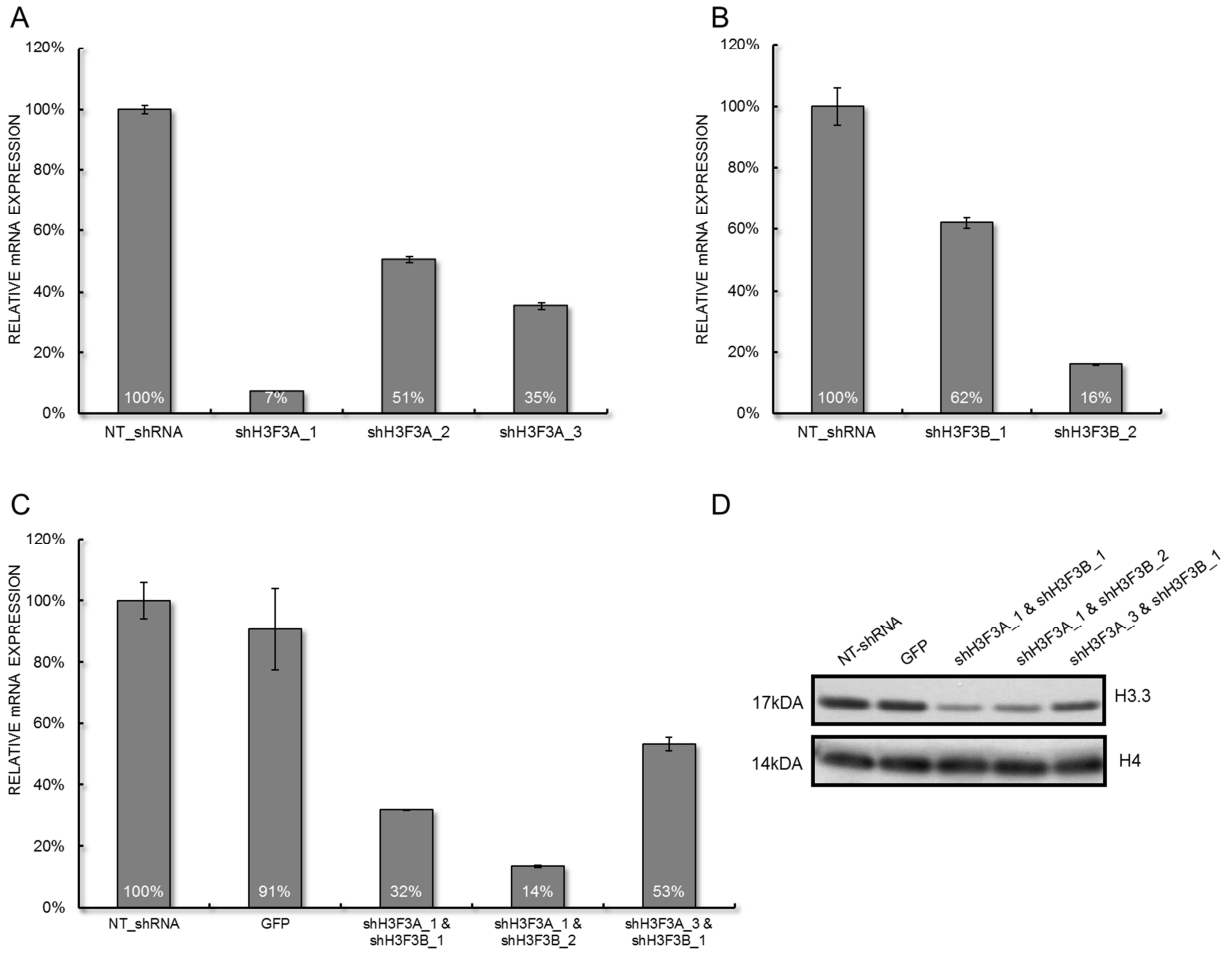


**Figure 11. Knockdown of endogenous H3.3 in SF188 Cells.** QRT-PCR results illustrating *H3F3A* **(A)** and *H3F3B* **(B)** mRNA expression upon lentiviral delivery of different shRNA constructs targeting the UTR of *H3F3A* or *H3F3B*. Relative gene expression is normalized to the housekeeping gene *SDHA*. *H3F3A/B* expression in SF188 cells simultaneously transduced with two different shRNAs targeting both H3.3 producing genes was evaluated by qRT-PCR **(C)** and Western blot analysis **(D)**. By using shH3F3A_1 and shH3F3B_2, total H3.3 protein level was downregulated to approximately 15%.

As reported for MCF7 human breast adenocarcinoma cells, inhibition of H3.3 expression may alter cell proliferation *in vitro* [164]. Based on this finding, cell cycle analysis of SF188 cells transduced with different combinations of shRNAs targeting endogenous *H3F3A* and *H3F3B* was carried out by performing the propidium iodide assay. The results indicate that knockdown of H3.3 expression in SF188 cells did not induce any change in cell cycle progression (Figure 12).

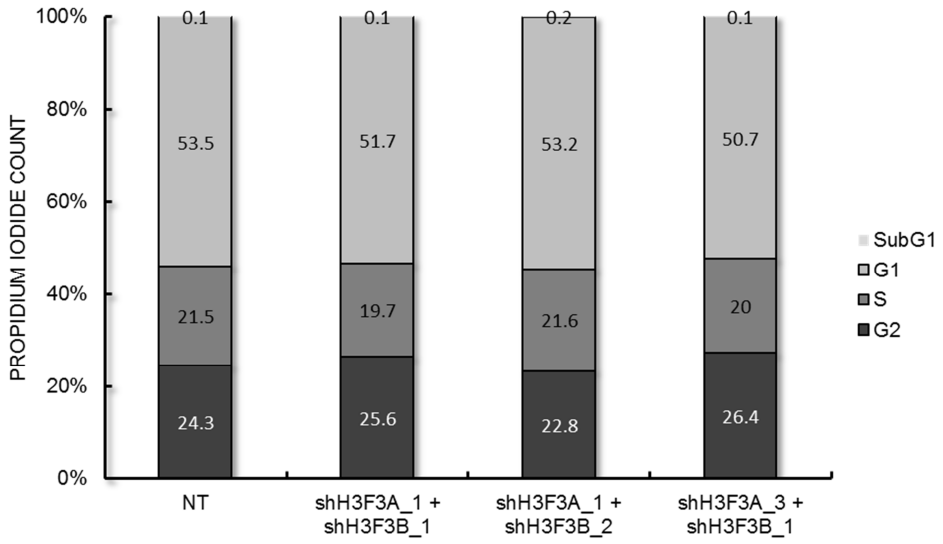


**Figure 12. Cell Cycle Analysis in SF188 Cells upon H3.3 Knockdown.** SF188 glioblastoma cells were transduced with different combinations of shRNAs targeting endogenous *H3F3A* or *H3F3B* for 14 days. Propidium iodide assay was conducted to compare cell cycle distribution of H3.3 knockdown cells to cells transduced with a non-target shRNA (NT).

Knockdown of endogenous H3.3 and simultaneous overexpression of mutant H3.3 requires two separate rounds of transduction. A simultaneous transduction with lentiviral particles delivering (i) the shRNA targeting *H3F3A* (ii) the shRNA targeting *H3F3B* and (iii) the respective H3.3 overexpression construct was not favored in order to avoid high virus loads resulting in cytotoxicity. As both lentiviral constructs, which were used to deliver shRNAs (pLKO.1-puro) or overexpression constructs (pLVX-puro), provide puromycin resistance to transduced cells, efficiency of the second round of transductions was of particular importance. Evaluation of transduction efficiencies in SF188 cells was conducted by using GFP overexpressing pLVX-Puro constructs followed by flow cytometry detecting GFP-positive cells. Using a MOI of 5, more than 90% of SF188 cells were detected to express GFP (Figure 13).

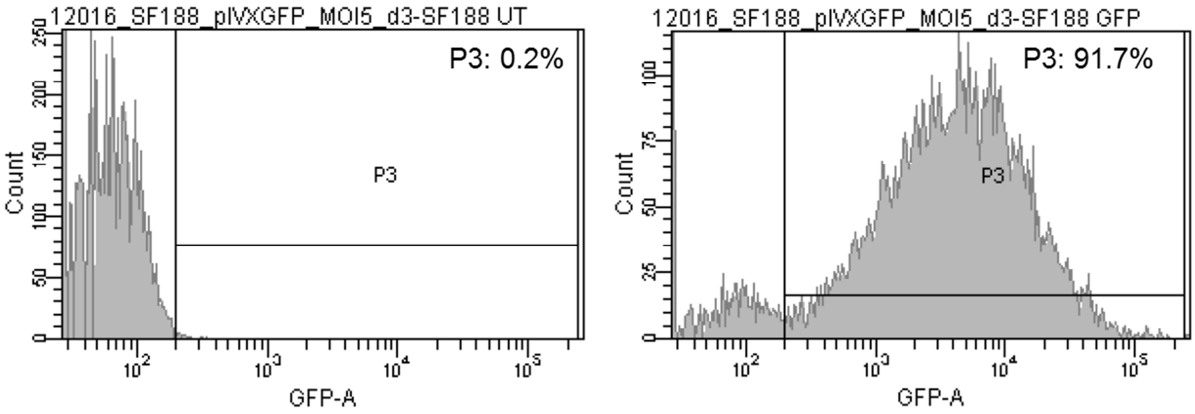


**Figure 13. Transduction Efficiency in SF188 Glioblastoma Cells.** SF188 cells were treated with lentiviral particles (MOI 5) resulting in expression of GFP. Percentage of GFP positive (transduced) cells was analyzed by flow cytometry three days later showing more than 90% GFP positive cells (right) compared to empty vector transduced cells (left).

The first round of transduction on SF188 cells was carried out to reduce the expression of endogenous H3.3 followed by selection with 3 µg/ml puromycin for 3 days. Afterwards, SF188 cells were treated with lentiviral particles mediating mutant H3.3 overexpression. Overall H3.3 mRNA expression (*H3F3A* and *H3F3B* transcripts) was measured by qRT-PCR 7 days after the second round of transductions. Compared to the non-target shRNA (NT-shRNA), H3.3 levels were significantly reduced in all SF188 cells treated with shRNAs targeting the UTR of *H3F3A* and *H3F3B* (shH3F3A_1 and shH3F3B_2) (Figure 14). SF188 cells additionally transduced with H3.3 overexpression constructs showed higher expression of H3.3 mRNA compared to empty vector or GFP transduced controls. However, the shRNA induced knockdown had stronger (down)regulatory effects on H3.3 expression compared to the H3.3 overexpression (Figure 14). Molecular characterization of SF188 cells combining knockdown of endogenous H3.3 and overexpression of one of the two mutants is subject to further studies.

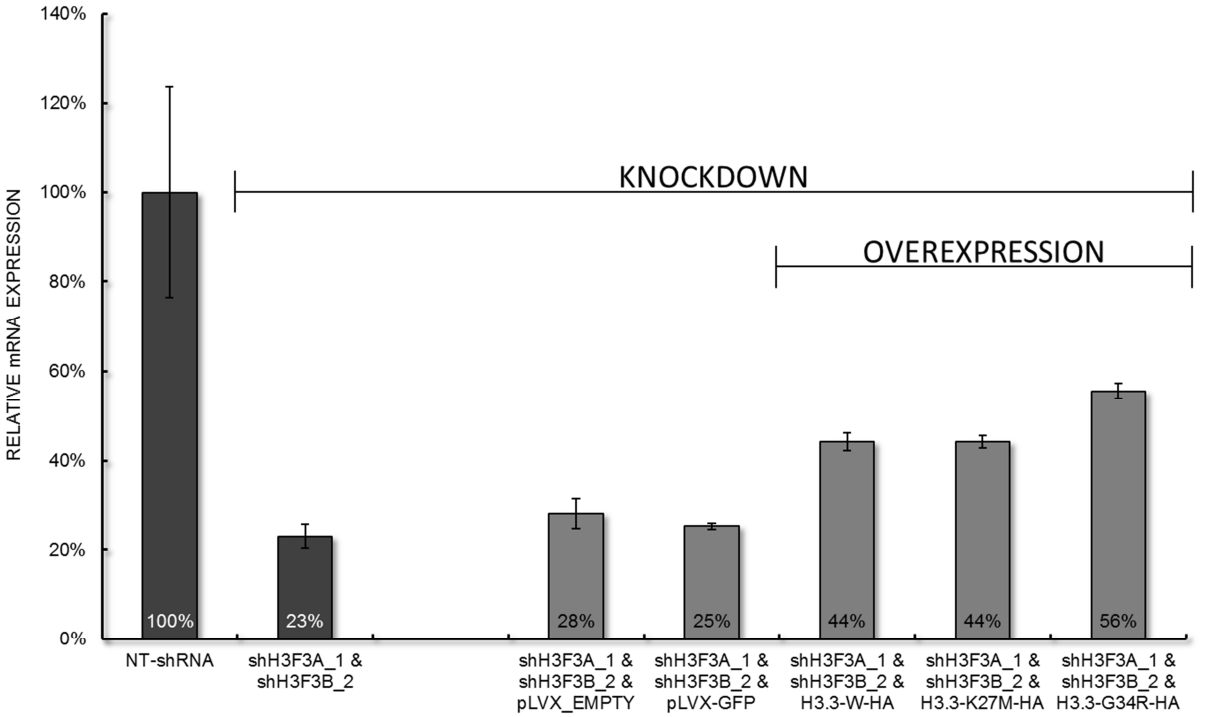


**Figure 14. Combined Knockdown and Overexpression Experiments.** Quantitative RT-PCR was conducted to determine H3.3 mRNA expression in SF188 cells transduced with shRNA targeting endogenous H3.3 (shH3F3A_1 & shH3F3B_2) and simultaneous overexpression of H3.3 variants (H3.3-WT-HA, H3.3-K27M-HA, H3.3-G34R-HA). Relative gene expression is normalized to the housekeeping gene SDHA. While down-regulatory effects are compared to a NT-shRNA, overexpression was normalized to an empty control vector (pLVX-EMPTY).

### 4.5 The Key Epigenetic Mark H3K27me3 in H3.3 mutant GBMs

Preliminary work of our laboratory indicated that each H3.3 mutation (K27M or G34R) defines an epigenetic subgroup of pedGBMs with a distinct gene expression and global DNA methylation pattern [30, 48]. Therefore, H3.3 mutated pedGBMs were analyzed for several posttranslational modifications, which are known to substantially influence chromatin structure and consequently gene expression [165]. Immunohistochemistry (IHC) was performed on 27 pedGBM tumors with known *H3F3A* mutation status. IHC staining was conducted for repressive histone marks including H3K9me3 and H3H27me3 as well as for the activating histone marks H3K4me3 and H3K36me3. While all 27 tumors showed immunopositivity for the two activating histone marks H3K4me3 and H3K36me3 and the repressive mark H3K9me3, all K27M mutated GBMs (n=8) showed absence or strong reduction of H3K27me3 expression (Figure 15A). The existence of H3K27me3 positive cells of blood vessels in the surrounding brain tissue further supports the fact, that H3K27me3 expression is specifically lost in K27M mutated tumor tissue (personal communication Prof. Andrey Korshunov). In contrast, all analyzed wildtype H3.3 tumors (n=13) as well as G34R mutated tumors (n=6) showed strong H3K27me3 immunopositivity (Figure 15B). These results indicate a dominant negative effect of the K27M mutant protein, since the

methylation specific H3K27 antibodies detect global H3K27me3 levels, including methylation at the highly abundant canonical histone H3.1 and H3.2.

To confirm the global reduction of H3K27 trimethylation in K27M mutated tumors by a different technique, histone proteins were isolated from additional pedGBM samples and subjected to H3K27me3 Western blot analysis. Thus, significantly lower K27 trimethylation levels were detected in the K27M mutated tumor compared to the G34R and wildtype tumor (Figure 15C). Moreover, an additional H3K27me3 specific antibody confirmed strong reduction of lysine 27 trimethylation in histone extracts of two independent K27M mutated pedGBM samples (Figure 15D). While K27 monomethylation (H3K27me1) did not show differences in expression, acetylation of lysine 27 (H3K27ac) was found to be increased in two K27M pedGBM samples (Figure 15E). These reciprocal changes in methylation and acetylation at H3K27 have been commonly described in literature [166, 167].

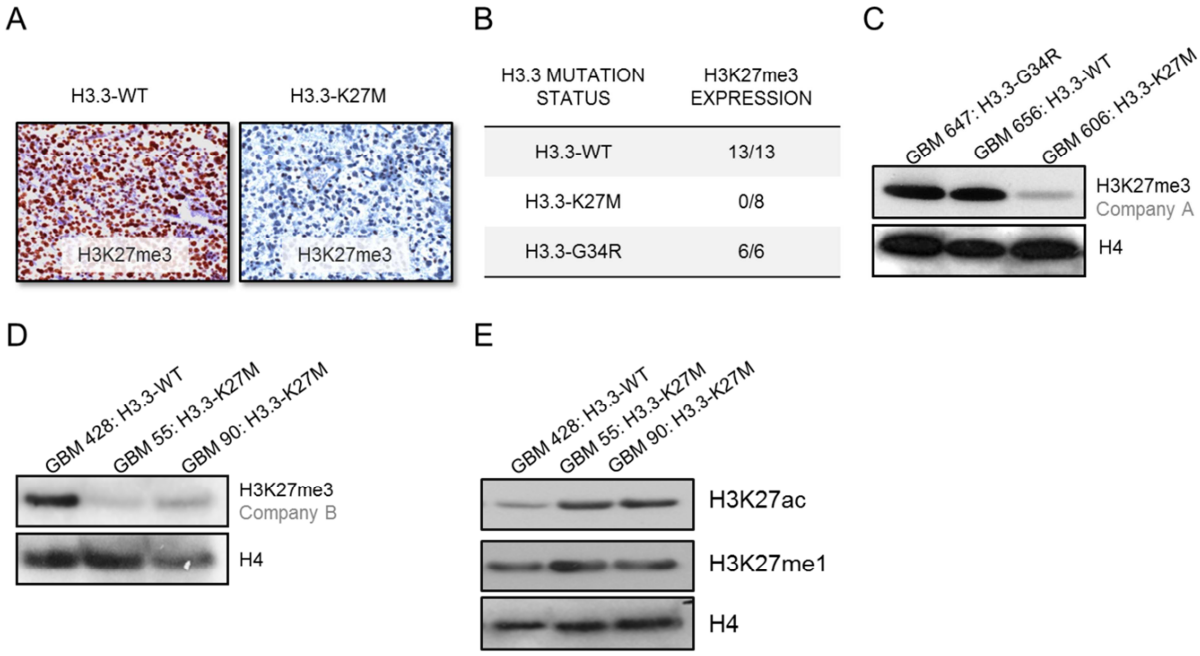


**Figure 15. H3K27me3 Expression in K27M mutant GBMs. (A)** H3K27me3 immunohistochemical stainings of primary GBM tumor tissues show strong immunopositivity in the H3.3 wildtype tumor but absence of this histone mark in the tumor expressing the H3.3 K27M mutant. **(B)** Overview of immunohistochemical stainings for H3K27me3 in pedGBMs with different H3.3 mutation status. **(C)** Western blot results illustrating H3K27Me3 reduction in histone extracts of a primary K27M GBM sample. Histone H4 protein expression indicates equal protein loading amounts. **(D)** Reduction of H3K27me3 was confirmed in histone extracts of additional primary GBMs using a different H3K27me3 specific antibody for Western blot analysis. **(E)** Western blot results showing unaltered levels of H3K27me1 but upregulated H3K27 acetylation in K27M mutated GBMs.

Since trimethylation at lysine 27 is established by the histone methyltransferase EZH2 as the catalytic component of the multiprotein complex PRC2, microarray data of 81 GBMs with known H3.3 mutation status was used to determine whether H3H27me3 reduction in K27M pedGBMs is reflected by altered mRNA expression of PRC2 core components. In doing so, PRC2 components EED, SUZ12 and RBAP48 as well as the H3K27me3 specific methyltransferase EZH2 (and its close homolog EZH1) did not show altered mRNA expression in K27M tumors (n=14) compared to G34R (n=11) or wildtype H3.3 samples (n=56) (see Supplementary Figure 2A-E). Accordingly, the H3K27me3 mediating histone demethylase UTX (KDM6A) is not transcriptionally upregulated in K27M mutant pedGBMs (see Supplementary Figure 2F).

Given that K27M mutant pedGBMs exhibiting low H3K27me3 expression also express a certain amount of wildtype H3.3 protein, Western blot analysis was carried out to elucidate if the global downregulation of H3K27 trimethylation can also be found in SF188 glioblastoma cells stably overexpressing the K27M mutant. However, Western blot analysis of H3K27me3 did no show differences 6 days after transduction (Figure 16A). At this (early) time point, several readouts described in 4.3 also did not show any phenotypic difference in K27M overexpressing cells. To assess, whether K27M induced downregulation of H3K27me3 expression might progress over time, transduced SF188 cells were cultivated for additional 50 days (15 passages). Subsequently, H3K27me3 levels were again determined by Western blot analysis. As shown in Figure 16B, H3K27me3 levels were found to be significantly reduced in SF188 cells expressing the K27M mutant. To test, whether the downregulation of H3K27me3 can be recapitulated *in vitro* independently of the used cell line, HEK293 cells overexpressing the H3.3 K27M mutant for 50 days were subjected to H3K27me3 Western blot analysis. As shown in Figure 16C, K27M expressing HEK293T cells also express reduced levels of global H3K27me3.

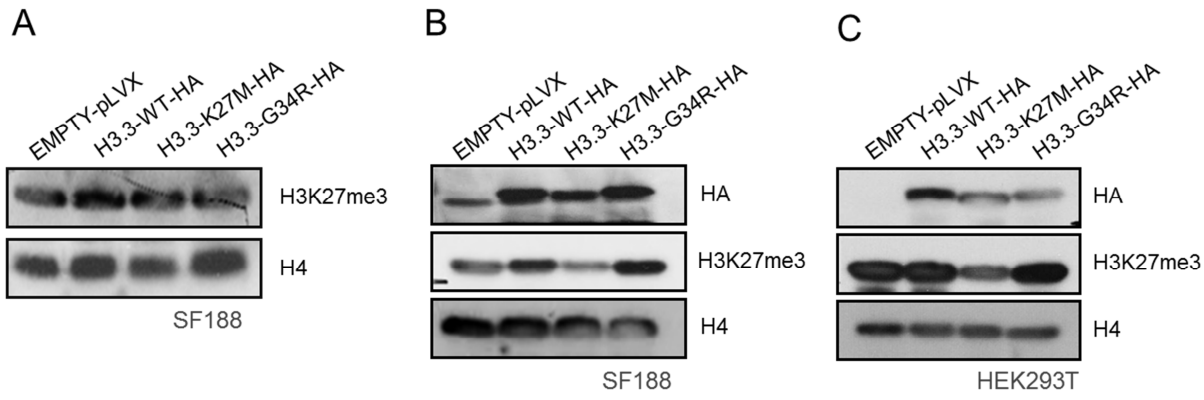


**Figure 16. H3K27me3 in K27M overexpressing Cell Lines. (A)** Western blot of transduced SF188 cells did not show differential H3K27me3 expression 6 days after transduction. (B) After 50 days K27M expressing SF188 cells exhibit a significant reduction of H3K27me3 levels as detected by Western blot analysis. (C) Reduced levels of H3K27me3 expression were detected on HEK293T cells, stably transduced to overexpress K27M mutant for 50 days.

### 4.6 The Histone Tail of mutated H3.3 shows Differences in PTMs

Changes in the balance and dynamics of histone posttranslational modifications directly influence the physicochemical properties of chromatin, resulting in chromatin (de)condensation and altered gene expression. For some PTMs it has been shown that they directly influence other PTMs at the same histone tail (cis crosstalk) or adjacent histone proteins (trans crosstalk). The crosstalk of PTMs was investigated directly at the amino-terminal tail of histone H3.3 and both H3.3 mutants. Discrimination of endogenous wildtype H3.3 (17 kDa) and overexpressed/exogenous H3.3 variants was ensured by transfecting EGFP-tagged H3.3 variants with a molecular weight of 47 kDa. Upon transfection of HEK293T cells, Western blot analysis was carried out to determine the expression of several key histone marks including H3K4me3, H3K9me3, H3K27me1, H3K27me3, H3K27ac, H3.3S31p and H3K36me3. As expected, H3K27me3 expression at the tail of K27M mutated H3.3 was completely abolished by the presence of methionine (Figure 17A). Moreover, none of the K27M transfected cells displayed a global downregulation of H3K27me3 three days after transfection. The existence of methionine at position 27 did not eliminate the signal for other position 27 specific modifications such as H3K27 acetylation and H3K27 monomethylation. For H3K27me1 this might partially be explained by the structural similarity of methionine and monomethylated lysine (see also Figure 21). While K4me3 was not detected at overexpressed H3.3, expression of K9me3 was unaltered between the three H3.3 variants. In contrary, H3S31p levels were downregulated at G34R mutated H3.3 and to a minor extent at K27M mutated H3.3 tails (Figure 17A). The activating histone mark H3K36me3 was significantly reduced at the tail of

the G34R mutant compared to the expression at the tail of K27M and wildtype H3.3 protein (Figure 17A). Finally, differential expression of all PTMs originally identified in H3K293T cells was confirmed in SF188 cells overexpressing EGFP-tagged H3.3 variants (Figure 17B).

Trimethylation of K36 at histone H3 protein is a key epigenetic modification, associated with active gene transcription. In subsequent experiments, global expression of H3K36me3, which is specifically downregulated at the tail of mutant histone H3.3, was analyzed by Western blot analysis in primary tumor samples. In doing so, H3K36me3 levels were found to be slightly downregulated in the tumor sample harboring a G34R mutation (Figure 17C).

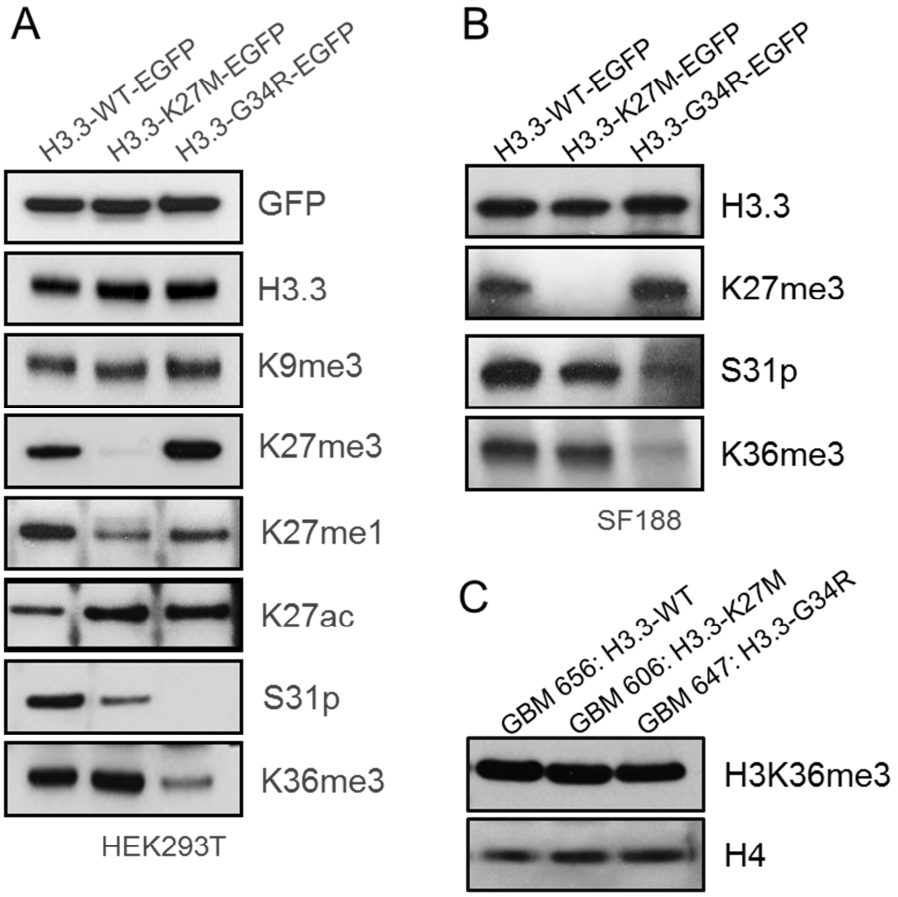


D

| MODIFICATION | H3.3-K27M-EGFP | H3.3-G34R-EGFP |
|---|---|---|
| H3K9me3 | NOT ALTERED | NOT ALTERED |
| H3K27ac | HIGH | HIGH |
| H3K27me1 | LOW | LOW |
| H3K27me3 | LOST | NOT ALTERED |
| H3S31p | LOW | LOW |
| H3K36me3 | NOT ALTERED | LOW |

**Figure 17. Posttranslational Modifications at the Histone Tail of H3.3 Variants. (A)** Western blot results of different PTMs at the amino-terminal tail of EGFP-tagged H3.3 variants in HEK293T cells. The expression of equal amounts of EGFP-tagged exogenous H3.3 (47kDA) is illustrated by GFP and H3.3 signals. **(B)** Western Blot results confirming differential expression of H3K27me3, H3.3S31p and H3K36me3 at the tail of H3.3 variants in SF188 glioblastoma cells. **(C)** Global H3K36me3 expression in primary GBMs detected by Western blot analysis. **(D)** Summary of histone modifications detected at the tail of overexpressed EGFP-tagged mutant H3.3. Expression is compared to levels detected at overexpressed wildtype EGFP-tagged H3.3.

### 4.7 Arginine 34 is posttranslationally modified at G34R mutated H3.3

Posttranslational modifications of the H3.3 amino-terminal tail include methylation of lysine and arginine residues. At the histone tail of G34R mutated H3.3, glycine 34 is replaced by an arginine, which represents a potential new site of methylation. While methylation of lysines includes mono-, di- and trimethylation, arginine residues can be found in mono- or dimethylated state, although dimethylation can occur in symmetric (SDMAs) as well as in asymmetric conformation (SDMAs). To find out, whether arginine 34 at G34R mutated H.3.3 is posttranslationally methylated, histone extracts of HEK293T cells overexpressing EGFP-tagged H3.3 variants were fractionated by reverse phase high-performance liquid chromatography (RP-HPLC). Subsequently, fractions containing the overexpressed H3.3 variants were identified by Western blot analysis and histone proteins were digested into peptides by trypsin in gel digestion. Finally, mass spectrometry (MS) was applied to analyze the modification status of arginine 34 at G34R mutated H3.3. As a result, dimethylation of arginine 34 was identified at the tail of G34R mutant H3.3 (Figure 18). The determination of R34me2 conformation (symmetric or asymmetric dimethylation) is still ongoing as it requires synthetically generated peptides as reference molecules.

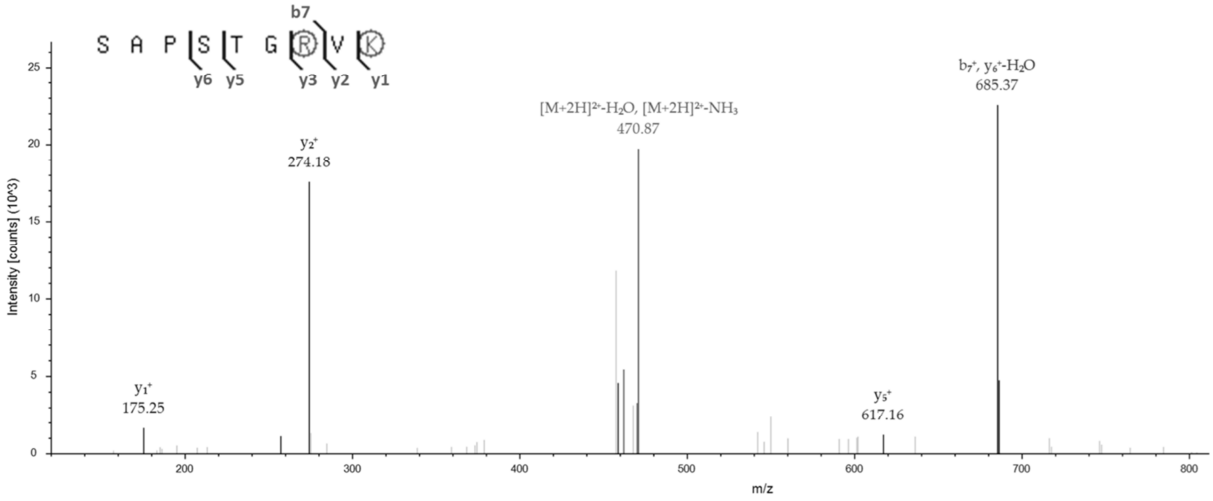


**Figure 18. Identification of R34 dimethylation at G34R mutant H3.3.** Mass spectrum of a digested peptide of G34R mutant H3.3 (SAPSTGRVK: amino acid position 28-36) overexpressed in HEK293T cells, showing dimethylation at arginine 34. The x-axis shows mass divided by charge (m/z).

Arginine methylation in humans is catalyzed by a family of up to 11 different arginine methyl transferases, which have been found frequently deregulated in human cancers [91]. To determine, whether expression of human PRMTs is altered in G34R mutated pedGBMs, expression profiling data of 81 GBMs with known *H3F3A* mutation status was analyzed. As a result, none of the 11 PRMTs was found to be specifically deregulated in G34R mutated tumors (see Supplementary Figure 3).

### 4.8 Tumorigenic Potential of mutated H3.3 in the Brain of neonatal Mice

To study, whether mutated H3.3 is able to induce high-grade gliomas *in vivo*, retroviral gene transfer was performed using the RCAS/Ntv-a system to selectively overexpress H3.3 mutants in neural progenitor cells in the brain of neonatal mice. Consequently, HA-tagged variants of H3.3 (H3.3-WT-HA, H3.3-K27M-HA or H3.3-G34R-HA) were cloned into the RCASBP(A) vector and transfected into DF-1 chicken fibroblasts. The production of infectious virus and the expression of HA-tagged H3.3 variants were confirmed by applying virus containing supernatant of transfected DF-1 cells to fresh DF-1 cells followed by Western blot analysis using a HA-specific antibody (Figure 19A). In addition, receptor-mediated cell infection was confirmed by applying virus-containing supernatant to murine XFM cells, expressing the virus-entry mediating Tv-a receptor at the cell surface.

Subsequently, virus producing DF-1 cells were injected into the brain of neonatal mice (maximum p3) expressing the Tv-a receptor from the nestin promoter (Ntv-a). Since K27M mutated GBMs were predominantly found in midline locations and G34R mutated GBMs are more prevalent in one of the two cerebral hemispheres, respective K27M or G34R transfected DF-1 cells were injected in midline or hemispheric parts of the mouse brain [48]. All injected animals were subjected to magnetic resonance imaging (MRI) every 4-8 weeks, displaying no tumors 7 months after injection of virus producing DF1 cells.

As described earlier, a frequent co-occurrence of *TP53* mutations is found in H3.3 mutant pedGBMs. All K27M mutated cases and approximately 67% of G34R mutated tumors had somatic mutations of *TP53* [30]. To determine the role of the TP53 pathway in enhancing the tumorigenic potential of mutated H3.3, mutant H3.3 and a dominant-negative variant of TP53 (dnTP53) were simultaneously overexpressed in the brain of Ntv-a mice. DnTP53 protein mainly consists of the TP53 tetramerization domain and has been shown to completely abolish endogenous TP53 function *in vivo* [168]. In order to inject dnTP53 together with H3.3 mutants, dnTP53 was cloned into the RCASBP(A) vector and transfected into DF-1 chicken fibroblasts. To detect the dnTP53 protein *in vivo* (separately from HA-tagged H3.3 variants), a carboxy-terminal AU1 tag was fused, which has been shown to have superior characteristics compared to other small epitope tags, when performing immunohistochemical detection of transgenes after CNS gene transfer [169, 170]. Before injection, expression of AU1-tagged dnTP53 in transfected DF-1 cells was confirmed by Western blot analysis (Figure 19B). Finally, fresh DF-1 cells were co-transfected with the AU1-tagged dnTP53 construct and one of the HA-tagged H3.3 variants. Injection of co-transfected DF-1 cells was again carried out in consideration of K27M or G34R relative tumor location (see above). A complete overview of all animals used for injection of mutated H3.3 and H3.3/dnTP53 co-injections is given in Figure 19C. As a result, 4 weeks post injection, one K27M/dnTP53 and one G34R/dnTP53 injected animal developed a brain tumor (Figure 19D). However, one of

the control animals, injected with wildtype H3.3 in combination with dnTP53 developed a brain tumor in the same time period. All other animals were sacrificed 6 months after injection without showing any brain abnormalities.

A

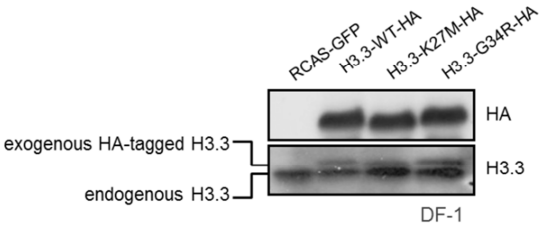


B

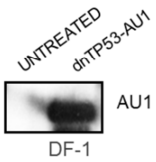


C

| CONSTRUCT | INJECTION SITE | NUMBER OF ANIMALS | TUMOR (TIMEPOINT) |
|---|---|---|---|
| H3.3-K27M-HA | Midline | 7 | 0 |
| H3.3-G34R-HA | Hemispheric | 6 | 0 |
| H3.3-WT-HA | Midline | 3 | 0 |
| H3.3-WT-HA | Hemispheric | 4 | 0 |
| H3.3-K27M-HA & dnTP53-AU1 | Midline | 6 | 1(d34) |
| H3.3-G34R-HA & dnTP53-AU1 | Hemispheric | 5 | 1(d34) |
| H3.3-WT-HA & dnTP53-AU1 | Midline | 2 | 1(d34) |
| H3.3-WT-HA & dnTP53-AU1 | Hemispheric | 2 | 0 |

D

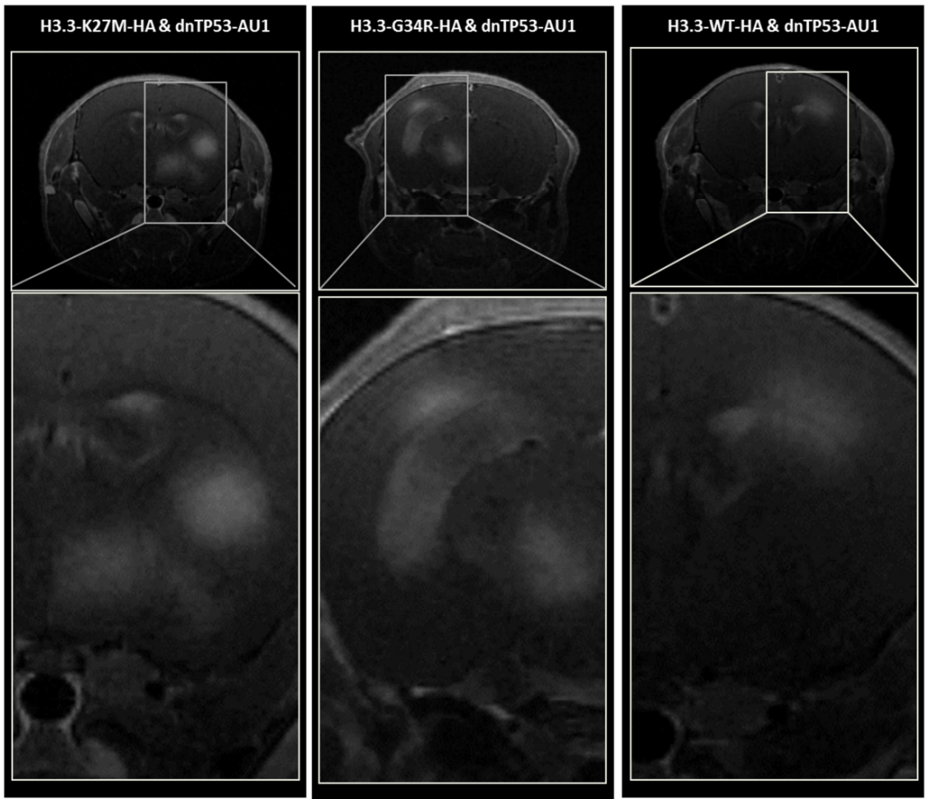


**Figure 19. *In vivo* tumorigenic potential of mutated H3.3.** Western blot analysis showing protein expression of HA-tagged H3.3 variants **(A)** and AU1-tagged dnTP53 **(B)** in transfected DF1 cells. **(C)** Overview of all *in vivo* experiments showing the respective construct, injection site, number of animals and the time point of tumor detection by MRI. **(D)** MRI images of brain tumors in mice after injection of the respective H3.3 variant and dnTP53.

# 5 DISCUSSION

The discovery of histone H3.3 mutations in nearly 50% of childhood glioblastoma and the identification of H3.3 mutation specific epigenetic subgroups has revolutionized our understanding of this devastating brain tumor. The data presented in this thesis provides novel insights into the complex alterations of the histone code induced by H3.3 mutants. The described findings set the stage for the translation of molecular advances into improved care for patients with this deadly disease.

## 5.1 Incorporation of mutant Histone H3.3

Since the successful cloning of the green fluorescent protein GFP of the jellyfish *Aequorea Victoria* in 1992, fluorescently labeled proteins have been used intensively to visualize protein localization *in vitro* and *in vivo* [171, 172]. Shortly after, the first fluorescently labeled histone proteins were generated leading to the observation that the fusion of relatively large epitope tags like GFP did not interfere with histone incorporation into nucleosomes [173]. Furthermore, it was shown that fluorescently labeled histone proteins, such as EGFP-tagged histone H3.3, undergo regular posttranslational modifications [160].

To determine whether the identified H3.3 mutations interfere with the nuclear import of the histone protein, EGFP-tagged variants of H3.3 were transfected into HEK293T or SF188 cells. Fluorescence microscopy revealed that both H3.3 mutant proteins were located exclusively within the cell nucleus of transfected cells (Figure 6). This is in line with published literature showing that nuclear localization of histone H3 proteins is not abolished by mutations affecting the histone tail or mutations resulting in truncated histone proteins, which are completely devoid of the histone tail [158].

Subsequent experiments were conducted to investigate potential spatial differences in the incorporation pattern of mutant H3.3 into chromatin. As an initial experiment, quantitative dual color fluorescence confocal imaging was applied to cells simultaneously expressing CFP-labeled wildtype H3.3 and one of the two H3.3 mutants tagged with EGFP. Data interpretation was performed by measuring the extent of signal overlap between both fluorophores. Recently, the same experimental setup was used to measure the degree of signal overlap between different fluorescently labeled histone proteins including H3.3. Moreover, this technique revealed that H3.3 is enriched in chromatin domains marked by activating histone modifications [160]. Based on the results presented here, no differences between mutant H3.3 and wildtype H3.3 localization were identified in SF188 glioblastoma cells. Although multichannel confocal imaging is a commonly used method in molecular biology to study the localization of distinct molecules in cellular environment, results might be misleading due to the limited spatial resolution of confocal microscopy of approximately 250 nm, which is mainly hampered by diffraction [174]. Compared to that, a single

nucleosome containing the complete histone octamer has a diameter of approximately 10 nm.

In a subsequent experiment, genome-wide incorporation profiles of mutant H3.3 were generated by performing chromatin immunoprecipitation followed by next generation sequencing (ChIP-Seq). ChIP-Seq offers the possibility to create genomic maps of precise protein incorporation sites at high resolution [175]. Within recent years, this method has been widely used to increase our knowledge about H3.3 incorporation sites in different cell types of various species [176-178]. By using an antibody targeting the HA-tag of overexpressed histone H3.3, genome-wide maps of incorporation sites of H3.3 mutants were generated and compared to the ChIP-Seq profile of (overexpressed) wildtype H3.3. In doing so, no apparent differences in protein incorporation of mutant and wildtype H3.3 have been identified (Figure 8).

Based on current literature, histone H3.3 is preferentially incorporated at sites of active transcription [157, 158, 179]. ChIP-Seq profiles illustrate that H3.3 is enriched at the transcriptional start site of actively transcribed genes but also in regions further downstream of the transcription termination signal [178]. At these sites, histone H3.3 is loaded onto DNA via the histone chaperone HIRA [122, 123]. Alternatively, H3.3 protein was found to be located at transcriptionally silent genomic regions at the telomeres and pericentromeric heterochromatin. Here, histone H3.3 is loaded onto DNA via an independent pathway including the chaperones ATRX and DAXX. A possible mechanism, how mutations of histone H3.3 affect its incorporation, is based on impaired interaction of the mutant protein with one of its chaperones. Up to now, the protein domains within histone H3.3, which mediate histone-chaperone interaction, are not elucidated in detail, but as it has recently been shown for the chaperone DAXX, a region located within the H3.3 core domain is responsible for H3.3-DAXX interaction [119]. Therefore, it is quite unlikely that the identified H3.3 mutations, which are located at the tail of H3.3, interfere with chromatin incorporation due to aberrant histone-chaperone interaction.

## 5.2 Global H3K27me3 Levels are reduced in K27M mutated pedGBMs

Posttranslational modifications of the amino-terminal tail of histone proteins including methylation of lysine residues have been known for decades to directly alter chromatin structure and gene expression. While histone H3 methylation of lysine 4 (H3K4me3) or lysine 36 (H3K36me3) are hallmarks of actively transcribed chromatin, methylation of lysine 9 (H3K9me3) or lysine 27 (H3K27me3) are overrepresented at inactive genes. In recent years, the status and establishment of the key histone mark H3K27me3 has become of particular interest in cancer biology. This is based on the fact that several factors involved

in the establishment or maintenance of H3K27me3 are known to be mutated or deregulated in a multitude of human cancer entities [137, 180].

The data depicted here also reports on the deregulation of H3K27me3 in K27M mutated pedGBMs. By using immunohistochemistry and Western blot analysis of primary tumor samples, it was demonstrated that pedGBMs, harboring the K27M mutation, show a global reduction of H3K27me3 levels (Figure 15). In contrast, G34R mutated tumors or tumors without *H3F3A* mutations exhibit high abundance of the H3K27me3 histone mark. As determined here, H3.3 protein in primary tumors is translated from transcripts of both H3.3 producing genes *H3F3A* and *H3F3B*. Furthermore, biallelic expression of *H3F3A* in pedGBMs was confirmed. In summary, this leads to the assumption that in tumors with heterozygous *H3F3A* mutations the relative amount of mutated H3.3 protein is approximately 25%. These findings together with the high abundance of canonical H3.1/H3.2, which is also detected by the H3K27me3 antibody, excludes the possibility that the global reduction of H3K27me3 is explained by the proportion of methionine containing H3.3, which never displays H3K27me3 (Figure 20). In conclusion, the data presented here reveals a strong dominant negative effect of K27M mutant H3.3 protein, which also impacts H3K27me3 expression at the amino-terminal tail of other histone proteins including canonical H3.1/H3.2.

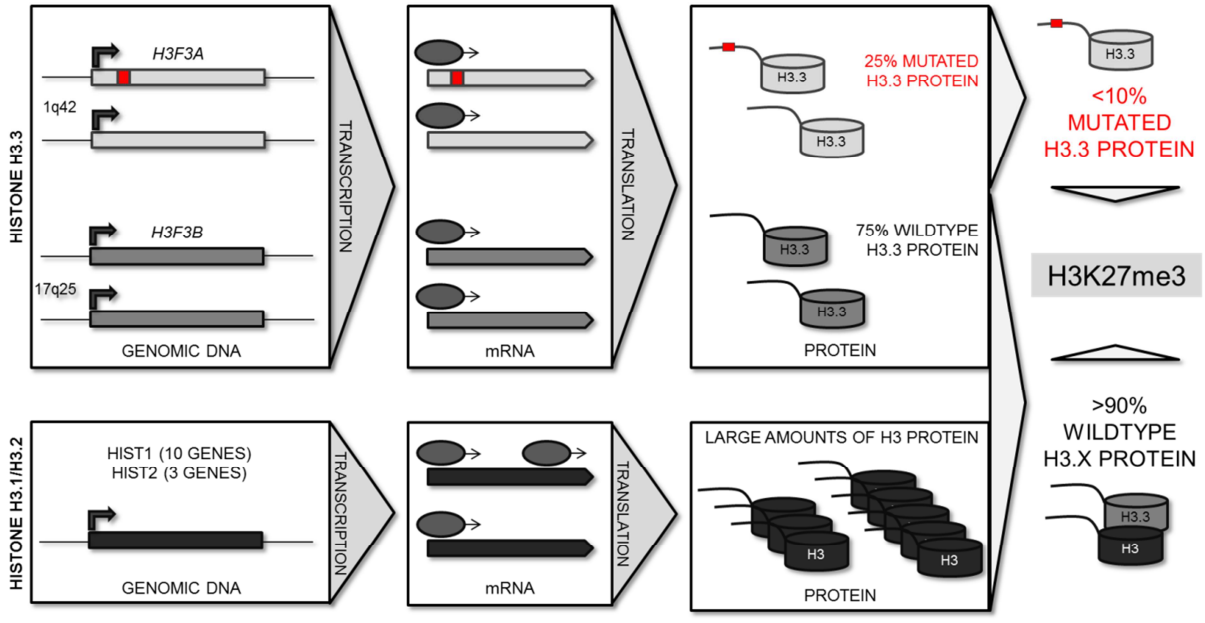


**Figure 20. Expression of mutant H3.3 in Primary Glioblastoma.** Both alleles of *H3F3A* (heterozygous mutation of *H3F3A* depicted in red) and *H3F3B* are transcribed into mRNA in primary glioblastoma. Therefore, only 25% of total H3.3 protein in a *H3F3A* mutated tumor cell harbors the mutation. In humans, canonical H3.1/H3.2 is transcribed from 13 different genes into polycistronic mRNA. Via translation, large amounts of H3 protein are synthesized during S-phase to wrap up the duplicated DNA. Finally, the amount of mutated H3.3 protein within a tumor cell does not exceed more than 10% of total H3 protein.

In line with our results, a strong dominant negative effect on global H3K27me3 expression has previously been reported for mutant canonical H3, which replaces lysine 27 by an arginine residue (H3K27R) [181]. In this study, global H3K27me3 levels were found to be dramatically reduced (approximately by 75%) by overexpressing the K27R mutant in CP70 human ovarian cancer cells. As in H3.3 mutated glioblastomas, gene expression is altered in CP70 cells overexpressing the H3 K27R mutant [181]. Furthermore, K27R overexpression lead to a significant reduction of global DNA methylation levels, resembling more the global DNA hypomethylation phenotype (CHOP) described in G34R mutant pedGBMs.

Two independent studies, focusing primarily on histone function in the development of flies and mice, showed that overexpression of K27R mutated H3.3 but not K27R mutated H3.1/3.2 induced severe developmental defects [182, 183]. Expression of H3.3 K27R resulted in accumulation of pericentromeric transcripts, localization defects of the heterochromatin protein HP1 as well as defective chromosome segregation. In addition, Santenard *et al.* revealed decreased levels of H3K27me3 expression to about 65% in H3.3 K27R overexpressing embryos. Besides that, H3K27me1 levels were decreased in the presence of K27R mutated H3.3, while other histone marks like H3K4me3 or H3K9me3 remained unaffected [182]. Taken together, this work concludes that the establishment of heterochromatin (reflected by H3K27me3 levels) in the early developing embryo is disturbed by the presence of K27R mutant H3.3. However, regulation of heterochromatin formation is not restricted to the early developing embryo. Dysregulation of heterochromatin is also known to increase susceptibility to cancer by several mechanisms. Less heterochromatin formation reflected by reduced H3K27me3 levels, for example, would lead to aberrant expression of oncogenes and increased genomic instability. Consistently, reduced H3K27me3 levels are associated with unfavorable prognosis in breast, ovarian and pancreatic cancers [70, 184]. Besides H3K27me3, impaired establishment of other heterochromatic histone marks such as H3K9me3 also increase tumor risk due to chromosomal instability *in vivo* [185]. Based on unpublished whole-genome sequencing data of our laboratory, however, K27M mutated pedGBMs do not show a higher frequency of chromosomal aberrations compared to non-mutated tumor samples.

Without reporting on heterochromatin formation, deregulated H3K27me3 levels have been demonstrated in a variety of human cancers. For most of these entities, H3K27me3 levels are altered due to genetic hits within the machinery responsible for H3K27me3 turnover. Elevated expression of the H3K27me3 establishing methyltransferase EZH2 is described in several human cancers including bladder, breast, gastric, lung and prostate cancer [186-189]. Here, the majority of tumors display activating mutations (e.g. Y641) or gene amplifications of EZH2. Other known mechanisms of EZH2 activation include the deletion of microRNA-101, which represents a negative regulator of EZH2 in prostate cancer [190].

These findings together with the identification of deleterious mutations of the H3K27me3 specific demethylase UTX (also known as KDM6A) point towards an oncogenic role of EZH2 and the H3K27me3 histone mark. [191]. However, the identification of several mutations leading to loss of EZH2 methyltransferase activity and reduced H3K27 trimethylation indicate a dual role of this histone mark. In pedGBMs, the presence of additional mutations (e.g. EZH2 or UTX), which would explain decreased H3K27me3 expression, was excluded by analyzing whole-exome sequencing data of K27M mutated tumor samples [30, 47].

As demonstrated here, the existence of deregulated H3K27me3 is a common event in human cancers. While for most of the entities the explanation is given by genetic hits in the H3K27me3 establishing machinery, the mechanism of H3K27me3 reduction by K27M mutant requires further investigation. One hypothesis about the mechanism of K27M induced reduction in H3K27me3 is based on the structural similarities between monomethylated lysine and its substituent methionine. The highly hydrophobic amino acid methionine represents the closest natural mimic of monomethylated lysine as it holds a terminal methyl group (Figure 21A). For this reason, methionine has already been used in other studies to imitate constitutively monomethylated lysine within H3 histone proteins [192]. Although the consequences of monomethylated H3K27 are discussed controversially, H3K27me1 is an essential intermediate in the establishment of H3K27 di- and trimethylation by the PRC1/2 complexes. Thus, the K27M mutant H3.3 protein could function as a permanently bound substrate due to the fact that the addition of a second methyl group to the sulfur atom of methionine is chemically not possible. In doing so, the K27M bound PRC1/2 complex is not able to methylate other H3 histones leading to a successive reduction of H3K27me3 levels.

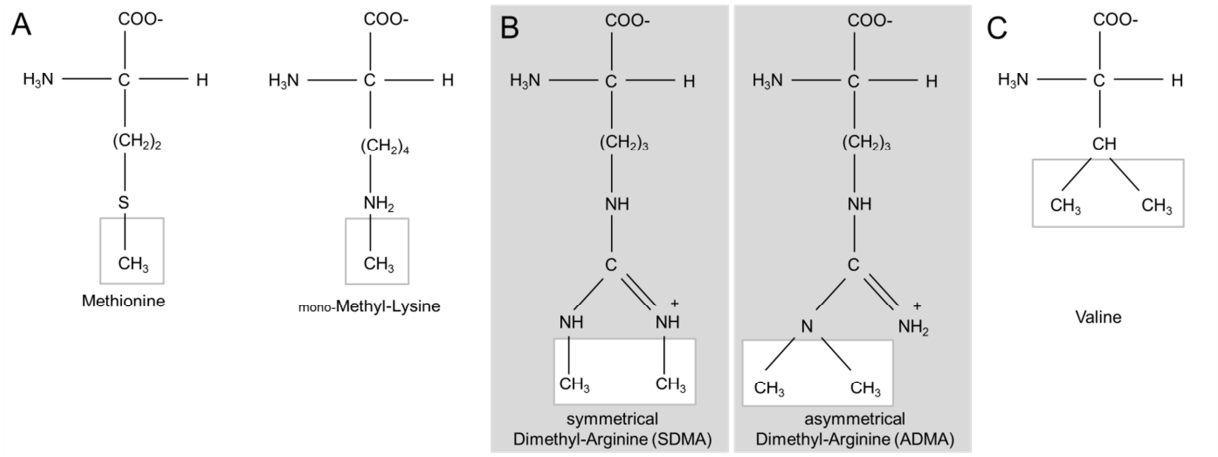


**Figure 21. Chemical Structure of (modified) Amino Acids. (A)** The highly hydrophobic amino acid methionine structurally resembles mono-methylated lysine as both complexes hold a terminal methyl group (framed). **(B)** Dimetylated arginines exist in symmetric (SDMA) or asymmetric conformation (ADMA) displaying differences in the linkage of the second methyl group (framed). **(C)** The amino acid valine structurally resembles dimethylated arginine based on the two terminal methyl groups.

A second potential mechanism of H3K27me3 downregulation via K27M mutant H3.3 is based on the maintenance model of the H3K27me3 histone mark during cell division [99, 193]. All controversially discussed models for the inheritance of histone methylation marks (reviewed in [70]) share one general feature: In order to preserve cellular identity, epigenetic marks including the repressive H3K27me3 mark, have to be transmitted to the next cell generation. Thus, the status of K27 methylation in the nucleosome at a respective genomic locus is copied to the daughter cell. Incorporated K27M mutant H3.3 protein, which is always devoid of methylation, would propagate the transmission of unmethylated lysine 27 to the daughter cell. If so, one would also assume that the effect of H3K27me3 downregulation is increasing over time because H3K27me3 needs to be diluted out with every round of cell division.

As demonstrated here, the K27M induced downregulation of the crucial epigenetic mark H3K27me3 was successfully recapitulated *in vitro* (see Figure 16). Overexpression of K27M mutant H3.3 in HEK293T and SF188 glioblastoma cells for 15 passages led to strongly decreased H3K27me3 levels. Since this phenotype was not detectable at earlier time points, it becomes apparent that H3K27me3 reduction progresses over time and is dependent on several rounds of cell divisions. Recently, Turcan *et al.* reported on the successive establishment of the CIMP phenotype in immortalized astrocytes by overexpression of R132H mutant IDH1 [194]. In these experiments, comprehensive changes in genome-wide DNA methylation were induced after an extended time of *in vitro* cultivation of astrocytes for up to 50 passages. An independent study reported on the constantly accumulating downregulation of transgene expression as a result of increasing DNA methylation and successive establishment of repressive histone marks in long time cultured chicken erythroid cells [195]. Thus, both studies consistently indicate that reshaping of the epigenome largely depends on extended time periods.

With respect to differential gene expression in K27M mutant primary pedGBMs, one should take into account that the presence of methionine at K27M mutant H3.3 also abolishes acetylation of this residue. H3K27 acetylation represents an epigenetic mark, which is directly implicated in the regulation of gene transcription [81, 196]. Acetylated H3K27 marks active enhancer regions, which are known to be highly enriched for H3.3 [197]. Western blot data presented here demonstrates that global H3K27ac levels are upregulated in tumors expressing K27M mutant H3.3. Loss of PRC2 activity, which results in reduced trimethylation of H3K27, has been described to result in a global increase in H3K27 acetylation [166, 167]. Thus, K27M induced downregulation of the repressive histone mark H3K27 might represent an essential step towards the establishment of transcriptional active chromatin via acetylation of H3K27.

### 5.3 Arginine 34 is posttranslationally modified at G34R mutated H3.3

While one of the H3.3 mutations found in pedGBMs abolishes an essential site of PTM by eliminating lysine 27, the second mutation creates a potential new site for PTMs by the presence of arginine instead of glycine 34 at the tail of G34R mutated histone H3.3. Mass spectrometry data presented here confirms this new site of PTM at the tail of G34R mutated H3.3 by detection of dimethylarginine 34 (R34me2).

In addition to the finding that arginine 34 is dimethylated at the tail of G34R mutant H3.3, this work also provides insights into potential functional consequences of the new PTM. As illustrated in Figure 17, R34me2 is associated with downregulation of K36 trimethylation in HEK293T cells and in the pediatric glioblastoma cell SF188. In general, trimethylation of lysine 36, which is located in close proximity to R34, is found at bodies of actively transcribed genes [198-200]. Notably, the crosstalk between arginine and lysine methylation is a wide-spread phenomenon at the tail of histone proteins, which has been named as arginine/lysine-methyl/methyl switches [201]. With regard to the histone tail of H3 (or H3.3), several arginine/lysine pairs are found including H3R2/H3K4, H3R8/H3K9 or H3R26/H3K27 (see also Figure 3). For all these arginine/lysine pairs, the arginine residue is located one or two amino acid position(s) upstream of the corresponding lysine residue. One of the best characterized arginine/lysine-methyl/methyl switches is the R2/K4 switch. For this switch it is well known that the methylation of arginine 2 by the protein arginine methyltransferase 6 (PRMT6) prevents the establishment of the K4me3 histone mark or *vice versa* [202, 203]. Trimethylation of lysine 4, which is established by the MLL1 complex, is (comparable to H3K36me3) an essential epigenetic mark in the establishment and maintenance of transcriptionally active chromatin [204]. Furthermore, the binding of H3K4 effector proteins such as the demethylase KDM4A (also referred to as JMJD2A), which contains a methylation-specific tudor domain, is sensitive for R2 methylation [205]. Interestingly, KDM4A was also reported to act on methyl groups at lysine 36 of histone H3 [206]. At the tail of G34R mutant H3.3, a similar conformation is generated by the presence of arginine at position 34. This conformation might represent the basis for a new arginie34/lysine36-methyl/methyl switch at G34R mutant H3.3. Remarkably, valine, the second amino acid, which was found to replace glycine 34 in G34V mutant H3.3 in some rare pedGBM cases, displays striking structural similarity to dimethylated arginine as it also holds two terminal methyl groups (Figure 21C).

Based on our mass spectrometry data, it cannot be distinguished, whether dimethylarginine 34 (R34me2) exists in symmetric (SDMA) or asymmetric (ADMA) conformation (Figure 21B). Since PRMTs show ADMA or SDMA specificity, the information about R34me2 conformation would be useful to narrow down the number of potential protein arginine methyltransferases (PRMTs) establishing R34 dimethylation. Although the number of PRMTs is constantly

growing, there are at least seven different PRMTs (PRMT1-4, 6, 8) catalyzing the production of asymmetric dimethyl arginine (ADMA) and two enzymes (PRMT 5, 7) producing the symmetrical variant [71]. Although numerous human cancers show aberrant PRMT expression, transcriptional deregulation of PRMTs has not been found in GBMs harboring a G34R mutation (Supplementary Figure 3). With the knowledge about the R34me2 establishing PRMT, specific PRMT inhibitors could be used, as they were shown to possess pharmacological and therapeutic potential [207-211].

In general, the histone tail of H3 has to adopt a conformation that fits into the substrate-binding groove of effector proteins without steric clashes. The conformation of G34R mutant H3.3 that fits into the binding groove of the H3K36me3 establishing machinery, might not only be negatively influenced by the presence of methyl groups at R34 but also by the elimination of glycine at position 34 itself. Both glycine residues at position 33 and 34 contribute to the overall flexibility of the H3 histone tail and consequently play an essential role in establishing the binding specificity of the H3K36 mediating demethylase KDM4A [212]. This H3K36 demethylase, which is also acting on H3K4, H3K9 and H4K20, is known to prefer small amino acid residues at the -2 position of the respective methylated lysine residue [206].

### 5.4 Establishment of a mutant H3.3 *in vitro* Cell Culture System

Pediatric glioblastomas expressing K27M or G34R mutated histone H3.3 are characterized by distinct gene expression profiles as well as different DNA methylation patterns [30, 48]. The work presented in this thesis was aiming at the establishment of an *in vitro* cell culture system, which can be used to recapitulate and characterize the molecular changes originally identified in H3.3 mutated pedGBMs.

Initially, several primary cell lines established from freshly dissected H3.3 mutated pedGBMs were used to study the functional consequences of H3.3 mutations *in vitro*. These cell lines were thought to represent the ideal cell culture model since these cells express mutant H3.3 from the endogenous *H3F3A* gene locus/gene promoter and include the genetic background, which in all likelihood contributes to the molecular phenotype of H3.3 mutated pedGBMs. After several months of *in vitro* cultivation, copy number data, which was produced as a by-product of genome-wide DNA-methylation analysis, revealed complex genetic changes for most of these primary cell lines (Supplementary Figure 4). In addition, sequencing of the *H3F3A* genomic locus failed to detect the respective *H3F3A* mutation in our primary cell line originally established from a K27M mutated tumor. Moreover, other scientists are also reporting on the unsuccessful *in vitro* cultivation of K27M mutant cell lines (private communication with Yoon-Jae Cho). Most likely, H3.3 mutated cells undergo negative

selection, leading to clonal expansion of non-mutated cells of the primary tumor. As a result, primary cell lines originating from H3.3 mutated tumors were not available to molecularly characterize H3.3 mutations *in vitro*.

Alternatively, overexpression of H3.3 mutants in previously established and well characterized glioblastoma cell lines was prioritized. As (nearly) all of the identified *H3F3A* mutations in pedGBMs were found to be monoallelic, expression of endogenous wildtype H3.3 seems to appropriately mimic the molecular phenotype detected in primary tumors. This is underlined by the presence of wildtype protein, which is produced from the second H3.3 producing gene *H3F3B* that has never been found to be mutated in pedGBMs. Thus, one would expect that the expression of mutant H3.3 *per se* induces changes, which cannot be compensated by co-expressed wildtype protein (dominant negative effect).

In order to determine, whether overexpression of mutant H3.3 induces similar effects on gene expression and DNA methylation *in vitro,* the pediatric glioblastoma cell line SF188 was used, since these cells carry *TP53* mutations, which were frequently found to co-exist in pedGBMs. In contrary, the use of HEK293T cells provides the advantage of characterizing mutant H3.3 in a more isolated way without any masking or amplifying effect due to other genetic hits. At first glance, SF188 cells as well as HEK293T cells did not show any significant alterations in gene expression, DNA methylation, PTMs or growth characteristics upon mutant H3.3 overexpression (see 4.3). At a later time point, it emerged that the dominant negative effect on H3K27me3 expression induced by the K27M mutant was only detectable after several rounds of *in vitro* passaging (see 4.5). Since this work has shown that primary pedGBMs express higher levels of mutant H3.3 compared to lentivirally transduced cells, the amount of mutant H3.3 protein might be of key importance to successfully recapitulate the phenotype of H3.3 mutated pedGBMs at a certain time point. Since ectopically expressed H3.3 has never been found to result in similar abundance of exogenous H3.3 compared to the endogenous protein, the combinatorial knockdown and overexpression approach described in 4.4 might help to induce the effects caused by mutant H3.3 at earlier time points [164, 213]. Currently, the investigation of cell lines overexpressing mutant H3.3 for at least 2 months as well as cells combining knockdown of endogenous H3.3 and mutant H3.3 overexpression is ongoing and includes genome-wide gene expression and DNA methylation profiling.

### 5.5 *In vivo* Tumorigenic Potential of mutant Histone H3.3

After infection of target cells by a retrovirus, the RNA genome of the virus is reversely transcribed into DNA and integrated into the host's genome. Due to this ability, retroviruses have been used intensively to shuttle genetic information into nearly any mammalian cell

type. By transfection of the avian sarcoma-leukosis virus-A derived vector RCAS into avian cells, infectious virus is produced, which is able to infect any cell type expressing the virus-entry mediating Tv-a receptor on its cell surface. The experiments conducted here used genetically modified mouse strains expressing the Tv-a receptor under the control of the nestin promoter (Ntv-a) to specifically target neural progenitor cells in the brain of newborn mice. This experimental setup has already been used to study the impact of other genes of interest in gliomagenesis [156, 214, 215]. The tumorigenic potential of mutant H3.3 was investigated by overexpression of mutant H3.3 in the brain of neonatal Ntv-a mice with consideration of the respective injection site (K27M midline; G34R hemispheric). In a second round of experiments, overexpression of H3.3 was introduced together with a dominant-negative variant of TP53 (dnTP53), which completely abrogates endogenous TP53 function [168]. While overexpression of mutant H3.3 alone was not sufficient to induce GBMs, the combination with dnTP53 resulted in brain tumors in one K27M, one G34R and one wildtype H3.3 overexpressing animal. This tumor distribution and the fact that all tumors were diagnosed at the same (early) time point suggest that impaired TP53 signaling was the major driving force of tumor induction. This is in line with published data showing that TP53 deficiency is heavily increasing the susceptibility to spontaneous tumors of various origin including brain tumors [216, 217]. *TP53* knockout mice will die due to cancer by the age of 10 months with 100% penetrance [218-220]. The high frequency of pedGBMs showing H3.3 and simultaneous *ATRX/DAXX* mutations might indicate that additional hits in chromatin modifiers within this pathway are required to induce tumors *in vivo*.

Targeting the respective cell of origin is of central importance to induce tumors *in vivo*. For H3.3 mutated pedGBMs, there is growing evidence that K27M and G34R mutated tumors are derived from different cells of origin, which is reflected by distinct tumor epigenomes. Moreover, both mutations are tightly linked to different tumor localization within the CNS and differential expression of well-known lineage markers like *OLIG1/2* and *FOXG1* [48]. In general, several cell types including neural stem cells and progenitor cells as well as astrocytes are discussed to represent the cell of origin of glioma [221]. Different genetic hits in quiescent neural progenitor cells have been proposed to specifically underlie the development of *IDH1* mutated gliomas [222]. In conclusion, the induction of GBM by expression of mutant histone H3.3 might be decisively dependent on targeting the correct cell type, which gives rise to this deadly brain tumor.

# 6 FUTURE PERSPECTIVES

Both mutations within the gene *H3F3A* coding for the replication independent histone variant H3.3 were shown to define distinct subgroups of pediatric glioblastoma, which are characterized by different genetic and epigenetic profiles. The molecular mechanisms leading to these defined genome-wide alterations are of particular relevance to develop new treatment options for patient suffering from this devastating brain tumor.

The molecular characterization of H3.3 mutations presented in this thesis provides evidence that H3.3 mutated pedGBMs are characterized by altered chromatin/histone modifications, which show mutation specificity. While K27M mutated pedGBMs are characterized by low levels of H3K27me3 due to the dominant negative effect of the K27M histone, the level of H3K36me3 at the tail of G34R mutant H3.3 is diminished, potentially caused by the presence of the new posttranslational modification identified in close proximity at arginine 34 of G34R mutant H3.3.

Future experiments concerning the K27M mutant should aim at the molecular mechanism of K27M induced H3K27me3 reduction. As a multitude of human cancers is characterized by dysregulation of the H3K27me3 establishing methyltransferase EZH2 and the PRC2 complex, localization of EZH2, its enzymatic activity and binding affinity to K27M mutant H3.3 should be investigated in more detail. In order to do so, co-IP experiments using modified synthetic peptides are currently conducted to determine the binding affinity of EZH2 to K27M mutant H3.3. Genome-wide DNA methylation analysis and gene expression profiling of K27M transduced cell lines together with H3K27me3 ChIP-Seq data of primary tumors and/or K27M overexpressing cell lines will further enhance our knowledge about the K27M induced epigenetic changes.

With respect to G34R mutated H3.3, the relationship between arginine 34 methylation and lysine 36 trimethylation needs further investigation. Therefore, mass spectrometry of primary tumor samples was initiated to dissect the pattern of PTMs at G34R mutant proteins. Furthermore, one should aim at the identification of R34me2 epigenetic readers by performing pulldown assays using unmodified and modified synthetic peptides of G34R mutant H3.3. In parallel, these co-IP experiments potentially lead to the identification of the R34me2 establishing protein arginine methyltransferase.

The establishment of *in vitro* cell culture models, which mimic the transcriptomic and epigenetic changes of H3.3 mutant pedGBM, is of particular importance. These *in vitro* models are desperately needed to make the next step and translate the molecular findings of mutant H3.3 into clinical settings. Comprehensive drug screening assays on *in vitro* and/or *in vivo* models will aim at the identification of compounds targeting H3.3 mutated tumor cells with high specificity.

Currently, the screening of additional primary cell lines of H3.3 mutated tumors is ongoing, to support additional *in vitro* experiments.

In conclusion, this thesis provides innovative insights into the genetic and epigenetic changes induced by mutant histone H3.3. In nearly 50% of pediatric glioblastomas, a genetic lesion within the *H3F3A* gene reshapes the epigenome of the tumor including DNA methylation and histone modifications, which consequently results in aberrant gene activation/repression. Thus, H3.3 mutated pedGBMs are a disease of the (epi)genome.

# 7 REFERENCES


1. *IUPAC-IUB Commission on Biochemical Nomenclature. A one-letter notation for amino acid sequences. Tentative rules.* Biochem J, 1969. **113**(1): p. 1-4.
2. Hansemann, D., *Ueber asymmetrische Zelltheilung in Epithelkrebsen und deren biologische Bedeutung. [On the asymmetrical cell division in epithelial cancers and its biological significance].* Arch Pathol Anat etc. Berl (Virchow's Arch), 1890(119): p. 299-326.
3. Boveri, T., *Concerning the origin of malignant tumours by Theodor Boveri. Translated and annotated by Henry Harris.* J Cell Sci, 2008. **121 Suppl 1**: p. 1-84.
4. Jemal, A., et al., *Global cancer statistics.* CA Cancer J Clin, 2011. **61**(2): p. 69-90.
5. World Health Organization, *Cancer Fact Sheet Reviewed January 2013.* 2013.
6. Siegel, R., D. Naishadham, and A. Jemal, *Cancer statistics, 2013.* CA Cancer J Clin, 2013. **63**(1): p. 11-30.
7. Hanahan, D. and R.A. Weinberg, *The hallmarks of cancer.* Cell, 2000. **100**(1): p. 57-70.
8. Cairns, R.A., I.S. Harris, and T.W. Mak, *Regulation of cancer cell metabolism.* Nat Rev Cancer, 2011. **11**(2): p. 85-95.
9. Hanahan, D. and R.A. Weinberg, *Hallmarks of cancer: the next generation.* Cell, 2011. **144**(5): p. 646-74.
10. Jones, D.T., et al., *Dissecting the genomic complexity underlying medulloblastoma.* Nature, 2012. **488**(7409): p. 100-5.
11. Northcott, P.A., et al., *Medulloblastomics: the end of the beginning.* Nat Rev Cancer, 2012. **12**(12): p. 818-34.
12. International Cancer Genome, C., et al., *International network of cancer genome projects.* Nature, 2010. **464**(7291): p. 993-8.
13. Feinberg, A.P. and B. Tycko, *The history of cancer epigenetics.* Nat Rev Cancer, 2004. **4**(2): p. 143-53.
14. Baylin, S.B. and P.A. Jones, *A decade of exploring the cancer epigenome - biological and translational implications.* Nat Rev Cancer, 2011. **11**(10): p. 726-34.
15. Berman, B.P., et al., *Regions of focal DNA hypermethylation and long-range hypomethylation in colorectal cancer coincide with nuclear lamina-associated domains.* Nat Genet, 2012. **44**(1): p. 40-6.
16. Hansen, K.D., et al., *Increased methylation variation in epigenetic domains across cancer types.* Nat Genet, 2011. **43**(8): p. 768-75.
17. Jones, P.A. and S.B. Baylin, *The fundamental role of epigenetic events in cancer.* Nat Rev Genet, 2002. **3**(6): p. 415-28.
18. Jemal, A., et al., *Global patterns of cancer incidence and mortality rates and trends.* Cancer Epidemiol Biomarkers Prev, 2010. **19**(8): p. 1893-907.
19. Cook, M.B., et al., *Sex disparities in cancer mortality and survival.* Cancer Epidemiol Biomarkers Prev, 2011. **20**(8): p. 1629-37.
20. CBTRUS, *CBTRUS Statistical Report: Primary Brain and Central Nervous System Tumors Diagnosed in the United States in 2004-2008 (March 23, 2012 Revision).* Central Brain Tumor Registry of the United States, Hinsdale, IL. website: www.cbtrus.org, 2012.
21. Hunger, S.P., et al., *Improved survival for children and adolescents with acute lymphoblastic leukemia between 1990 and 2005: a report from the children's oncology group.* J Clin Oncol, 2012. **30**(14): p. 1663-9.
22. Gilbertson, R., *Paediatric embryonic brain tumours. biological and clinical relevance of molecular genetic abnormalities.* Eur J Cancer, 2002. **38**(5): p. 675-85.
23. Khatua, S., et al., *Brain tumors in children--current therapies and newer directions.* Indian J Pediatr, 2012. **79**(7): p. 922-7.
24. Pfaff, E., et al., *TP53 mutation is frequently associated with CTNNB1 mutation or MYCN amplification and is compatible with long-term survival in medulloblastoma.* J Clin Oncol, 2010. **28**(35): p. 5188-96.

25. Garre, M.L., et al., *Medulloblastoma variants: age-dependent occurrence and relation to Gorlin syndrome--a new clinical perspective.* Clin Cancer Res, 2009. **15**(7): p. 2463-71.
26. Hamilton, S.R., et al., *The molecular basis of Turcot's syndrome.* N Engl J Med, 1995. **332**(13): p. 839-47.
27. Farrell, C.J. and S.R. Plotkin, *Genetic causes of brain tumors: neurofibromatosis, tuberous sclerosis, von Hippel-Lindau, and other syndromes.* Neurol Clin, 2007. **25**(4): p. 925-46, viii.
28. Pollack, I.F., *Pediatric brain tumors.* Semin Surg Oncol, 1999. **16**(2): p. 73-90.
29. Paugh, B.S., et al., *Integrated molecular genetic profiling of pediatric high-grade gliomas reveals key differences with the adult disease.* J Clin Oncol, 2010. **28**(18): p. 3061-8.
30. Schwartzentruber, J., et al., *Driver mutations in histone H3.3 and chromatin remodelling genes in paediatric glioblastoma.* Nature, 2012. **482**(7384): p. 226-31.
31. Lannering, B., et al., *Long-term sequelae after pediatric brain tumors: their effect on disability and quality of life.* Med Pediatr Oncol, 1990. **18**(4): p. 304-10.
32. Rutkowski, S., et al., *Treatment of early childhood medulloblastoma by postoperative chemotherapy alone.* N Engl J Med, 2005. **352**(10): p. 978-86.
33. Gilbertson, R.J. and J.N. Rich, *Making a tumour's bed: glioblastoma stem cells and the vascular niche.* Nat Rev Cancer, 2007. **7**(10): p. 733-6.
34. Percival Bailey, H.C., *Classification of the Tumours of the Glioma Group on a Histogenetic Basis With a Correlated Study of Prognosis.* JB Lippincott, Philadelphia 1926.
35. Gladson, C.L., R.A. Prayson, and W.M. Liu, *The pathobiology of glioma tumors.* Annu Rev Pathol, 2010. **5**: p. 33-50.
36. Louis, D.N., et al., *The 2007 WHO classification of tumours of the central nervous system.* Acta Neuropathol, 2007. **114**(2): p. 97-109.
37. Preusser, M., et al., *Current concepts and management of glioblastoma.* Ann Neurol, 2011. **70**(1): p. 9-21.
38. Stupp, R., et al., *Radiotherapy plus concomitant and adjuvant temozolomide for glioblastoma.* N Engl J Med, 2005. **352**(10): p. 987-96.
39. Kleihues, P. and H. Ohgaki, *Primary and secondary glioblastomas: from concept to clinical diagnosis.* Neuro Oncol, 1999. **1**(1): p. 44-51.
40. Ohgaki, H. and P. Kleihues, *Genetic pathways to primary and secondary glioblastoma.* Am J Pathol, 2007. **170**(5): p. 1445-53.
41. Bax, D.A., et al., *A distinct spectrum of copy number aberrations in pediatric high-grade gliomas.* Clin Cancer Res, 2010. **16**(13): p. 3368-77.
42. Parsons, D.W., et al., *An integrated genomic analysis of human glioblastoma multiforme.* Science, 2008. **321**(5897): p. 1807-12.
43. Qu, H.Q., et al., *Genome-wide profiling using single-nucleotide polymorphism arrays identifies novel chromosomal imbalances in pediatric glioblastomas.* Neuro Oncol, 2010. **12**(2): p. 153-63.
44. Yan, H., et al., *IDH1 and IDH2 mutations in gliomas.* N Engl J Med, 2009. **360**(8): p. 765-73.
45. Korshunov, A., et al., *Molecular staging of intracranial ependymoma in children and adults.* J Clin Oncol, 2010. **28**(19): p. 3182-90.
46. Lokker, N.A., et al., *Platelet-derived growth factor (PDGF) autocrine signaling regulates survival and mitogenic pathways in glioblastoma cells: evidence that the novel PDGF-C and PDGF-D ligands may play a role in the development of brain tumors.* Cancer Res, 2002. **62**(13): p. 3729-35.
47. Wu, G., et al., *Somatic histone H3 alterations in pediatric diffuse intrinsic pontine gliomas and non-brainstem glioblastomas.* Nat Genet, 2012. **44**(3): p. 251-3.
48. Sturm, D., et al., *Hotspot Mutations in H3F3A and IDH1 Define Distinct Epigenetic and Biological Subgroups of Glioblastoma.* Cancer Cell, 2012. **22**(4): p. 425-37.

49. Khuong-Quang, D.A., et al., *K27M mutation in histone H3.3 defines clinically and biologically distinct subgroups of pediatric diffuse intrinsic pontine gliomas.* Acta Neuropathol, 2012. **124**(3): p. 439-47.
50. Chowdhury, R., et al., *The oncometabolite 2-hydroxyglutarate inhibits histone lysine demethylases.* EMBO Rep, 2011. **12**(5): p. 463-9.
51. Xu, W., et al., *Oncometabolite 2-hydroxyglutarate is a competitive inhibitor of alpha-ketoglutarate-dependent dioxygenases.* Cancer Cell, 2011. **19**(1): p. 17-30.
52. Noushmehr, H., et al., *Identification of a CpG island methylator phenotype that defines a distinct subgroup of glioma.* Cancer Cell, 2010. **17**(5): p. 510-22.
53. Heaphy, C.M., et al., *Altered telomeres in tumors with ATRX and DAXX mutations.* Science, 2011. **333**(6041): p. 425.
54. Liu, X.Y., et al., *Frequent ATRX mutations and loss of expression in adult diffuse astrocytic tumors carrying IDH1/IDH2 and TP53 mutations.* Acta Neuropathol, 2012. **124**(5): p. 615-25.
55. Luger, K., et al., *Crystal structure of the nucleosome core particle at 2.8 A resolution.* Nature, 1997. **389**(6648): p. 251-60.
56. Kornberg, R.D., *Chromatin structure: a repeating unit of histones and DNA.* Science, 1974. **184**(4139): p. 868-71.
57. Akey, C.W. and K. Luger, *Histone chaperones and nucleosome assembly.* Curr Opin Struct Biol, 2003. **13**(1): p. 6-14.
58. McGhee, J.D., et al., *Orientation of the nucleosome within the higher order structure of chromatin.* Cell, 1980. **22**(1 Pt 1): p. 87-96.
59. Graziano, V., et al., *Histone H1 is located in the interior of the chromatin 30-nm filament.* Nature, 1994. **368**(6469): p. 351-4.
60. Felsenfeld, G. and J.D. McGhee, *Structure of the 30 nm chromatin fiber.* Cell, 1986. **44**(3): p. 375-7.
61. Grigoryev, S.A. and C.L. Woodcock, *Chromatin organization - the 30 nm fiber.* Exp Cell Res, 2012. **318**(12): p. 1448-55.
62. Maeshima, K., S. Hihara, and M. Eltsov, *Chromatin structure: does the 30-nm fibre exist in vivo?* Curr Opin Cell Biol, 2010. **22**(3): p. 291-7.
63. Fussner, E., R.W. Ching, and D.P. Bazett-Jones, *Living without 30nm chromatin fibers.* Trends Biochem Sci, 2011. **36**(1): p. 1-6.
64. Horn, P.J. and C.L. Peterson, *Molecular biology. Chromatin higher order folding--wrapping up transcription.* Science, 2002. **297**(5588): p. 1824-7.
65. Filipski, J., et al., *Periodicity of DNA folding in higher order chromatin structures.* EMBO J, 1990. **9**(4): p. 1319-27.
66. McBryant, S.J., V.H. Adams, and J.C. Hansen, *Chromatin architectural proteins.* Chromosome Res, 2006. **14**(1): p. 39-51.
67. Arents, G. and E.N. Moudrianakis, *The histone fold: a ubiquitous architectural motif utilized in DNA compaction and protein dimerization.* Proc Natl Acad Sci U S A, 1995. **92**(24): p. 11170-4.
68. Cox, S.G., et al., *An essential role of variant histone h3.3 for ectomesenchyme potential of the cranial neural crest.* PLoS Genet, 2012. **8**(9): p. e1002938.
69. Murray, K., *The Occurrence of Epsilon-N-Methyl Lysine in Histones.* Biochemistry, 1964. **3**: p. 10-5.
70. Greer, E.L. and Y. Shi, *Histone methylation: a dynamic mark in health, disease and inheritance.* Nat Rev Genet, 2012. **13**(5): p. 343-57.
71. Di Lorenzo, A. and M.T. Bedford, *Histone arginine methylation.* FEBS Lett, 2011. **585**(13): p. 2024-31.
72. Nowak, S.J. and V.G. Corces, *Phosphorylation of histone H3: a balancing act between chromosome condensation and transcriptional activation.* Trends Genet, 2004. **20**(4): p. 214-20.
73. Eberharter, A. and P.B. Becker, *Histone acetylation: a switch between repressive and permissive chromatin. Second in review series on chromatin dynamics.* EMBO Rep, 2002. **3**(3): p. 224-9.

74. Weake, V.M. and J.L. Workman, *Histone ubiquitination: triggering gene activity.* Mol Cell, 2008. **29**(6): p. 653-63.
75. Shiio, Y. and R.N. Eisenman, *Histone sumoylation is associated with transcriptional repression.* Proc Natl Acad Sci U S A, 2003. **100**(23): p. 13225-30.
76. Camporeale, G., et al., *K8 and K12 are biotinylated in human histone H4.* Eur J Biochem, 2004. **271**(11): p. 2257-63.
77. Messner, S., et al., *PARP1 ADP-ribosylates lysine residues of the core histone tails.* Nucleic Acids Res, 2010. **38**(19): p. 6350-62.
78. Liebich, H.M., et al., *Non-enzymatic glycation of histones.* Biol Mass Spectrom, 1993. **22**(2): p. 121-3.
79. Garcia-Gimenez, J.L., et al., *Histone carbonylation occurs in proliferating cells.* Free Radic Biol Med, 2012. **52**(8): p. 1453-64.
80. Tan, M., et al., *Identification of 67 histone marks and histone lysine crotonylation as a new type of histone modification.* Cell, 2011. **146**(6): p. 1016-28.
81. Strahl, B.D. and C.D. Allis, *The language of covalent histone modifications.* Nature, 2000. **403**(6765): p. 41-5.
82. Jenuwein, T. and C.D. Allis, *Translating the histone code.* Science, 2001. **293**(5532): p. 1074-80.
83. Downs, J.A., M.C. Nussenzweig, and A. Nussenzweig, *Chromatin dynamics and the preservation of genetic information.* Nature, 2007. **447**(7147): p. 951-8.
84. Soria, G., S.E. Polo, and G. Almouzni, *Prime, repair, restore: the active role of chromatin in the DNA damage response.* Mol Cell, 2012. **46**(6): p. 722-34.
85. Campos, E.I. and D. Reinberg, *Histones: annotating chromatin.* Annu Rev Genet, 2009. **43**: p. 559-99.
86. Kolasinska-Zwierz, P., et al., *Differential chromatin marking of introns and expressed exons by H3K36me3.* Nat Genet, 2009. **41**(3): p. 376-81.
87. Young, M.D., et al., *ChIP-seq analysis reveals distinct H3K27me3 profiles that correlate with transcriptional activity.* Nucleic Acids Res, 2011. **39**(17): p. 7415-27.
88. Bernstein, B.E., et al., *A bivalent chromatin structure marks key developmental genes in embryonic stem cells.* Cell, 2006. **125**(2): p. 315-26.
89. Roh, T.Y., et al., *The genomic landscape of histone modifications in human T cells.* Proc Natl Acad Sci U S A, 2006. **103**(43): p. 15782-7.
90. Shi, Y., et al., *Histone demethylation mediated by the nuclear amine oxidase homolog LSD1.* Cell, 2004. **119**(7): p. 941-53.
91. Yang, Y. and M.T. Bedford, *Protein arginine methyltransferases and cancer.* Nat Rev Cancer, 2013. **13**(1): p. 37-50.
92. Chang, B., et al., *JMJD6 is a histone arginine demethylase.* Science, 2007. **318**(5849): p. 444-7.
93. Gershey, E.L., et al., *Chemical studies of histone methylation. Evidence for the occurrence of 3-methylhistidine in avian erythrocyte histone fractions.* J Biol Chem, 1969. **244**(18): p. 4871-7.
94. Banerjee, T. and D. Chakravarti, *A peek into the complex realm of histone phosphorylation.* Mol Cell Biol, 2011. **31**(24): p. 4858-73.
95. Liokatis, S., et al., *Phosphorylation of histone H3 Ser10 establishes a hierarchy for subsequent intramolecular modification events.* Nat Struct Mol Biol, 2012. **19**(8): p. 819-23.
96. Margueron, R. and D. Reinberg, *The Polycomb complex PRC2 and its mark in life.* Nature, 2011. **469**(7330): p. 343-9.
97. Schmitges, F.W., et al., *Histone methylation by PRC2 is inhibited by active chromatin marks.* Mol Cell, 2011. **42**(3): p. 330-41.
98. Cao, R. and Y. Zhang, *SUZ12 is required for both the histone methyltransferase activity and the silencing function of the EED-EZH2 complex.* Mol Cell, 2004. **15**(1): p. 57-67.
99. Hansen, K.H., et al., *A model for transmission of the H3K27me3 epigenetic mark.* Nat Cell Biol, 2008. **10**(11): p. 1291-300.

100. Margueron, R., et al., *Role of the polycomb protein EED in the propagation of repressive histone marks.* Nature, 2009. **461**(7265): p. 762-7.
101. Shen, X., et al., *EZH1 mediates methylation on histone H3 lysine 27 and complements EZH2 in maintaining stem cell identity and executing pluripotency.* Mol Cell, 2008. **32**(4): p. 491-502.
102. Mousavi, K., et al., *Polycomb protein Ezh1 promotes RNA polymerase II elongation.* Mol Cell, 2012. **45**(2): p. 255-62.
103. Yang, Y., et al., *Computer modeling reveals that modifications of the histone tail charges define salt-dependent interaction of the nucleosome core particles.* Biophys J, 2009. **96**(6): p. 2082-94.
104. Musselman, C.A. and T.G. Kutateladze, *Handpicking epigenetic marks with PHD fingers.* Nucleic Acids Res, 2011. **39**(21): p. 9061-71.
105. Qiu, C., et al., *The PWWP domain of mammalian DNA methyltransferase Dnmt3b defines a new family of DNA-binding folds.* Nat Struct Biol, 2002. **9**(3): p. 217-24.
106. Jones, D.O., I.G. Cowell, and P.B. Singh, *Mammalian chromodomain proteins: their role in genome organisation and expression.* Bioessays, 2000. **22**(2): p. 124-37.
107. Dhalluin, C., et al., *Structure and ligand of a histone acetyltransferase bromodomain.* Nature, 1999. **399**(6735): p. 491-6.
108. Dawson, M.A., T. Kouzarides, and B.J. Huntly, *Targeting epigenetic readers in cancer.* N Engl J Med, 2012. **367**(7): p. 647-57.
109. Pusarla, R.H. and P. Bhargava, *Histones in functional diversification. Core histone variants.* FEBS J, 2005. **272**(20): p. 5149-68.
110. Young, N.L., P.A. Dimaggio, and B.A. Garcia, *The significance, development and progress of high-throughput combinatorial histone code analysis.* Cell Mol Life Sci, 2010. **67**(23): p. 3983-4000.
111. Thatcher, T.H. and M.A. Gorovsky, *Phylogenetic analysis of the core histones H2A, H2B, H3, and H4.* Nucleic Acids Res, 1994. **22**(2): p. 174-9.
112. Ederveen, T.H., I.K. Mandemaker, and C. Logie, *The human histone H3 complement anno 2011.* Biochim Biophys Acta, 2011. **1809**(10): p. 577-86.
113. Jaeger, S., et al., *Expression of metazoan replication-dependent histone genes.* Biochimie, 2005. **87**(9-10): p. 827-34.
114. Smith, S. and B. Stillman, *Purification and characterization of CAF-I, a human cell factor required for chromatin assembly during DNA replication in vitro.* Cell, 1989. **58**(1): p. 15-25.
115. Shibahara, K. and B. Stillman, *Replication-dependent marking of DNA by PCNA facilitates CAF-1-coupled inheritance of chromatin.* Cell, 1999. **96**(4): p. 575-85.
116. Hake, S.B., et al., *Serine 31 phosphorylation of histone variant H3.3 is specific to regions bordering centromeres in metaphase chromosomes.* Proc Natl Acad Sci U S A, 2005. **102**(18): p. 6344-9.
117. Schulmeister, A., M. Schmid, and E.M. Thompson, *Phosphorylation of the histone H3.3 variant in mitosis and meiosis of the urochordate Oikopleura dioica.* Chromosome Res, 2007. **15**(2): p. 189-201.
118. Postberg, J., et al., *The evolutionary history of histone H3 suggests a deep eukaryotic root of chromatin modifying mechanisms.* BMC Evol Biol, 2010. **10**: p. 259.
119. Liu, C.P., et al., *Structure of the variant histone H3.3-H4 heterodimer in complex with its chaperone DAXX.* Nat Struct Mol Biol, 2012. **19**(12): p. 1287-92.
120. Tagami, H., et al., *Histone H3.1 and H3.3 complexes mediate nucleosome assembly pathways dependent or independent of DNA synthesis.* Cell, 2004. **116**(1): p. 51-61.
121. Elsaesser, S.J. and C.D. Allis, *HIRA and Daxx constitute two independent histone H3.3-containing predeposition complexes.* Cold Spring Harb Symp Quant Biol, 2010. **75**: p. 27-34.
122. Ray-Gallet, D., et al., *HIRA is critical for a nucleosome assembly pathway independent of DNA synthesis.* Mol Cell, 2002. **9**(5): p. 1091-100.
123. Loppin, B., et al., *The histone H3.3 chaperone HIRA is essential for chromatin assembly in the male pronucleus.* Nature, 2005. **437**(7063): p. 1386-90.

124. Konev, A.Y., et al., *CHD1 motor protein is required for deposition of histone variant H3.3 into chromatin in vivo.* Science, 2007. **317**(5841): p. 1087-90.
125. Hake, S.B., et al., *Expression patterns and post-translational modifications associated with mammalian histone H3 variants.* J Biol Chem, 2006. **281**(1): p. 559-68.
126. Lewis, P.W., et al., *Daxx is an H3.3-specific histone chaperone and cooperates with ATRX in replication-independent chromatin assembly at telomeres.* Proc Natl Acad Sci U S A, 2010. **107**(32): p. 14075-80.
127. Cui, B. and M.A. Gorovsky, *Centromeric histone H3 is essential for vegetative cell division and for DNA elimination during conjugation in Tetrahymena thermophila.* Mol Cell Biol, 2006. **26**(12): p. 4499-510.
128. Sakai, A., et al., *Transcriptional and developmental functions of the H3.3 histone variant in Drosophila.* Curr Biol, 2009. **19**(21): p. 1816-20.
129. Hodl, M. and K. Basler, *Transcription in the absence of histone H3.3.* Curr Biol, 2009. **19**(14): p. 1221-6.
130. Witt, O., W. Albig, and D. Doenecke, *Testis-specific expression of a novel human H3 histone gene.* Exp Cell Res, 1996. **229**(2): p. 301-6.
131. Tachiwana, H., et al., *Nucleosome formation with the testis-specific histone H3 variant, H3t, by human nucleosome assembly proteins in vitro.* Nucleic Acids Res, 2008. **36**(7): p. 2208-18.
132. Schenk, R., et al., *H3.5 is a novel hominid-specific histone H3 variant that is specifically expressed in the seminiferous tubules of human testes.* Chromosoma, 2011. **120**(3): p. 275-85.
133. Wiedemann, S.M., et al., *Identification and characterization of two novel primate-specific histone H3 variants, H3.X and H3.Y.* J Cell Biol, 2010. **190**(5): p. 777-91.
134. Sullivan, K.F., M. Hechenberger, and K. Masri, *Human CENP-A contains a histone H3 related histone fold domain that is required for targeting to the centromere.* J Cell Biol, 1994. **127**(3): p. 581-92.
135. Palmer, D.K., et al., *Purification of the centromere-specific protein CENP-A and demonstration that it is a distinctive histone.* Proc Natl Acad Sci U S A, 1991. **88**(9): p. 3734-8.
136. Chi, P., C.D. Allis, and G.G. Wang, *Covalent histone modifications--miswritten, misinterpreted and mis-erased in human cancers.* Nat Rev Cancer, 2010. **10**(7): p. 457-69.
137. Chase, A. and N.C. Cross, *Aberrations of EZH2 in cancer.* Clin Cancer Res, 2011. **17**(9): p. 2613-8.
138. Chang, C.J. and M.C. Hung, *The role of EZH2 in tumour progression.* Br J Cancer, 2012. **106**(2): p. 243-7.
139. Ansari, K.I., S. Kasiri, and S.S. Mandal, *Histone methylase MLL1 has critical roles in tumor growth and angiogenesis and its knockdown suppresses tumor growth in vivo.* Oncogene, 2012.
140. Hasselblatt, M., et al., *Nonsense mutation and inactivation of SMARCA4 (BRG1) in an atypical teratoid/rhabdoid tumor showing retained SMARCB1 (INI1) expression.* Am J Surg Pathol, 2011. **35**(6): p. 933-5.
141. Hasselblatt, M., et al., *High-resolution genomic analysis suggests the absence of recurrent genomic alterations other than SMARCB1 aberrations in atypical teratoid/rhabdoid tumors.* Genes Chromosomes Cancer, 2013. **52**(2): p. 185-90.
142. Wang, G.G., et al., *NUP98-NSD1 links H3K36 methylation to Hox-A gene activation and leukaemogenesis.* Nat Cell Biol, 2007. **9**(7): p. 804-12.
143. Berdasco, M. and M. Esteller, *Aberrant epigenetic landscape in cancer: how cellular identity goes awry.* Dev Cell, 2010. **19**(5): p. 698-711.
144. Lu, C., et al., *IDH mutation impairs histone demethylation and results in a block to cell differentiation.* Nature, 2012. **483**(7390): p. 474-8.
145. Jakovcevski, M. and S. Akbarian, *Epigenetic mechanisms in neurological disease.* Nat Med, 2012. **18**(8): p. 1194-204.
146. Kurotaki, N., et al., *Haploinsufficiency of NSD1 causes Sotos syndrome.* Nat Genet, 2002. **30**(4): p. 365-6.

147. Berdasco, M., et al., *Epigenetic inactivation of the Sotos overgrowth syndrome gene histone methyltransferase NSD1 in human neuroblastoma and glioma.* Proc Natl Acad Sci U S A, 2009. **106**(51): p. 21830-5.
148. Amir, R.E., et al., *Rett syndrome is caused by mutations in X-linked MECP2, encoding methyl-CpG-binding protein 2.* Nat Genet, 1999. **23**(2): p. 185-8.
149. Iwase, S., et al., *The X-linked mental retardation gene SMCX/JARID1C defines a family of histone H3 lysine 4 demethylases.* Cell, 2007. **128**(6): p. 1077-88.
150. De La Fuente, R., C. Baumann, and M.M. Viveiros, *Role of ATRX in chromatin structure and function: implications for chromosome instability and human disease.* Reproduction, 2011. **142**(2): p. 221-34.
151. Miller, S.A., D.D. Dykes, and H.F. Polesky, *A simple salting out procedure for extracting DNA from human nucleated cells.* Nucleic Acids Res, 1988. **16**(3): p. 1215.
152. Pfaffl, M.W., *A new mathematical model for relative quantification in real-time RT-PCR.* Nucleic Acids Res, 2001. **29**(9): p. e45.
153. Li, H., et al., *The Sequence Alignment/Map format and SAMtools.* Bioinformatics, 2009. **25**(16): p. 2078-9.
154. Cory, A.H., et al., *Use of an aqueous soluble tetrazolium/formazan assay for cell growth assays in culture.* Cancer Commun, 1991. **3**(7): p. 207-12.
155. Nicoletti, I., et al., *A rapid and simple method for measuring thymocyte apoptosis by propidium iodide staining and flow cytometry.* J Immunol Methods, 1991. **139**(2): p. 271-9.
156. Gronych, J., et al., *An activated mutant BRAF kinase domain is sufficient to induce pilocytic astrocytoma in mice.* J Clin Invest, 2011. **121**(4): p. 1344-8.
157. Mito, Y., J.G. Henikoff, and S. Henikoff, *Genome-scale profiling of histone H3.3 replacement patterns.* Nat Genet, 2005. **37**(10): p. 1090-7.
158. Ahmad, K. and S. Henikoff, *The histone variant H3.3 marks active chromatin by replication-independent nucleosome assembly.* Mol Cell, 2002. **9**(6): p. 1191-200.
159. Jin, C. and G. Felsenfeld, *Distribution of histone H3.3 in hematopoietic cell lineages.* Proc Natl Acad Sci U S A, 2006. **103**(3): p. 574-9.
160. Delbarre, E., et al., *Chromatin environment of histone variant H3.3 revealed by quantitative imaging and genome-scale chromatin and DNA immunoprecipitation.* Mol Biol Cell, 2010. **21**(11): p. 1872-84.
161. Bax, D.A., et al., *Molecular and phenotypic characterisation of paediatric glioma cell lines as models for preclinical drug development.* PLoS One, 2009. **4**(4): p. e5209.
162. Rutka, J.T., et al., *Establishment and characterization of five cell lines derived from human malignant gliomas.* Acta Neuropathol, 1987. **75**(1): p. 92-103.
163. Chen, P., et al., *Constitutional p53 mutations associated with brain tumors in young adults.* Cancer Genet Cytogenet, 1995. **82**(2): p. 106-15.
164. Kim, H., et al., *Histone variant H3.3 stimulates HSP70 transcription through cooperation with HP1gamma.* Nucleic Acids Res, 2011. **39**(19): p. 8329-41.
165. Cedar, H. and Y. Bergman, *Linking DNA methylation and histone modification: patterns and paradigms.* Nat Rev Genet, 2009. **10**(5): p. 295-304.
166. Tie, F., et al., *CBP-mediated acetylation of histone H3 lysine 27 antagonizes Drosophila Polycomb silencing.* Development, 2009. **136**(18): p. 3131-41.
167. Pasini, D., et al., *Characterization of an antagonistic switch between histone H3 lysine 27 methylation and acetylation in the transcriptional regulation of Polycomb group target genes.* Nucleic Acids Res, 2010. **38**(15): p. 4958-69.
168. Bowman, T., et al., *Tissue-specific inactivation of p53 tumor suppression in the mouse.* Genes Dev, 1996. **10**(7): p. 826-35.
169. Shevtsova, Z., et al., *Evaluation of epitope tags for protein detection after in vivo CNS gene transfer.* Eur J Neurosci, 2006. **23**(8): p. 1961-9.
170. Lobbestael, E., et al., *Immunohistochemical detection of transgene expression in the brain using small epitope tags.* BMC Biotechnol, 2010. **10**: p. 16.
171. Prasher, D.C., et al., *Primary structure of the Aequorea victoria green-fluorescent protein.* Gene, 1992. **111**(2): p. 229-33.

172. Misteli, T. and D.L. Spector, *Applications of the green fluorescent protein in cell biology and biotechnology.* Nat Biotechnol, 1997. **15**(10): p. 961-4.
173. Kanda, T., K.F. Sullivan, and G.M. Wahl, *Histone-GFP fusion protein enables sensitive analysis of chromosome dynamics in living mammalian cells.* Curr Biol, 1998. **8**(7): p. 377-85.
174. Buckers, J., et al., *Simultaneous multi-lifetime multi-color STED imaging for colocalization analyses.* Opt Express, 2011. **19**(4): p. 3130-43.
175. Park, P.J., *ChIP-seq: advantages and challenges of a maturing technology.* Nat Rev Genet, 2009. **10**(10): p. 669-80.
176. Goldberg, A.D., et al., *Distinct factors control histone variant H3.3 localization at specific genomic regions.* Cell, 2010. **140**(5): p. 678-91.
177. Stroud, H., et al., *Genome-wide analysis of histone H3.1 and H3.3 variants in Arabidopsis thaliana.* Proc Natl Acad Sci U S A, 2012. **109**(14): p. 5370-5.
178. Ray-Gallet, D., et al., *Dynamics of histone H3 deposition in vivo reveal a nucleosome gap-filling mechanism for H3.3 to maintain chromatin integrity.* Mol Cell, 2011. **44**(6): p. 928-41.
179. Chow, C.M., et al., *Variant histone H3.3 marks promoters of transcriptionally active genes during mammalian cell division.* EMBO Rep, 2005. **6**(4): p. 354-60.
180. Martinez-Garcia, E. and J.D. Licht, *Deregulation of H3K27 methylation in cancer.* Nat Genet, 2010. **42**(2): p. 100-1.
181. Abbosh, P.H., et al., *Dominant-negative histone H3 lysine 27 mutant derepresses silenced tumor suppressor genes and reverses the drug-resistant phenotype in cancer cells.* Cancer Res, 2006. **66**(11): p. 5582-91.
182. Santenard, A., et al., *Heterochromatin formation in the mouse embryo requires critical residues of the histone variant H3.3.* Nat Cell Biol, 2010. **12**(9): p. 853-62.
183. Gunesdogan, U., H. Jackle, and A. Herzig, *A genetic system to assess in vivo the functions of histones and histone modifications in higher eukaryotes.* EMBO Rep, 2010. **11**(10): p. 772-6.
184. Wei, Y., et al., *Loss of trimethylation at lysine 27 of histone H3 is a predictor of poor outcome in breast, ovarian, and pancreatic cancers.* Mol Carcinog, 2008. **47**(9): p. 701-6.
185. Peters, A.H., et al., *Loss of the Suv39h histone methyltransferases impairs mammalian heterochromatin and genome stability.* Cell, 2001. **107**(3): p. 323-37.
186. Varambally, S., et al., *The polycomb group protein EZH2 is involved in progression of prostate cancer.* Nature, 2002. **419**(6907): p. 624-9.
187. Kleer, C.G., et al., *EZH2 is a marker of aggressive breast cancer and promotes neoplastic transformation of breast epithelial cells.* Proc Natl Acad Sci U S A, 2003. **100**(20): p. 11606-11.
188. Raman, J.D., et al., *Increased expression of the polycomb group gene, EZH2, in transitional cell carcinoma of the bladder.* Clin Cancer Res, 2005. **11**(24 Pt 1): p. 8570-6.
189. Watanabe, H., et al., *Deregulation of histone lysine methyltransferases contributes to oncogenic transformation of human bronchoepithelial cells.* Cancer Cell Int, 2008. **8**: p. 15.
190. Cao, P., et al., *MicroRNA-101 negatively regulates Ezh2 and its expression is modulated by androgen receptor and HIF-1alpha/HIF-1beta.* Mol Cancer, 2010. **9**: p. 108.
191. van Haaften, G., et al., *Somatic mutations of the histone H3K27 demethylase gene UTX in human cancer.* Nat Genet, 2009. **41**(5): p. 521-3.
192. Hyland, E.M., et al., *An evolutionarily 'young' lysine residue in histone H3 attenuates transcriptional output in Saccharomyces cerevisiae.* Genes Dev, 2011. **25**(12): p. 1306-19.
193. Zeng, X., S. Chen, and H. Huang, *Phosphorylation of EZH2 by CDK1 and CDK2: a possible regulatory mechanism of transmission of the H3K27me3 epigenetic mark through cell divisions.* Cell Cycle, 2011. **10**(4): p. 579-83.

194. Turcan, S., et al., *IDH1 mutation is sufficient to establish the glioma hypermethylator phenotype.* Nature, 2012. **483**(7390): p. 479-83.
195. Mutskov, V. and G. Felsenfeld, *Silencing of transgene transcription precedes methylation of promoter DNA and histone H3 lysine 9.* EMBO J, 2004. **23**(1): p. 138-49.
196. Sterner, D.E. and S.L. Berger, *Acetylation of histones and transcription-related factors.* Microbiol Mol Biol Rev, 2000. **64**(2): p. 435-59.
197. Creyghton, M.P., et al., *Histone H3K27ac separates active from poised enhancers and predicts developmental state.* Proc Natl Acad Sci U S A, 2010. **107**(50): p. 21931-6.
198. Bannister, A.J., et al., *Spatial distribution of di- and tri-methyl lysine 36 of histone H3 at active genes.* J Biol Chem, 2005. **280**(18): p. 17732-6.
199. Barski, A., et al., *High-resolution profiling of histone methylations in the human genome.* Cell, 2007. **129**(4): p. 823-37.
200. Edmunds, J.W., L.C. Mahadevan, and A.L. Clayton, *Dynamic histone H3 methylation during gene induction: HYPB/Setd2 mediates all H3K36 trimethylation.* EMBO J, 2008. **27**(2): p. 406-20.
201. Migliori, V., et al., *Arginine/lysine-methyl/methyl switches: biochemical role of histone arginine methylation in transcriptional regulation.* Epigenomics, 2010. **2**(1): p. 119-37.
202. Hyllus, D., et al., *PRMT6-mediated methylation of R2 in histone H3 antagonizes H3 K4 trimethylation.* Genes Dev, 2007. **21**(24): p. 3369-80.
203. Guccione, E., et al., *Methylation of histone H3R2 by PRMT6 and H3K4 by an MLL complex are mutually exclusive.* Nature, 2007. **449**(7164): p. 933-7.
204. Bernstein, B.E., et al., *Methylation of histone H3 Lys 4 in coding regions of active genes.* Proc Natl Acad Sci U S A, 2002. **99**(13): p. 8695-700.
205. Iberg, A.N., et al., *Arginine methylation of the histone H3 tail impedes effector binding.* J Biol Chem, 2008. **283**(6): p. 3006-10.
206. Couture, J.F., et al., *Specificity and mechanism of JMJD2A, a trimethyllysine-specific histone demethylase.* Nat Struct Mol Biol, 2007. **14**(8): p. 689-95.
207. Krause, C.D., et al., *Protein arginine methyltransferases: evolution and assessment of their pharmacological and therapeutic potential.* Pharmacol Ther, 2007. **113**(1): p. 50-87.
208. Dillon, M.B., et al., *Novel inhibitors for PRMT1 discovered by high-throughput screening using activity-based fluorescence polarization.* ACS Chem Biol, 2012. **7**(7): p. 1198-204.
209. Heinke, R., et al., *Virtual screening and biological characterization of novel histone arginine methyltransferase PRMT1 inhibitors.* ChemMedChem, 2009. **4**(1): p. 69-77.
210. Spannhoff, A., et al., *A novel arginine methyltransferase inhibitor with cellular activity.* Bioorg Med Chem Lett, 2007. **17**(15): p. 4150-3.
211. Spannhoff, A., et al., *Target-based approach to inhibitors of histone arginine methyltransferases.* J Med Chem, 2007. **50**(10): p. 2319-25.
212. Chen, Z., et al., *Structural basis of the recognition of a methylated histone tail by JMJD2A.* Proc Natl Acad Sci U S A, 2007. **104**(26): p. 10818-23.
213. Tamura, T., et al., *Inducible deposition of the histone variant H3.3 in interferon-stimulated genes.* J Biol Chem, 2009. **284**(18): p. 12217-25.
214. Hambardzumyan, D., et al., *Modeling Adult Gliomas Using RCAS/t-va Technology.* Transl Oncol, 2009. **2**(2): p. 89-95.
215. Doucette, T., et al., *Mesenchymal stem cells display tumor-specific tropism in an RCAS/Ntv-a glioma model.* Neoplasia, 2011. **13**(8): p. 716-25.
216. Jacks, T., et al., *Tumor spectrum analysis in p53-mutant mice.* Curr Biol, 1994. **4**(1): p. 1-7.
217. Symonds, H., et al., *p53-dependent apoptosis suppresses tumor growth and progression in vivo.* Cell, 1994. **78**(4): p. 703-11.
218. Kenzelmann Broz, D. and L.D. Attardi, *In vivo analysis of p53 tumor suppressor function using genetically engineered mouse models.* Carcinogenesis, 2010. **31**(8): p. 1311-8.

219. Johnson, T.M. and L.D. Attardi, *Dissecting p53 tumor suppressor function in vivo through the analysis of genetically modified mice.* Cell Death Differ, 2006. **13**(6): p. 902-8.
220. Donehower, L.A., et al., *Effects of genetic background on tumorigenesis in p53-deficient mice.* Mol Carcinog, 1995. **14**(1): p. 16-22.
221. Zong, H., R.G. Verhaak, and P. Canoll, *The cellular origin for malignant glioma and prospects for clinical advancements.* Expert Rev Mol Diagn, 2012. **12**(4): p. 383-94.
222. Lai, A., et al., *Evidence for sequenced molecular evolution of IDH1 mutant glioblastoma from a distinct cell of origin.* J Clin Oncol, 2011. **29**(34): p. 4482-90.

## 8 LIST OF FIGURES

# 9 PUBLICATIONS

1. **Hotspot mutations in H3F3A and IDH1 define distinct epigenetic and biological subgroups of glioblastoma.**

   *Cancer Cell. 2012 Oct 16;22(4):425-37.*

   Sturm D, Witt H, Hovestadt V, Khuong-Quang DA, Jones DT, Konermann C, Pfaff E, Tönjes M, Sill M, **Bender S**, Kool M, Zapatka M, Becker N, Zucknick M, Hielscher T, Liu XY, Fontebasso AM, Ryzhova M, Albrecht S, Jacob K, Wolter M, Ebinger M, Schuhmann MU, van Meter T, Frühwald MC, Hauch H, Pekrun A, Radlwimmer B, Niehues T, von Komorowski G, Dürken M, Kulozik AE, Madden J, Donson A, Foreman NK, Drissi R, Fouladi M, Scheurlen W, von Deimling A, Monoranu C, Roggendorf W, Herold-Mende C, Unterberg A, Kramm CM, Felsberg J, Hartmann C, Wiestler B, Wick W, Milde T, Witt O, Lindroth AM, Schwartzentruber J, Faury D, Fleming A, Zakrzewska M, Liberski PP, Zakrzewski K, Hauser P, Garami M, Klekner A, Bognar L, Morrissy S, Cavalli F, Taylor MD, van Sluis P, Koster J, Versteeg R, Volckmann R, Mikkelsen T, Aldape K, Reifenberger G, Collins VP, Majewski J, Korshunov A, Lichter P, Plass C, Jabado N, Pfister SM.

2. **Dissecting the genomic complexity underlying medulloblastoma.**

   *Nature. 2012 Aug 2;488(7409):100-5.*

   Jones DT, Jäger N, Kool M, Zichner T, Hutter B, Sultan M, Cho YJ, Pugh TJ, Hovestadt V, Stütz AM, Rausch T, Warnatz HJ, Ryzhova M, **Bender S**, Sturm D, Pleier S, Cin H, Pfaff E, Sieber L, Wittmann A, Remke M, Witt H, Hutter S, Tzaridis T, Weischenfeldt J, Raeder B, Avci M, Amstislavskiy V, Zapatka M, Weber UD, Wang Q, Lasitschka B, Bartholomae CC, Schmidt M, von Kalle C, Ast V, Lawerenz C, Eils J, Kabbe R, Benes V, van Sluis P, Koster J, Volckmann R, Shih D, Betts MJ, Russell RB, Coco S, Tonini GP, Schüller U, Hans V, Graf N, Kim YJ, Monoranu C, Roggendorf W, Unterberg A, Herold-Mende C, Milde T, Kulozik AE, von Deimling A, Witt O, Maass E, Rössler J, Ebinger M, Schuhmann MU, Frühwald MC, Hasselblatt M, Jabado N, Rutkowski S, von Bueren AO, Williamson D, Clifford SC, McCabe MG, Collins VP, Wolf S, Wiemann S, Lehrach H, Brors B, Scheurlen W, Felsberg J, Reifenberger G, Northcott PA, Taylor MD, Meyerson M, Pomeroy SL, Yaspo ML, Korbel JO, Korshunov A, Eils R, Pfister SM, Lichter P.

3. **Genome sequencing of pediatric medulloblastoma links catastrophic DNA rearrangements with TP53 mutations.**

   *Cell. 2012 Jan 20;148(1-2):59-71.*

   Rausch T, Jones DT, Zapatka M, Stütz AM, Zichner T, Weischenfeldt J, Jäger N, Remke M, Shih D, Northcott PA, Pfaff E, Tica J, Wang Q, Massimi L, Witt H, **Bender S**, Pleier S, Cin H, Hawkins C, Beck C, von Deimling A, Hans V, Brors B, Eils R, Scheurlen W, Blake J, Benes V, Kulozik AE, Witt O, Martin D, Zhang C, Porat R, Merino DM, Wasserman J, Jabado N, Fontebasso A, Bullinger L, Rücker FG, Döhner K, Döhner H, Koster J, Molenaar JJ, Versteeg R, Kool M, Tabori U, Malkin D, Korshunov A, Taylor MD, Lichter P, Pfister SM, Korbel JO.

4. **FSTL5 is a marker of poor prognosis in non-WNT/non-SHH medulloblastoma.**

   *J Clin Oncol. 2011 Oct 10;29(29):3852-61.*

   Remke M, Hielscher T, Korshunov A, Northcott PA, **Bender S**, Kool M, Westermann F, Benner A, Cin H, Ryzhova M, Sturm D, Witt H, Haag D, Toedt G, Wittmann A, Schöttler A, von Bueren AO, von Deimling A, Rutkowski S, Scheurlen W, Kulozik AE, Taylor MD, Lichter P, Pfister SM.

**5. Delineation of two clinically and molecularly distinct subgroups of posterior fossa ependymoma.**

*Cancer Cell. 2011 Aug 16;20(2):143-57.*

Witt H, Mack SC, Ryzhova M, **Bender S**, Sill M, Isserlin R, Benner A, Hielscher T, Milde T, Remke M, Jones DT, Northcott PA, Garzia L, Bertrand KC, Wittmann A, Yao Y, Roberts SS, Massimi L, Van Meter T, Weiss WA, Gupta N, Grajkowska W, Lach B, Cho YJ, von Deimling A, Kulozik AE, Witt O, Bader GD, Hawkins CE, Tabori U, Guha A, Rutka JT, Lichter P, Korshunov A, Taylor MD, Pfister SM.

6. **The transcription factor evi-1 is overexpressed, promotes proliferation, and is prognostically unfavorable in infratentorial ependymomas.**

*Clin Cancer Res. 2011 Jun 1;17(11):3631-7.*

Koos B**, Bender S**, Witt H, Mertsch S, Felsberg J, Beschorner R, Korshunov A, Riesmeier B, Pfister S, Paulus W, Hasselblatt M.

7. **Oncogenic FAM131B-BRAF fusion resulting from 7q34 deletion comprises an alternative mechanism of MAPK pathway activation in pilocytic astrocytoma.**

*Acta Neuropathol. 2011 Jun;121(6):763-74.*

Cin H, Meyer C, Herr R, Janzarik WG, Lambert S, Jones DT, Jacob K, Benner A, Witt H, Remke M, **Bender S**, Falkenstein F, Van Anh TN, Olbrich H, von Deimling A, Pekrun A, Kulozik AE, Gnekow A, Scheurlen W, Witt O, Omran H, Jabado N, Collins VP, Brummer T, Marschalek R, Lichter P, Korshunov A, Pfister SM.

8. **FGFR3 is a target of the homeobox transcription factor SHOX in limb development.**

*Hum Mol Genet. 2011 Apr 15;20(8):1524-35.*

Decker E, Durand C, **Bender S**, Rödelsperger C, Glaser A, Hecht J, Schneider KU, Rappold G.

9. **Role of LIM and SH3 protein 1 (LASP1) in the metastatic dissemination of medulloblastoma.**

*Cancer Res. 2010 Oct 15;70(20):8003-14.*

Traenka C, Remke M, Korshunov A, **Bender S**, Hielscher T, Northcott PA, Witt H, Ryzhova M, Felsberg J, Benner A, Riester S, Scheurlen W, Grunewald TG, von Deimling A, Kulozik AE, Reifenberger G, Taylor MD, Lichter P, Butt E, Pfister SM.

10. **Molecular staging of intracranial ependymoma in children and adults.**

*J Clin Oncol. 2010 Jul 1;28(19):3182-90.*

Korshunov A, Witt H, Hielscher T, Benner A, Remke M, Ryzhova M, Milde T, **Bender S**, Wittmann A, Schöttler A, Kulozik AE, Witt O, von Deimling A, Lichter P, Pfister S.

## 10 ACKNOWLEDGEMENTS

First of all, I would like to express my deepest thanks to Prof. Stefan M. Pfister and Prof. Peter Lichter for making it possible to conduct my thesis at the German Cancer Research Center (DKFZ).

I am indebted to Prof. Stefan M. Pfister for his continuous advice and guidance. I would like to thank him for the opportunity to work in an outstanding scientific environment and I'm very grateful for letting me be a member of (t)his extraordinary group.

Likewise, I am very thankful to Prof. Peter Lichter for guiding me with his incredible scientific expertise.

I would like to thank Prof. Werner Buselmaier and Prof. Olaf Witt for critical thinking during my TAC meetings. In addition, I'm thankful to Prof. Stefan Frings and PD Karsten Rippe for being willing to be in my defense committee.

I am grateful to for the excellent support of my colleagues Dr. Marcel Kool, Dr. Hendrik Witt, Dr. Marc Zapatka, Dominik Sturm, Dr. Pascal Johann, Dr. Sebastian Stark and Dr. Jan Gronych as well as my collaborator Dr. Weijun Feng. Especially I would like to mention the help of Prof. Andrey Korshunov, Dr. Huriye Cin and Dr. David TW Jones.

Special thanks to my colleagues and friends Josephine Bageritz, Dr. Sabrina Pleier and Verena Thewes. I really had a great time with you!

It was a pleasure to work in such a wonderful atmosphere with my further colleagues Sonja Hutter, Elke Pfaff and Theophilos Tzaridis and Dr. Jan Meier.

Special thanks to Anna Schöttler, Andrea Wittmann and Laura Sieber for excellent technical assistance. I also would like to appreciate the assistance of Frauke Devens and Magdalena Schlotter.

I would like to highlight the contribution of Michael Hain, who solved all hardware and software problems.

Moreover, I am grateful to Birgit Weiss and Ralph Röth for introducing me to basic lab work in a fantastic lab atmosphere.

I also would like to acknowledge Dr. Stephan Wolf for pointing me in the right direction.

For giving so much happiness and strength, I wish to thank Z&W.

My very warm thanks go to Güler: She is (by far) the most important "finding" of my research time at the DKFZ.

Finally, I would like to express my warmest thanks to my wonderful parents Ursula and Gerhard for their continuous support and for always believing in me and my decisions. This thesis is dedicated to you!

## 11 SUPPLEMENTARY DATA

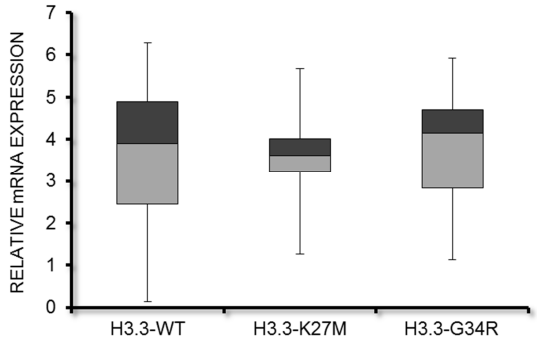


**Supplementary Figure 1. Expression of canonical Histone H3 in primary GBMs.** Histone H3 microarray expression data (Probe set 214522_x) of 81 pedGBM samples, which were grouped according to their *H3F3A* mutation status (WT: n=56; K27M: n=14; G34R: n=11).

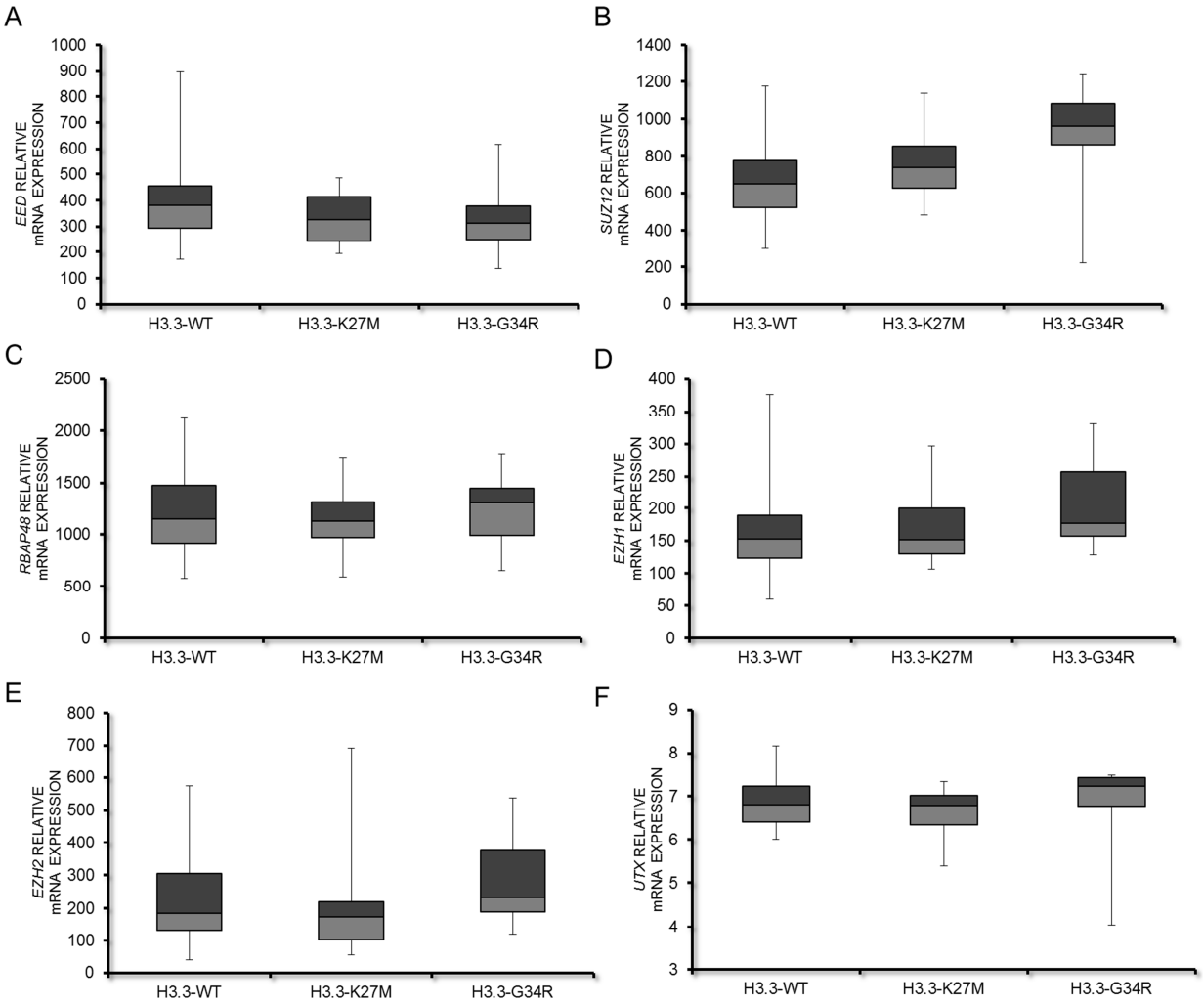


**Supplementary Figure 2. Expression of H3K27me3 modifying Enzymes.** Microarray expression data of 81 pedGBM samples grouped according to their H3F3A mutation status (WT: n=56; K27M: n=14; G34R: n=11). Messenger RNA expression is illustrated for the PRC2 core components EED **(A)**, EZH1 **(B)**, EZH2 **(C)**, RBAP48 **(D)** and SUZ12 **(E)** as well as for the H3K27me demethylase UTX **(F)**. Following probe sets were used: EED (209572_s_at), EZH1 (32259_at), EZH2 (203358_s_at), RBAP48 (210371_s_at), SUZ12 (212287_at) and UTX (203992_s_at).

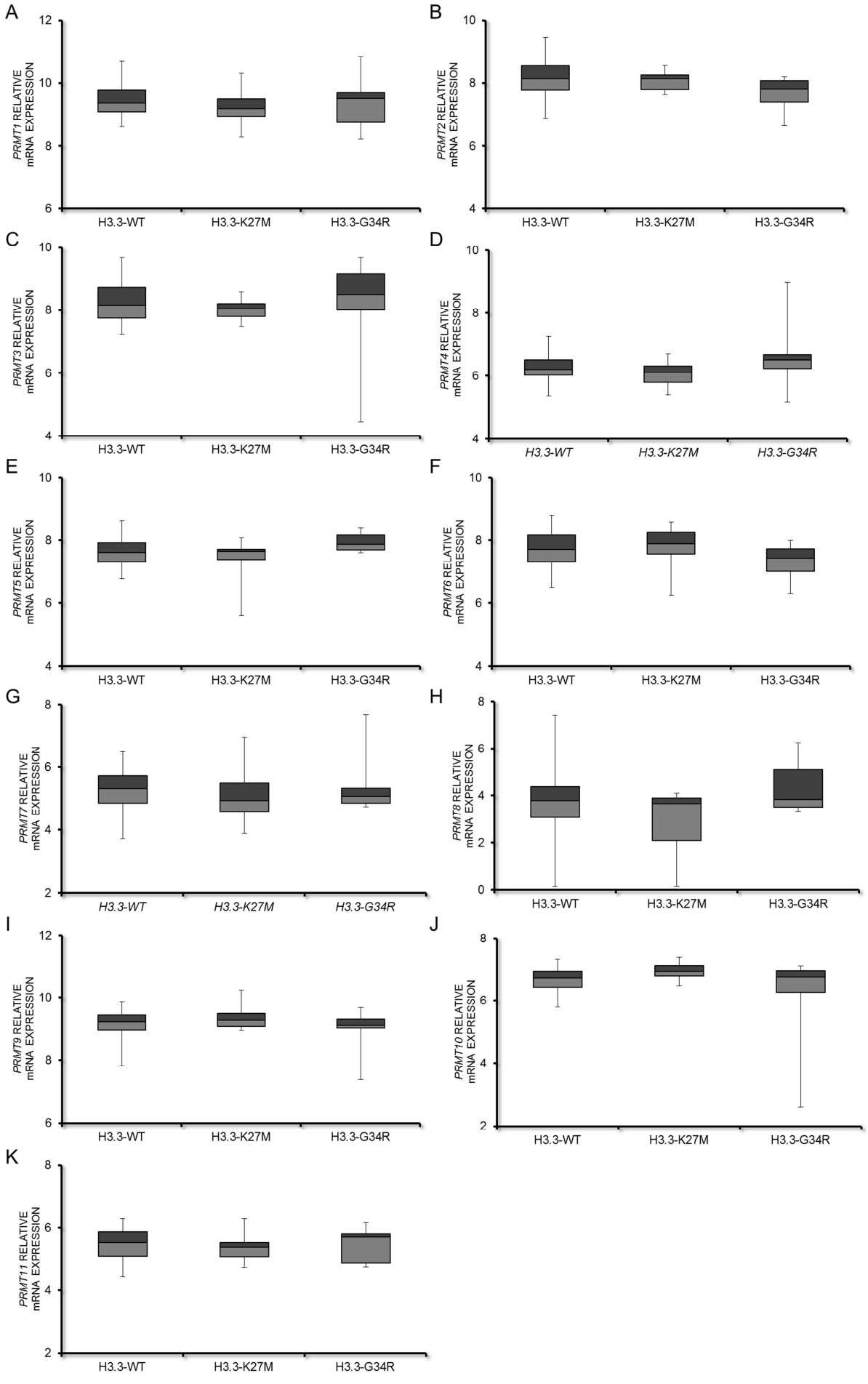
A
PRMT1 RELATIVE mRNA EXPRESSION
12
10
8
6
H3.3-WT
H3.3-K27M
H3.3-G34R
B
PRMT2 RELATIVE mRNA EXPRESSION
10
8
6
4
H3.3-WT
H3.3-K27M
H3.3-G34R
C
PRMT3 RELATIVE mRNA EXPRESSION
10
8
6
4
H3.3-WT
H3.3-K27M
H3.3-G34R
D
PRMT4 RELATIVE mRNA EXPRESSION
10
8
6
4
H3.3-WT
H3.3-K27M
H3.3-G34R
E
PRMT5 RELATIVE mRNA EXPRESSION
10
8
6
4
H3.3-WT
H3.3-K27M
H3.3-G34R
F
PRMT6 RELATIVE mRNA EXPRESSION
10
8
6
4
H3.3-WT
H3.3-K27M
H3.3-G34R
G
PRMT7 RELATIVE mRNA EXPRESSION
8
6
4
2
H3.3-WT
H3.3-K27M
H3.3-G34R
H
PRMT8 RELATIVE mRNA EXPRESSION
8
6
4
2
0
H3.3-WT
H3.3-K27M
H3.3-G34R
I
PRMT9 RELATIVE mRNA EXPRESSION
12
10
8
6
H3.3-WT
H3.3-K27M
H3.3-G34R
J
PRMT10 RELATIVE mRNA EXPRESSION
8
6
4
2
H3.3-WT
H3.3-K27M
H3.3-G34R
K
PRMT11 RELATIVE mRNA EXPRESSION
8
6
4
2
H3.3-WT
H3.3-K27M
H3.3-G34R

**Supplementary Figure 3. Expression of PRMTs in primary GBMs.** Microarray expression data of 81 pedGBM samples with known *H3F3A* mutation status (WT: n=56; K27M: n=14; G34R: n=11) are illustrated as box blots for *PRMT1* **(A)**, *PRMT2* **(B)**, *PRMT3* **(C)**, *PRMT4* **(D)**, *PRMT5* **(E),** *PRMT6* **(F)**, *PRMT7* **(G)**, *PRMT8* **(H)**, *PRMT9* **(I)**, *PRMT10* (**J)** and PRMT11 **(K)**. Following probe sets were used: PRMT1 (206445_s_at), PRMT2 (202098_s_at), PRMT3 (213320_at), PRMT4 (CARM1) (212512_s_at), PRMT5 (217786_at), PRMT6 (223275_at), PRMT7 (219408_at), PRMT8 (230839_at), PRMT9 (FBXO11) (222119_s_at), PRMT10 (228536_at) and PRMT11 (FBXO10) (227222_at).

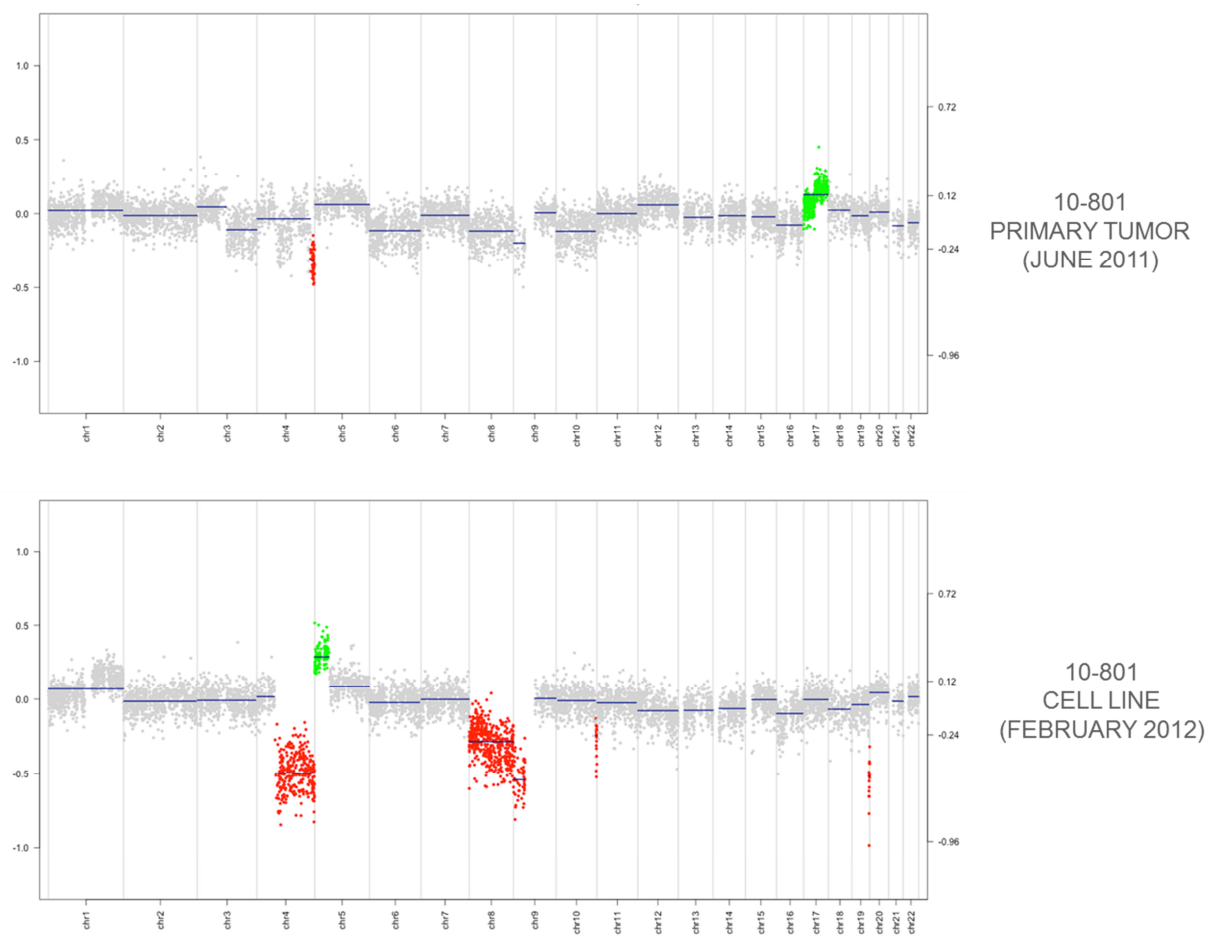


**Supplementary Figure 4. Genomic Aberrations in H3.3 mutated Cell Line 10-801.** The cell line 10-801 was derived from a G34R mutated pedGBM displaying several genomic aberrations (top). After several month of *in vitro* cultivation, numerous new genetic abnormalities are detectable (bottom).